Test Functions for Elliptic Problems Satisfying Linear Essential Edge Conditions on Both Convex and Concave Polygons

Elisabeth Anna Malsch

Submitted in partial fulfillment of the
requirements for the degree
of Doctor of Philosophy
in the Graduate School of Arts and Sciences

COLUMBIA UNIVERSITY

2003

© 2003

Elisabeth Anna Malsch
All Rights Reserved

ABSTRACT

Test Functions for Elliptic Problems Satisfying Linear Essential Edge Conditions on Both Convex and Concave Polygons

Elisabeth Anna Malsch

Interpolations which are smooth and bounded can be constructed over any two dimensional polygonal domain, including those with concavities and inclusions. Like boundary element test functions, they depend only on the boundary values. Unlike the boundary element method formulations, they satisfy linear essential boundary conditions exactly and do not depend on a Greens' function solution to the governing field equation. In other words, they are Ritz type coordinate functions which apply to any polygonal domain. The interpolations satisfy element level constancy and linear patch tests and perform well in approximation of potential field solutions. Similar functions, applicable only to convex polygons, have been applied successfully to biomedical problems including skull growth and heart function analyses. No smooth kinematic concave polygonal element description of any type is presented in the available finite element, boundary element or computational geometry literature.

Contents

1 Introduction **1**

1.1 Stiffness and tessellation 7

1.1.1 Modal approach 10

1.1.2 Element level degree of freedom 13

1.2 Review of linear edged geometric test function formulations . . 17

1.2.1 An interpolation which is both bounded and linear exists for every polygonal domain 18

1.2.2 Interpolation within convex polygons 22

2 Linear transformation **25**

2.1 General construction of a quadrilateral test function for a non-concave polygon 27

2.2 Perspective transformation 29

2.2.1 Local coordinate derivation 31

2.2.2 Transformed unit square 33

2.2.3 Jacobian of the perspective transformation 35

2.2.4 General integration in cartesian coordinates 37
2.3 Testing applicability of a transformation by deriving the elliptic field equation 38
2.3.1 Non-uniqueness of a smooth linear interpolation 40

3 Approximating concavity **42**
3.1 Available methods for concave element construction 43
3.1.1 Conformal mapping 44
3.1.2 Application to the concave quadrilateral 46
3.2 Concave element construction from path-lines 49
3.2.1 Satisfying the first order continuity requirement 49
3.3 General methods for all polygons 56
3.3.1 Smooth zeroth order concave shape 57
3.3.2 Construction of a linear edged interpolation 60
3.3.3 A general linear edged interpolation 64
3.3.4 Smooth first order bounded interpolations 66
3.4 Comparison of concave representations 68

4 Order of approximation **73**
4.1 Taylor Expansion 75
4.2 Form of the shape function 77
4.3 Padé approximation 79
4.4 Quadratic Shafer (Hermite-Padé) 81
4.4.1 Degenerate side-node element 83

4.5 Numerical test: impact of the number of element nodes to the approximation . . . 84
4.5.1 Comparison of the general methods . . . 89
4.5.2 Counter example to closure . . . 91
4.6 Interior behavior and convergence . . . 94

5 Elliptic problems **95**
5.1 The potential problem . . . 96
5.1.1 Test case: triangulation vs. side nodes . . . 97
5.2 Interpolation and stability . . . 102
5.2.1 Single element properties . . . 106
5.2.2 Closure test for the skew quadrilateral . . . 107
5.2.3 Test case: concavity . . . 109

6 Summary and applications **113**

A Code examples **127**
A.1 Lagrange polynomial from Taylor Series . . . 128
A.2 Shape function routine for convex polygons . . . 129
A.3 Shape function for an element with side nodes . . . 131
A.4 Concave quadrilateral shape function routine . . . 132

B Methods **135**
B.1 One-dimensional formulation and solution . . . 136
B.1.1 *h*-method . . . 137

B.1.2 p-method 138
B.1.3 One dimensional modal solution 138
B.2 Conformal Mapping 140
B.3 Shape function generation and boundedness 141
B.4 Rational polynomial basis functions 143

List of Figures

1.1 Bar in tension 4

1.2 Discrete boundary value problem. 5

1.3 Mesh composed of triangles. 8

1.4 Mesh composed of quadrilaterals. 8

1.5 Lagrange elements with one, two and three side nodes. 14

1.6 Lagrange approximation to the Runge function $\frac{1}{x^2+1}$ using equally spaced nodes. 14

1.7 Lagrange approximation to $|x|$ using equally spaced nodes. . . 15

1.8 Discontinuous zeroth order approximation 23

1.9 Interpolation within sub-triangles 23

1.10 Smooth first order interpolation 23

2.1 Sketches of fluid flow path lines 27

2.2 Normed square 29

2.3 Convex element 29

2.4 Side node 29

3.1 Semi-infinite → polygonal 45
3.2 Symmetric element 48
3.3 Asymmetric element 48
3.4 Concave quadrilateral element approximated by triangles and the associated gradient. 50
3.5 Smooth concave element sketch. 51
3.6 Coordinate system for quadrilateral analysis 52
3.7 Skew concave element 53
3.8 Remaining shape functions from patch test 54
3.9 Functions which are minimum along a line 56
3.10 Behavior of finite lines at a reentrant corner. 57
3.11 Concave quadrilateral element with smooth interpolation contours 59
3.12 Concave pentagonal element with smooth interpolation contours 60
3.13 Smooth interpolation on a concave element with eighteen nodes 61
3.14 Elliptical contours. 62
3.15 General linear edged interpolation within a square. 63
3.16 Smooth linear edged interpolation within a concave domain. . 64
3.17 Linear boundary behavior, even along reentrant boundaries. . 66
3.18 Smooth, bounded interpolation contours within reentrant shapes. 67
3.19 Smooth first order interpolation within a square. 68
3.20 Smooth first order interpolation within a concave domain. . . 69
3.21 C^0 Tessellated model 69

3.22 C^1 Smooth model 69
3.23 Linear edged test function behavior. 70
3.24 Zeroth order test function behavior along the diagonal from the concave and opposite concave nodes. 70
3.25 Linear edged test function behavior along the diagonal. 71
3.26 Behavior from the concave node to the opposite concave node. 72

4.1 Error for constant and linear fields is zero 84
4.2 Error with respect to the field xy for a convex triangle, quadrilateral, pentagon, hexagon, septagon and octagon respectively 86
4.3 Error with respect to the field x^2 for a convex triangle, quadrilateral, pentagon, hexagon, septagon and octagon respectively 86
4.4 Error with respect to the field y^2 for a convex triangle, quadrilateral, pentagon, hexagon, septagon and octagon respectively 87
4.5 Error with respect to the quadratic x^2 field for a quadrilateral with five, six, seven and eight nodes 87
4.6 Error with respect to the quadratic y^2 field for a quadrilateral with five, six, seven and eight nodes 87
4.7 Error with respect to the field x, y, x^2, xy and y^2 for a reentrant quadrilateral 92
4.8 Error with respect to the field x, y, x^2, xy and y^2 for a reentrant hexagon 93
4.9 Error between two linear skew quadrilateral representations . . 93

5.1 **L**, **U** and **O** shaped concave domains. 110

6.1 Modeling the structure of material, the torsion problem. . . . 115

6.2 Interpolants for modeling planar torsion. 116

6.3 Soil structure interaction with concave cells. 117

6.4 Concave cell interpolation. 119

6.5 Analysis of biological structures defined by a limited number of data points. 119

6.6 Smooth gradient colorings can be generated at any desired resolution without tessellation. 120

Acknowledgement

I am deeply grateful for the opportunity to work and play on a single idea, to be able to watch it grow, and to form it into something which I want to share with other people. I am especially indebted to my advisor (Doktorvater) Gautam Dasgupta. And also to Dr. Wachspress for his insights and interest. The advice of my Thesis Committee, Professors Rimas Vaicaitis, Raimondo Betti, Guillaume Bal and Jeffrey Holmes, is also much appreciated. The financial support for this research was provided through National Science Foundation Grants numbers CMS 9820353 and CMS 02022232, the Department of Civil Engineering and Engineering Mechanics, and the Guggenheim Flight Fellowship. To my parents and especially John for patiently listening and trying to understand what all the funny sketches mean. To Christian, who I have watched and studied so intently, I was proud of you too, as much as that was possible. From you I saw that there is a certain special benefit to sticking out, being loud and accepting nothing. Would that some of life had been as easy for you as it has been for me.

Notation

Determinant: $|\cdot|$ or $\det(\cdot)$

Absolute value of a determinant: $|\det(\cdot)|$

Kronecker Delta: $\delta_{ij} = \begin{cases} 1 & i = j \\ 0 & i \neq j \end{cases}$

Operator $\mathcal{L}$: $\mathcal{L}[\cdot]$

Matrix K with dimensions m and n: $[\mathbf{K}]^{mxn}$

Vector a of dimension n: $\{\vec{a}_n\}$

Approximate: $\approx$

Equal: $=$

Minimum value of a function g dependent on i over a set S: $\min_{i \in S}(g(i))$

Maximum value of a function g dependent on i over a set S: $\max_{i \in S}(g(i))$

For every point at each location $\{x, y\}$ in the domain $\mathcal{D}$: $\forall \{x, y\} \in \mathcal{D}$

Interelement continuity of order n: $\mathtt{C}^n$

Area Coordinates

$$\text{cartesian coordinates of point } i: \quad \{x_i, y_i\} \tag{1}$$

$$\text{area of triangle with vertices at points } a, b \,\&\, c.: \quad \triangle(a,b,c) \hat{=} \frac{1}{2!} \begin{vmatrix} x_a & y_a & 1 \\ x_b & y_b & 1 \\ x_c & y_c & 1 \end{vmatrix} \tag{2}$$

$$\text{zero line through points } b \,\&\, c: \quad \triangle(\vec{x},b,c) \hat{=} \frac{1}{2!} \begin{vmatrix} x & y & 1 \\ x_b & y_b & 1 \\ x_c & y_c & 1 \end{vmatrix} \tag{3}$$

Chapter 1

Introduction

Approximate representations of systems described by an elliptic functional operator can be constructed using geometric test functions. Similar to the finite element and boundary element methods a trial function is formulated as an assumed interpolation which prescribes the influence of a value, given at a point, upon the behavior of the solution everywhere else in the problem domain. Test functions can be constructed such that linear essential boundary conditions are satisfied exactly on any polygonal domain. Unlike the conventional approaches, the resulting representation depends neither on the fundamental solution of the governing field equation nor on a domain tessellation. Consequently, the method is more flexible than the boundary element method and more stable than the finite element method.

An exact test function formulation is characterized by interpolations which satisfy the kinematic boundary conditions and the governing field equa-

tion. The quality of the approximation is a function only of the amount of boundary and domain node data which is included in the model. A domain dependent Green's function is such a representation. If a unique solution exists, then the corresponding Green's function exists and is unique on the same domain.[1] In most cases the domain and governing field equation can not be satisfied by a simple closed form solution. Alternatively, the exact solution can be represented by an infinite summation. A set of orthogonal functions which each describe a different modal behavior of the solution exactly are combined to describe the behavior of any function. The nature of the eigenfunction is dependent on the governing field equation and the geometry of the domain.

A number of methods for constructing approximate test functions have been developed. In 1877, Lord Rayleigh developed a method for finding eigenvalues according a quotient representation and a choice of trial functions which satisfy the rigid boundary conditions.[2] Independently, in his 1908 and 1909 papers Ritz referred to a set of coordinate functions, which satisfy the essential boundary conditions and are complete within the domain.[3] In 1943 Courant introduced an "admissible coordinate function" applicable to a triangular element. A trial function applicable to a specific finite domain was later termed shape function. Unlike trial and test functions, shape functions

[1] See reference for rigorous description and proof [56, pp.54–56].

[2] A test function is constructed as a linear combination of such trial functions. A secondary reference is cited [26, pp. 183–191].

[3] A secondary reference is cited [13].

need not satisfy essential boundary conditions. A large class of non-conformal shape functions have been developed.[4] In the context of boundary element literature, the term test function has been redefined such that it refers to the fundamental solution satisfying the governing equation and does not necessarily satisfy the boundary conditions [7].

The developed method is termed geometric test function since it applies to the entire boundary domain and —unlike the boundary element— satisfies the essential boundary conditions. The geometric test functions satisfy all the conditions of coordinate functions, including boundedness and smoothness, except completeness. There is no other mention of the practical construction of this type of test function on any concave domain, in the available finite element, boundary element or computational geometry literature.[5]

The goal of any approximate method is to capture as many of the properties of the exact solution using as few data points and trial functions as possible. Accordingly, it is imperative to select functions which most closely capture the salient features of the solution. In cases where the modal behavior of a system governs its performance, a truncated series solution is most useful. Similarly, for a system governed by its boundary behavior a geometric test function solution which satisfies the essential boundary conditions and a required set of field behaviors is preferable.

[4] A collection of elements are presented in the reference [67, pp.290–316].

[5] An overview of available finite element methods are presented in the reference [67]. The boundary element method is similarly discussed [8]. An overview of methods of computational geometry is cited [21].

The simplest interpolation is the one-dimensional line which uniquely and optimally connects two points. The description of a line in terms of a trial function definition, consists of two nodal points and two associated linear interpolations. On a one dimensional domain, where the domain description requires only continuity at nodal points and infinite smoothness between nodes, a unique approximation can be constructed as a combination of such linear elements.[6]

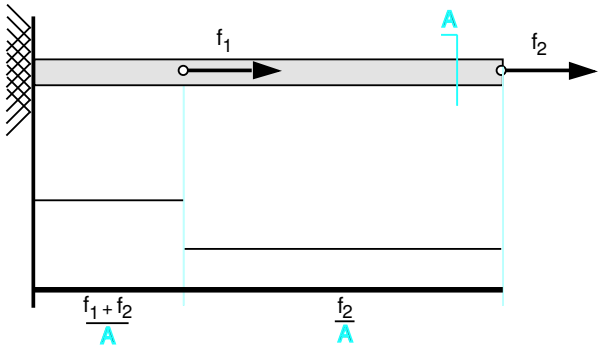


Figure 1.1: Bar in tension

A linear interpolation within a two dimensional domain can not be defined so simply. There is no unique or optimal description except along the boundary where the behavior is one dimensional. Additional restrictions on an interpolation depend on global requirements of the application. For example, the suitability of a two dimensional finite element approximation depends on the so called 'patch test' condition.[7] The set of shape functions

[6] A one dimensional bar for example can be modeled accurately with discontinuous elements, see figure 1.1.

[7] The 'patch test' condition was first introduced by Irons and Razzaque in 1972 [30,

which describe a linear interpolation must, in linear combination, reproduce constant and linear fields. Interpolations which do not satisfy this condition produce models that dissipate energy when no work has been done on the system; in mechanical problems translating or rotating the model produces strain energy.[8] Other global requirements include constraints introduced by material incompressibility and restrictions on plane section behavior.

Given a two dimensional boundary value problem where strain and stress discontinuities occur only on the boundary, the addition of any interior nodes, and associated meshing, mars the continuity of the model.[9] Any elements

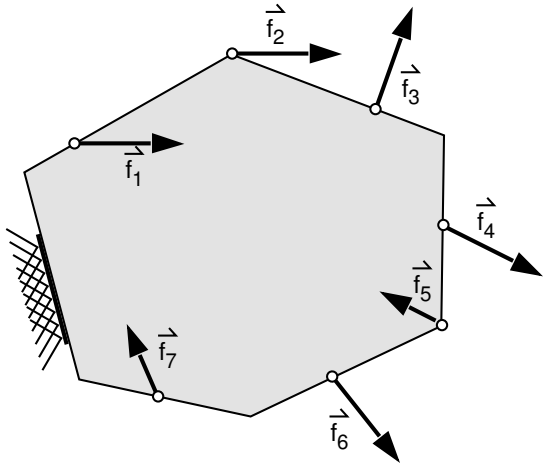


Figure 1.2: Discrete boundary value problem.

pp. 149–157]. Shape functions must necessarily reproduce a polynomial of degree m if the approximate solution to an n-dimensional elliptic variational problem of order m is to converge to the continuous solution. The proof was constructed by Strang and Fix in 1973 [57, pp. 105–116, 300–302].

[8]This pathology is also termed rigid-body failure [38, pp. 488]. Mathematically the requirement is termed a consistency condition, a force which adds no energy to the system must be associated with a zero energy mode [56, p. 223]

[9]For example see figure 1.2.

added inside the mesh are defined by boundaries which are constrained to be linear in a domain which is characterized only by its continuity and governing field equation. As a result, some models are significantly stiffer than the physical system they represent [37]. Methods for relaxing the model include: reduced integration, bubble functions, selective under-integration, and reduced strain. Each adds spurious data and results in a model whose reliability is unknown [38, pp. 500–511]. While it is possible to achieve a balance of errors that adequately represents a particular problem, there is no general guarantee that such a scheme will accurately predict the behavior of even a slightly different system under the same displacement and loading conditions.[10]

The domain dependent Green's function, satisfies the governing equation and the rigid boundary conditions. It most exactly interpolates the effect of boundary behavior into the interior of the domain. If it is available, no other interpolation is required [14, 56]. If it is possible to find fundamental solutions to the governing field equation, then a boundary element formulation is constructible [7]. For applications where the governing field equation is unknown or too complicated to solve explicitly, only the displacement based solution applies [13, 46, 57]. Especially for such cases, a method of two dimensional interpolation which captures any desired number of kinematic

[10]These terms which describe the pathologies of shape function failure are explained in detail in the reference [38, pp. 488]. Some of the more successful remediation attempts can be reformulated as a mixed method [50]. A predictor of convergence exists for mixed methods is the 'inf-sup' condition. It is difficult to apply in general [4].

degrees of freedom and linear essential boundary conditions is required.

1.1 Stiffness and tessellation

To better construct a simple approximate solution which satisfies the rigid boundary conditions, in 1943 Courant introduced a domain discretization. The interpolations within the triangular sub-domains are linear:

$$\phi_i^{\triangle}(x, y) = a_i x + b_i y + c_i \tag{1.1}$$

The approximation is applied to a problem of plane torsion. The accuracy of the convergent solution is dependent on the subdivision size [13].

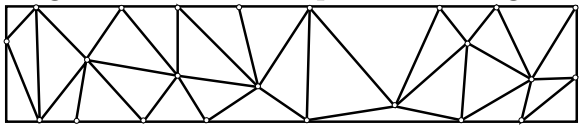
In 1960 the term finite element method was applied to the method of dividing domains into sub-domains and calculating the minimum of a function separately on each domain.[11] The quality of an approximation is governed either by the decrease in the subdivision size h or an increase in the order p of a polynomial which is satisfied exactly by the interpolation [13].[12]

Approximate solutions to many two dimensional problems are constructed using Courant's linear shape functions. Any polygonal space can be triangulated according to methods of Computational Geometry such as Delaunay Triangulation [21]. Nevertheless, triangular elements behave too stiffly in some applications such that the approximate solution never converges [38]. The kinematic flexibility of an element is dependent on the number of nodes

[11] The term 'finite element method' was coined by Clough in his 1960 article [12, 22].
[12] One dimensional examples are included in the appendix B.1.

which define it. A triangle exhibits $3n$ degree's of freedom where n is the number of generalized parameters associated with each node.

Figure 1.3: Mesh composed of triangles.



A quadrilateral element with linear edges can similarly be constructed. It exhibits $4n$ degrees of freedom. In 1961, I. C. Taig introduced a convex quadrilateral element formulation which is defined using a computational coordinate frame $\{s, t\}$:

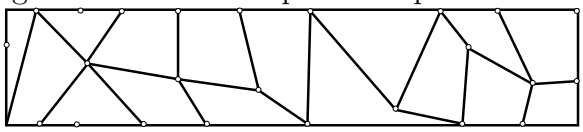
$$\phi_i^{\diamond}(s,t) = a_i s + b_i t + c_i st + d_i \tag{1.2}$$

The local cartesian coordinates $\{x, y\}$ are described with respect to an affine transformation:

$$x = \sum_{i=1}^{4} x_i \, \phi_i \quad \text{and} \quad y = \sum_{i=1}^{4} y_i \, \phi_i \tag{1.3}$$

Where $\{x_i, y_i\}$ are the vertices of the convex quadrilateral. The quadrilat-

Figure 1.4: Mesh composed of quadrilaterals.



eral shape functions can not be applied in general. For example, the concave

elements in figure 1.4 can not be described as a geometrically linear transformation of a polynomial.

Linear edged triangular meshes can not model in-plane bending modes [38, pp. 224–227]. Quadrilateral meshes behave somewhat better, but nevertheless produce a model which is excessively stiff if any quadrilateral's aspect ratio is too great [38, pp. 499-517]. Similarly, modeling a higher order field may require an element with more nodes. Errors arising from the mismatch of modes are termed 'locking' errors.[13] Increasing the subdivision or the number of elements does not alleviate such pathologies. A collection of overly stiff elements results only in an overly stiff system, not a more flexible model [44].

Accordingly, the behavior of a finite element approximation can be improved somewhat by increasing the element level degree of freedom. Using kinematic test functions, the degree of freedom of an element can be increased without violating the boundary requirements. In the absence of a general geometric test function method applicable to any polygon, approaches which disregard the essential boundary conditions or employ boundary element type test functions have been developed.[14]

Alternatively, a set of test functions can be constructed such that the global constraints and local boundary requirements are satisfied exactly. The triangular serendipity element, for example, is a direct consequence of

[13] Locking is the condition of grossly excessive stiffness bordering on rigidity [38, pp. 203].

[14] Many multi-node methods have been developed, a short description is given in §1.1.2. The stress based formulation was developed by T.H. Pian in 1964 [48]

the linearity and constancy requirements [13]. Imposing material requirements, such as incompressibility, result in test functions which depend on non-dimensional material parameters. A beam in bending can be described by functions which will not lock at any aspect ratio and depend on Poisson's Ratio [15].

The presented general method for geometric test function construction guarantees only that the interpolations satisfy the constancy conditions and are linear along the boundary. Additional conditions, such as the linearity requirement, are assured by defining three functions in terms of the others. The feasibility of imposing higher order requirements requires further research.

1.1.1 Modal approach

In an approximation over more than one-dimension, the order of approximation within an element is not clearly first order. In a one dimensional element a node can only be connected to its two neighbors. The resulting finite element has only two degrees of freedom, a rigid body mode and a linear strain mode. Combining a number of linear elements allows for the approximation to higher order behaviors. In a more-than-one dimensional element the connection of boundary nodes is dictated by the domain, or element, geometry. The number of eigenvalues associated with an element is a function of the number of nodes which describe it [44]. A two dimensional element, for example, can model higher order behaviors while faithfully representing

linear boundary conditions and nodal discontinuities along its boundary. Unlike the one dimensional case, combining elements with fewer nodes does not necessarily allow for the approximation of a higher order field [38].

The finite element method, based on the Rayleigh-Ritz method, is fundamentally an approach for approximating the spectrum of a linear subspace $[\mathbf{K}]$ which is most equivalent to the elliptic linear operator $\mathcal{L}[\cdot]$; the displacements $u(x, y)$ are obtained as a side effect of the approximation [56, pp. 228–231]. The spectral theory of operators suggests that every self-adjoint operator can be represented as a linear series:

$$\mathcal{L}[\vec{u}(x, y)] \approx [\mathbf{A}]^{n\times n}\{\vec{u}_n\} = \{\vec{f}_n\} \tag{1.4}$$

In the finite element method the stiffness matrices $[\mathbf{A}]$ are determined independently for each m-noded element, before being combined into a general matrix. The rigid body condition is reflected in the three zero eigenvalues related to the displacement and rotation modes. If one element fails to reproduce the condition then the entire mesh will fail to model rigid body modes [56, pp. 220–223].

If orthogonal trial functions which satisfy the boundary conditions and the governing equation exist then the construction of an m mode solution poses no difficulty. If a higher order element is characterized by the number of orthogonal eigenvectors and corresponding eigenvalues it can represent, then the degree of an element is a function of the number of nodes which define it—not the terms of the Taylor series which it can represent exactly.[15]

[15] A comparison of a modal solution and a nodal, finite element, solution is presented

In terms of modal approximation the more test functions the better the solution [56, pp. 228–231]. Orthogonal functions would result in a diagonal stiffness matrix [**A**]. Linearly independent trial functions can be applied instead. The resulting system matrix is symmetric and positive definite but not necessarily diagonal. The degree of approximation can be increased by adding another node. The location of the node is not prescribed by the modal formulation. Consequently, a node can be added in the interior of the domain —and cause a discontinuity where none is prescribed— or it can be added along the boundary. Accordingly, bounded and smooth test functions can provide an approximation to any elliptic functional and its associated boundary conditions.

The stability of the approximation can be measured according to the condition number. The condition number is a measure of the independence of the geometric test functions [57, pp. 205–215].

$$\kappa = \frac{\lambda_{\max}([\mathbf{A}])}{\lambda_{\min}([\mathbf{A}])} \tag{1.5}$$

Where the $\lambda_{\min}(\cdot)$ is the smallest eigenvalue of the matrix and $\lambda_{\max}(\cdot)$ the largest eigenvalue. For an orthonormal basis $\kappa = 1$. A system is stable if the condition number remains bounded as the number of nodes which define an element increases [46]. For a test function solution to be convergent the set of approximation functions must be complete with respect to all possible solutions. The presented geometric test functions do not necssarily

by R. H. MacNeal. According to his analysis, finite elements are limited because of their inability to remain conformal and capture higher order fields associated with a power series expansion, beyond constancy and linearity [38, pp. 500–511].

satisfy this requirement. Nevertheless, they can provide an ever more exact approximation to the behavior of a given domain with respect to an elliptic functional. Extending the formulation to include interior points, and ensure closure, is the subject of ongoing research [39].

1.1.2 Element level degree of freedom

Conventionally, the order of an element is defined by the terms of a polynomial series p which it can reproduce exactly [57]. In this respect the rectangular element is higher order than the triangular since it can reproduce the xy term. Accordingly, the degree of the formulation is often related to the kinematic degrees of freedom of an element [67, pp. 228–230]. Common p element formulations are the Lagrange and Serendipity elements. The number of nodes, and order of polynomial approximation, is increased by adding mid-side nodes and changing the linear boundary interpolation into a quadratic or higher order interpolation [38, pp. 76–80]. Consequently, the boundary behavior is forced to be smooth and any gradient dislocations are removed [30, pp. 395–396]. In general, Lagrange and Serendipity elements with nodal points located only on the boundary, do not exactly reproduce constant and linear fields.

The simplest two dimensional Lagrange elements are constructed by multiplying two one dimensional Lagrange interpolations, see figure 1.5. More complicated domains can also be described [35]. Different geometries are constructed by isoparametric transformation [30]. Even some curved boundaries

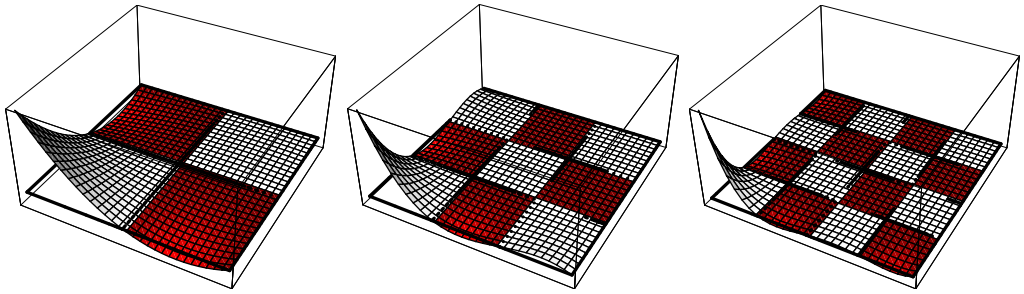


Figure 1.5: Lagrange elements with one, two and three side nodes.

can be accommodated [67]. The introduction of a computational coordinate system and a method for numerical integration by Gauss points allows for efficient procedural algorithms [30, pp. 396–406].

Unfortunately, the Lagrange Interpolation does not necessarily exhibit uniform convergence. In the approximation of functions with large gradients or discontinuities, increasing the number of nodes does not increase the degree of approximation; eventually round-off error overtakes the result entirely, see figures 1.6 and 1.7.[16] Oscillatory errors and inconsistent representations are common [38, 50].

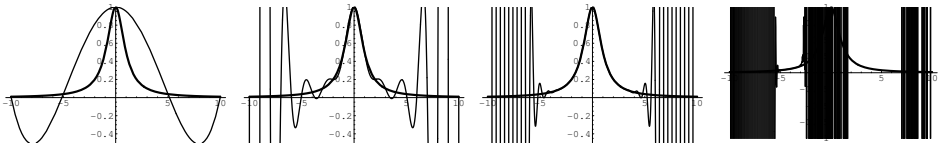


Figure 1.6: Lagrange approximation to the Runge function $\frac{1}{x^2+1}$ using equally spaced nodes.

[16]Convergence of a monotonically increasing power series is not assured. Alternatively a set of piecewise continuous lines are uniformly convergent [20].

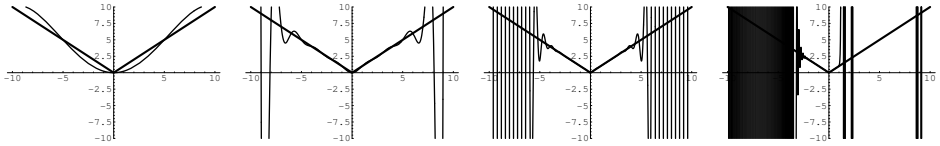


Figure 1.7: Lagrange approximation to $|x|$ using equally spaced nodes.

Methods other than Lagrange interpolation, for increasing element level degree of freedom have also been applied in finite element approximations. S. A. Coons developed an interpolation formula for arbitrarily shaped CAD (Computer Aided Drafting) patches. There is more flexibility in constructing the interpolator than is possible for a Lagrange element, and the resulting function is more bounded [53, pp. 422–425]. These global interpolations have been applied extensively in computer graphics applications and recently to axisymmetric problems. Nevertheless, the Coon's functions have similar drawbacks as p method constructions. They do not allow discontinuity at the boundary and they are not strictly bounded between the nodal values.[17]

Other graphics based algorithms, such as b-spline interpolation and NURBS have also been applied to finite element analysis [51]. Each suffers from the same pathologies as the Lagrange, and Coons element formulations. The kinematic constraints of the problem, the rigid boundary conditions, and the constancy and linearity requirements need to be satisfied within the displacement type element formulation if it is to converge efficiently and predictably

[17]Nonetheless the global method constructed from the interpolation produced a better result than the mesh based finite element method in a shorter time than the boundary element method for the same number of nodal points [51].

[57, 30, 59].

Motivated in part by these failures, a number of approaches designed to avoid increasing the kinematic degrees of freedom at the element level have been developed. Most can be shown to be variations of mixed field formulations [50, pp. 401]. If displacement and stress, for example, are considered to be separate fields then the governing variational formulation can be constructed to minimize the mismatch [3]. In general, multi-field methods are employed when the displacement field alone cannot adequately capture the behavior of the domain [10]. The efficiency of multi-field variational methods is a function of a heuristic choice of a Lagrange multiplier and quantifiable by the 'inf-sup' condition.[18]

One popular method is the reduced integration technique. When applied accurately, it weights the known values at the boundary more heavily than the points derived by interpolation. Consequently the integrated model may describe the physical behavior more closely than the original shape function. By construction, reduced integration minimizes the influence of higher order behaviors, of Lagrange elements with side nodes. In effect, the oscillatory boundary behavior is replaced by a piecewise constant or piecewise linear approximation [67, pp. 357]. The method of choosing which points to include in the integration, and which to ignore, can be described using a multi-field variational representation [50]. The method of reduced or under-integration

[18]The test is attributed to Ladysvenskaya, Babuška and Brezzi, a detailed description is available in the reference [47]. The condition can not always be evaluated analytically, some numerical approximations exist [4].

does not necessarily provide a stable or convergent approximation. Spurious mechanisms and modes often result [38, pp. 261–316].

The only available large-element construction which accommodates linear sides and discontinuity at the nodes is based on a rational polynomial formulation.[19] Wachspress developed a method for shape function construction which is applicable to any convex polygon. The approach is based on projective geometry. The resulting interpolations necessarily satisfy the rigid body conditions, boundedness and linear boundary behavior. The resulting test functions are equivalent to Padé expansions [61]. The representation captures characteristics of higher order fields behavior without sacrificing the lower order requirements. Extensions to the rational polynomial formulation on a convex element have been constructed, including three dimensional analogs and higher order boundary behavior [62, 35, 25].

1.2 Review of linear edged geometric test function formulations

Even for a first order representation, it is useful to model any known characteristics of the exact solution as closely as possible.[20] The domain dependent

[19] In this context, a large-element is defined as a displacement based element with more than four nodes. The term large-element formulation has been applied to the description of the displacement based Coons' element and to Trefftz type boundary elements [51, 31].

[20] For a first order representation the first two terms of the power series expansion of a smooth function (constant and linear terms) are reproduced exactly by the approximation [23, p.16]

Green's function solution to an elliptic operator is necessarily bounded. Accordingly, the test functions should be similarly bounded. Given a domain $\mathcal{D}$ described by n boundary nodes and n function values f^i given at each node-i.

$$\min_{i\in(1,n)}(f^i) \leq \hat{f}(x,y) \leq \max_{i\in(1,n)}(f^i) \quad \forall\ \{x,y\} \in \mathcal{D} \tag{1.6}$$

Where $\hat{f}(x,y)$ is the test function. The enforcement of this restriction—the Chebyshev condition—is especially necessary when bounded values, such as temperature in Kelvin, are being distributed.

The goal then is to construct an element with the required number of degrees of freedom to model higher order behaviors without corrupting the lower order variational requirements. The $\mathtt{C}^0$ version of such an element formulation would be require inter-element continuity and the faithful reproduction of constant and linear fields.

$$\sum_{i=1}^{n}\phi_i(x,y) = 1 \quad \sum_{i=1}^{n}x_i\,\phi_i(x,y) = x \quad \text{and} \quad \sum_{i=1}^{n}y_i\,\phi_i(x,y) = y \tag{1.7}$$

Where, the $\phi_i(x,y)$ are the geometric trial functions in global cartesian $\{x,y\}$ coordinates and the nodal points which define the n-sided polygon are located at the points $\{x_i,y_i\}$ where i ranges from 1 to n.

1.2.1 An interpolation which is both bounded and linear exists for every polygonal domain

A geometric test function method which satisfies the variational requirements and is smooth within the given domain requires a smooth linear interpolation.

An interpolation within a polygonal domain need not be restricted in number of nodes or domain convexity. Solutions to linear second order elliptic operators for linear boundary conditions are valid bounded, linear interpolation functions. Evaluation of elliptic functions on polygonal domains, even concave, is a well-posed problem with an analytic solution. Conformal mapping on polygonal domains can be performed equally well if the polygon is concave or convex using Schwartz-Christoffel Mapping (see §3). Temperature distributions over homogeneous materials and two dimensional irrotational fluid flow provide experimental evidence of smooth solutions.

A steady state heat distribution within a rectangular domain can be modeled using Laplace's equation, letting the boundary conditions be linear, following the example in the reference [26, pp. 67–72]:

$$\begin{aligned} \text{Elliptic equation :} \quad & \nabla^2 u(x,y) = \frac{\partial^2 u}{\partial x^2} + \frac{\partial^2 u}{\partial y^2} = 0 \\ \text{Boundary conditions :} \quad & u(0,y) = y\frac{u_4}{H} + u_1,\ u(L,y) = y\frac{u_3}{H} + u_2, \\ & u(x,0) = x\frac{u_2}{L} + u_1,\ u(x,H) = x\frac{u_3}{L} + u_4 \end{aligned} \tag{1.8}$$

The solution in terms of an eigenfunction expansion is:

$$\begin{aligned} u(x,y) &= \sum_{n=1}^{\infty} A_n \sin\frac{n\pi y}{H} \sinh\frac{n\pi}{H}(x-L) + (\text{three similar terms}) \\ \text{where} \quad A_n &= \frac{2}{H\sinh\left(n\pi\frac{(-L)}{H}\right)} \int_0^H \left(y\frac{u_4}{H} + u_1\right) \sin\frac{n\pi y}{H} \mathrm{d}y \end{aligned} \tag{1.9}$$

or

$$u(x,y) = \begin{array}{ccccc} u_1\left(1-\frac{x}{L}\right)\left(1-\frac{y}{H}\right) & + & u_2\left(\frac{x}{L}\right)\left(1-\frac{y}{H}\right) \\ + & u_3\left(\frac{x}{L}\right)\left(\frac{y}{H}\right) & + & u_4\left(1-\frac{x}{L}\right)\left(\frac{y}{H}\right) \end{array}. \tag{1.10}$$

The solution, equation 1.10, is equivalent to the standard first order interpolation function within a rectangle. The eigenfunction solution is also valid, although more time consuming to evaluate, equation 1.9. Using complex variable theory and conformal mapping, many solutions can be constructed to Laplace's equation for simple boundary conditions. For example, two dimensional fluid flow around corners, through rectangular slots and around air foils can be computed for an ideal flow [58, pp.105, 145, 120].

If a test function satisfies a elliptic operation and linear boundary conditions the remaining requirements of boundedness, smoothness and integrability are satisfied automatically [24, pp. 31–35]. The solution can be mapped to any polygonal domain. Consequently a first order interpolation should be constructible on any linearly bounded domain, even one containing concavities, see appendix B.2. The solution is unique for the elliptic function and the given boundary conditions [14].

The ellipticity of an operator $\mathcal{L}(\cdot)$ of order m over N variables depends on its principle portion $\mathcal{L}_p(\cdot)$.

$$\mathcal{L}(\cdot) = \sum_{|k|\leq m} a_k(\vec{x})D^k(\cdot) \quad \text{and} \quad \mathcal{L}_p(\cdot) = \sum_{|k|=m} a_k(\vec{x})D^k(\cdot) \tag{1.11}$$

Where D is a generalized differential operator. For a second order elliptic operator in cartesian $\{x, y\}$ coordinates, the principle part is of the form

$$a\frac{\partial^2(\cdot)}{\partial x^2} + c\frac{\partial^2(\cdot)}{\partial x \partial y} + b\frac{\partial^2(\cdot)}{\partial y^2} \tag{1.12}$$

where a,b, and c can also be functions of x and y. The operator is elliptic if the coefficients form a positive definite matrix:

$$\{ \tfrac{\partial}{\partial x} \quad \tfrac{\partial}{\partial y} \} \begin{pmatrix} a & \frac{c}{2} \\ \frac{c}{2} & b \end{pmatrix} \begin{Bmatrix} \frac{\partial}{\partial x} \\ \frac{\partial}{\partial y} \end{Bmatrix} \quad \text{where} \quad 4(ab) - c > 0. \tag{1.13}$$

A set of n trial functions ϕ_i which satisfy the same linear elliptic operator $\mathcal{L}$, for each of the boundary conditions, should also satisfy the linearity requirements.

$$\mathcal{L}[\phi_i] = 0 \quad i = 1, 2, \ldots, n \tag{1.14}$$

If the operator is linear:

$$\mathcal{L}\left[\sum_{i=1}^{n} \phi_i\right] = 0. \tag{1.15}$$

The solution to an elliptic operator is necessarily maximum or minimum only along the boundary. For the constant boundary condition the only solution which satisfies the maxima requirements is the constancy condition $\sum_{i=1}^{n} \phi_i = 1$. Similarly, given the nodal positions $\{x_i, y_i\}$ the solution to the linear combination of operators:

$$\mathcal{L}\left[\sum_{i=1}^{n} x_i \phi_i\right] = 0 \quad \text{and} \quad \mathcal{L}\left[\sum_{i=1}^{n} y_i \phi_i\right] = 0 \tag{1.16}$$

leads to the linear solutions $\sum_{i=1}^{n} x_i \phi_i = x$ and $\sum_{i=1}^{n} y_i \phi_i = y$. The constancy and linearity requirements are satisfied at every point in the domain, including the boundary.

Consequently, the solution which satisfies the same elliptic operator for all shape functions, also satisfies the first order interpolation requirements.

Accordingly, all domains upon which such an operator can be evaluated for linear boundary conditions can be described, without discretization, with boundary nodal values and linear trial functions. Also, the test functions within the domain are only unique with respect to the elliptic operator they satisfy, they are not unique in general. The aim is to find the simplest function which satisfies the boundary conditions.

1.2.2 Interpolation within convex polygons

A consistent discontinuous zeroth order approximation can be constructed using a first order Voronoi diagram [6, pp. 425–428]. It applies to any configuration of nodes, concave or convex. The boundaries of the diagram define the areas of influence of each node. The constant valued test functions depend only on the domain of influence and the nodal values. The resulting elements would not be differentiable since continuity within the element is lost. Nonetheless, similar collocation methods are applied in numerical analysis of continuous problems [8, pp. 22–31].

The lowest order linear interpolation is based on Delaunay triangulation [6]. The three trial functions for any triangle can be derived directly from the three constancy and linearity requirements, according to the Courant Triangle [13].

First order interpolations which are smooth, and necessarily linear only on the boundary, can be constructed within any polygonal domain. Wachspress derived rational polynomial interpolations based on projective geometry. It

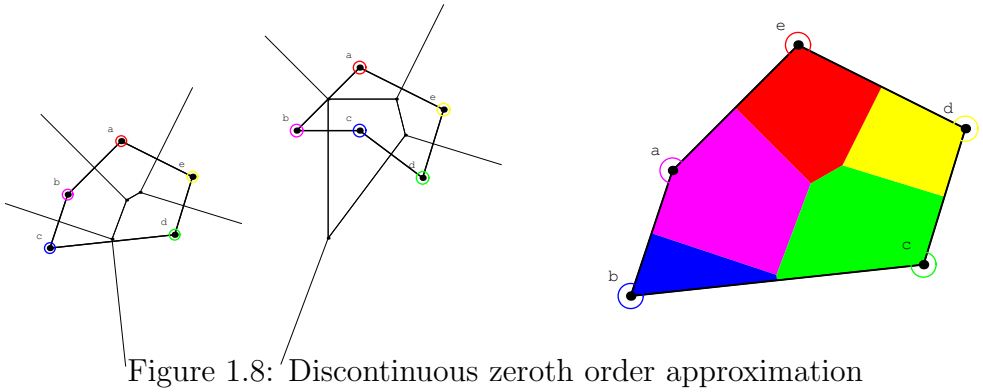


Figure 1.8: Discontinuous zeroth order approximation

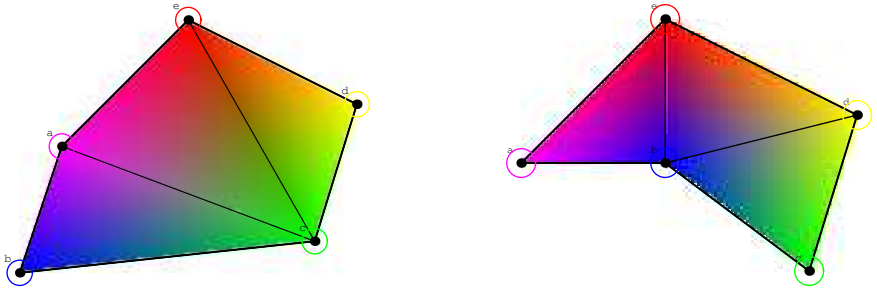


Figure 1.9: Interpolation within sub-triangles

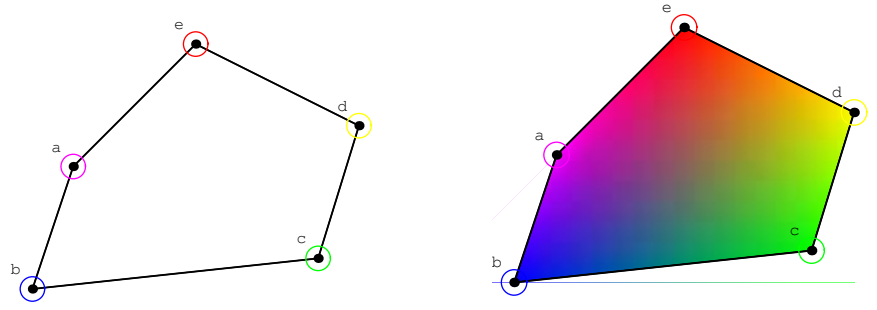


Figure 1.10: Smooth first order interpolation

applies to any convex polygon [61, pp. 52–87]. Quadrilateral domains are described in local (eg. cartesian $\{x, y\}$ coordinates) by a perspective transformation (§2.2.2). Degenerate two-dimensional elements with any number of side nodes are representable if the test functions for the elements of the same geometry without side nodes are known (§4.4.1). Even concave and multiply connected polygons can be represented consistently (§3).

Chapter 2

Global cartesian coordinates: element construction by linear transformation

The linear interpolation within a domain polygon may be derived as a transformation of a similar domain, for which a linear test function is known. Isoparametric elements are an example of a transformation based shape function [67]. The procedure is simplified further if the transition from the undeformed to the deformed shape can be described as a linear transformation. The suitability of a transformation can be calculated using to the Jacobian [30, pp. 58–64]. It need only be non-zero in the domain for the boundary transformation to be invertible [40]. The resulting representation automatically satisfies the geometric test function conditions if the perspective

transformation is valid.[1]

Discontinuities along the boundary of an element which do not propagate into the interior of the domain do not violate the linear test function requirements, see 1.2. Appropriately, the discontinuity is consistent with the application of a point force. In one dimensional problems, such as transverse loading of a string, the discontinuity is essential to the construction of the exact solution using Green's function. The boundary discontinuity poses no additional mathematical problems since the application of a point force can be considered within the tenets of the theory of distributions [56, pp. 1–58]. However, for numerical integration extra care must be taken around any points where discontinuities occur.

By representing interpolations in global coordinates, for example cartesian $\{x, y\}$, it is possible to evaluate if a boundary discontinuity adversely effects domain continuity. Accordingly, the isoparametric transformation can be constructed as a three dimensional affine transformation, and the Wachspress rational polynomial representation as a perspective transformation. Solving the inverse transformations results in polynomial and rational polynomial test functions which are smooth and satisfy the linear boundary conditions.

Additionally, irrational polynomial representations are derived for skew quadrilaterals and triangles with a side node. The discontinuity along the boundary of the triangle does not propagate into the interior or the domain.[2]

[1] A perspective transformation preserves the linearity of lines.

[2] The suggestion that a transformation is invalid if the Jacobian is zero anywhere in

Consequently, valid test functions can be constructed in $\{x, y\}$ coordinates even if the linear transformation is not invertible at a boundary point.

2.1 General construction of a quadrilateral test function for a non-concave polygon

The shape functions for quadrilaterals are a combination of interpolations between opposite lines of finite length. The simplest interpolation between values on two different lines is defined by the simplest path which connects those points, see figures 2.2, 2.3 and 2.4. The shortest path between two known points on a plane is linear. Restrictions on the interpolation lines include that they can neither exit the domain, nor overlap. In this respect interpolation path-lines are analogous to fluid flow path-lines, see figure 2.1 [65, 49, pp., pp.123–188].

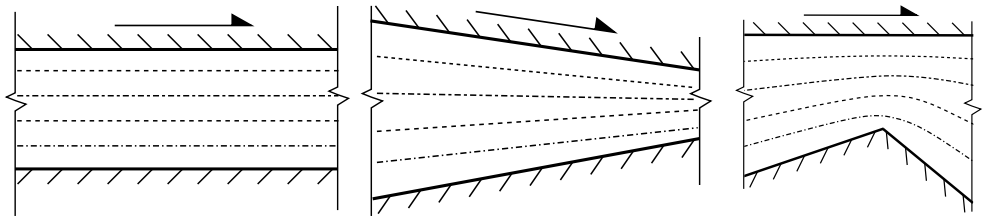


Figure 2.1: Sketches of fluid flow path lines

the domain including the boundary is too strong a requirement. Standard textbooks for finite element analysis suggest that the element with a side node can not be represented using the isoparametric transformation, despite the fact that the resulting shape function is smooth and integrable throughout the triangular domain [29, 67].

The bilinear shape function within a square exhibits linear path lines. Given a unit square with vertices at:

$$\{\{0,0\},\{1,0\},\{1,1\},\{0,1\}\} \tag{2.1}$$

the shape functions are are:

$$\begin{aligned} N_a(s,t) &= (1-s)(1-t) & N_b(s,t) &= s\,(1-t) \\ N_c(s,t) &= st & N_d(s,t) &= (1-s)\,t \end{aligned} \tag{2.2}$$

The shape functions are bounded and they can, in linear combination, reproduce constant and linear fields.

Within a unit cube the interpolation lines are linear and run parallel to the boundary. The interpolation from one edge to the other is analogous to the sum of two adjacent test functions: $N_3(s,t) + N_4(s,t)$ or simply s, according to equations 2.2. Perspective transformations of the unit cube preserve linearity; the linear interpolation paths remain linear even after perspective transformation.[3] In a concave element the interpolation path can not be linear and remain confined to the domain. This is the definition of concavity.[4] Consequently a concave element test function can not be derived from perspective transformations of a unit cube. This conclusion can be proven more rigorously using the tenants of projective geometry [28, 61].

Elements with nodal points that occur at any point other than the vertex

[3]The resulting surfaces are algebraic [54].

[4]Notions of convexity and conversely concavity were recorded by Archimedes around 300 BC, a modern reference is [6, p. 125], see also §3.

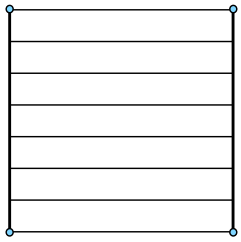


Figure 2.2: Normed square

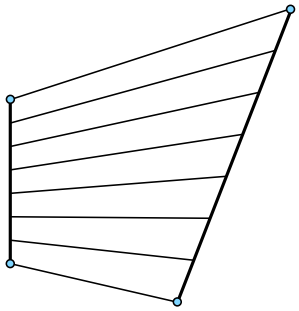


Figure 2.3: Convex element

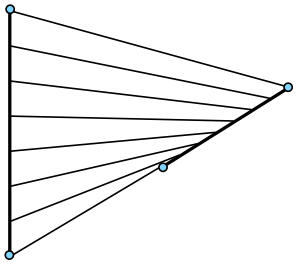


Figure 2.4: Side node

are referred to as degenerate elements. Interpolation paths within a convex element, with a node located anywhere along the boundary, are derivable from a perspective transformation since there is no impediment to the linearity of such paths. While the interpolations can not be derived from in-plane transformations (eg. cartesian coordinates $\{x, y\}$) they can be found by transformations in a third out-of-plane dimension (eg. $\{z\}$). Accordingly, the test function for a triangle with a side node can not be captured by a function in rational polynomial form. It can, nonetheless, be described using parametrized coordinates [40].

2.2 Perspective transformation

The test function within a rectangular element is bilinear.[5] Any quadrilateral shapes which are similarly described by linear internal path-lines can be constructed from the representation for the square by perspective transfor-

[5] A bilinear interpolation exhibits linear contours in both coordinate directions. More general examples can be found in the reference [53].

mation. Desargues Theorem states that if two similar triangles are situated such that their sides are parallel then the lines joining their vertices pass through the same point or are parallel [28, p. 72]. An affine transformation of a shape preserves parallel lines and is equivalent to changing the angles and positions of the similar triangles. All the lines which are parallel under affine transformation remain linear, but not parallel, under perspective transformation. Lines which pass through the vertices of the scaled similar triangles meet at a vanishing point.

The proof, and the construction of the projection, requires that the point at position $\{x, y, z\}$ be related to the line described by the ratio of four segments $(r : u : v : w)$. The following represents the condition for the common position of the point and line [28, pp. 72–73]:

$$rx + uy + vz + w = 0 \tag{2.3}$$

The general description of a point then can be formulated in terms of homogenous coordinates: $\{x, y, z, 1\}$ [53, pp. 81–83]. Accordingly a general linear transformation of a point in two dimensions is constructed.

2.2.1 Local coordinate derivation

To represent the full shape function in homogenous coordinates, and apply a general perspective transformation [**A**] (with coefficients a_{ij}):

$$\{x', y', \psi', h\} = \{s, t, \phi(s,t), 1\} \begin{Bmatrix} a_{11} & a_{12} & a_{13} & a_{14} \\ a_{21} & a_{22} & a_{23} & a_{24} \\ a_{31} & a_{32} & a_{33} & a_{34} \\ a_{41} & a_{42} & a_{43} & a_{44} \end{Bmatrix}. \tag{2.4}$$

Where:

$$\phi(s,t) = \phi_a N_1(s,t) + \phi_b N_2(s,t) + \phi_c N_3(s,t) + \phi_4 N_d(s,t). \tag{2.5}$$

The ϕ_i are constants and $N_i(s,t)$ are given by equation 2.2.

The solution then, parametrized by s and t, is

$$x = \frac{x'}{h} = \frac{a_{11}s + a_{21}t + a_{31}\phi(s,t) + a_{41}}{a_{14}s + a_{24}t + a_{34}\phi(s,t) + a_{44}} \tag{2.6}$$

$$y = \frac{y'}{h} = \frac{a_{12}s + a_{22}t + a_{32}\phi(s,t) + a_{42}}{a_{14}s + a_{24}t + a_{34}\phi(s,t) + a_{44}} \tag{2.7}$$

$$\psi = \frac{\psi'}{h} = \frac{a_{13}s + a_{23}t + a_{33}\phi(s,t) + a_{43}}{a_{14}s + a_{24}t + a_{34}\phi(s,t) + a_{44}} \tag{2.8}$$

The linearity of a line in the unit cube $\{s, t, \phi(s,t)\}$ is preserved in the local coordinates $\{x, y, \psi(x,y)\}$ [53, pp. 90-100]. Accordingly, the boundary lines which are linear in the computational frame $\phi(s,t)$ remain so for the interpolation in local coordinates $\psi(x,y)$.

To solve for the shape function in local coordinates it is simpler to solve for s, t and $s * t$ separately.[6] The solution then is parametrized by x and y. For convenience rename the the constants and describe the result in matrix form:

$$\{s,t,st\} \;=\; \{x\,b_{44}-b_{41}, y\,b_{44}-b_{42}, \psi b_{44}-b_{43}\} \begin{pmatrix} b_{11}-x\,b_{14} & b_{12}-y\,b_{14} & b_{13}-\psi b_{14} \\ b_{21}-x\,b_{24} & b_{22}-y\,b_{24} & b_{23}-\psi b_{24} \\ b_{31}-x\,b_{34} & b_{32}-y\,b_{34} & b_{33}-\psi b_{34} \end{pmatrix}^{-1} \tag{2.11}$$

[6] The solution should be in terms of the local coordinates $\{x, y\}$ not parametrized by $\{s, t\}$, equations 2.6 and 2.7. The value of the specific constants is less important than the form of the equation. The representation can be simplified by introducing new constants.

$$s = \frac{(\alpha_1 x + \alpha_2)t + (\alpha_3 x + \alpha_4)}{(\beta_1 x + \beta_2)t + (\beta_3 x + \beta_4)} \quad \text{and} \quad t = \frac{(\gamma_1 y + \gamma_2)s + (\gamma_3 y + \gamma_4)}{(\delta_1 y + \delta_2)s + (\delta_3 y + \delta_4)} \tag{2.9}$$

Solving for s and t, again introducing more convenient constants. Let $\eta_i(x,y) = \eta_{1i}x + \eta_{2i}y + \eta_{3i}xy + \eta_{4i}$, then:

$$\eta_1(x,y)s^2 + \eta_2(x,y)s + \eta_3(x,y) = \eta_4(x,y)t^2 + \eta_5(x,y)t + \eta_6(x,y) = 0 \tag{2.10}$$

Substituting these results into equation 2.8, again only the form of the equation is important. Solving in terms of x and y, $\psi(x,y)$:

$$\frac{\begin{array}{l} \mathtt{C}_1\left(\frac{-\eta_2(x,y)\pm\sqrt{\eta_2^2(x,y)-4\eta_1(x,y)\eta_3(x,y)}}{2\eta_1(x,y)}\right) + \mathtt{C}_3\left(\frac{-\eta_5(x,y)\pm\sqrt{\eta_5^2(x,y)-4\eta_4(x,y)\eta_6(x,y))}}{2\eta_4(x,y)}\right) + \\ \mathtt{C}_5\left(\frac{-\eta_2(x,y)\pm\sqrt{\eta_2^2(x,y)-4\eta_1(x,y)\eta_3(x,y)}}{2\eta_1(x,y)}\right)\left(\frac{-\eta_5(x,y\pm\sqrt{\eta_5^2(x,y)-4\eta_4(x,y)\eta_6(x,y))}}{2\eta_4(x,y)}\right) + \mathtt{C}_7 \end{array}}{\begin{array}{l} \mathtt{C}_2\left(\frac{-\eta_2(x,y)\pm\sqrt{\eta_2^2(x,y)-4\eta_1(x,y)\eta_3(x,y)}}{2\eta_1(x,y)}\right)\mathtt{C}_4\left(\frac{-\eta_5(x,y)\pm\sqrt{\eta_5^2(x,y)-4\eta_4(x,y)\eta_6(x,y))}}{2\eta_4(x,y)}\right) + \\ \mathtt{C}_6\left(\frac{-\eta_2(x,y)\pm\sqrt{\eta_2^2(x,y)-4\eta_1(x,y)\eta_3(x,y)}}{2\eta_1(x,y)}\right)\left(\frac{-\eta_8(x,y)\pm\sqrt{\eta_5^2(x,y)-4\eta_4(x,y)\eta_6(x,y))}}{2\eta_4(x,y)}\right) + \mathtt{C}_8 \end{array}}$$

This equation is not in standard form.

To represent the solution in standard form substitute the values for s, t and st:

$$s \cdot t - st = 0 \tag{2.12}$$

After rearranging and renaming the constants the numerator must be zero for the equality, equation 2.12, to be true. The final simplified representation is:

$$\begin{aligned} 0 = \; & \alpha\,\psi^2 + (\beta_1\,x + \beta_2\,y + \beta_3)\psi \\ & +(\gamma_1\,x^2 + \gamma_2\,y^2 + \gamma_3\,xy + \gamma_4\,x + \gamma_5\,y + \gamma_6) \end{aligned} \tag{2.13}$$

The general perspective transformation of a unit square is quadratic in terms of the shape function ψ. α, β_i and γ_i are the constants of polynomials in x and y. If α is zero the transformation results in a rational polynomial. The eight independent constants are determined uniquely by the location of the eight nodes which outline a quadrilateral. Any equation which satisfies the form of equation 2.13 is a perspective transformation. Both the isoparametric and rational polynomial forms can be described using equation 2.13.[7]

2.2.2 Transformed unit square

The interpolation within a quadrilateral shape is not unique within skew quadrilaterals. Both the projective geometry formulation and the isopara-

[7]Examples are included in a journal paper [40].

metric formulation can be derived from perspective transformations performed on a unit cube. Given a unit square with the following nodal points:

$$\{\{0,0\},\{1,0\},\{1,1\},\{0,1\}\} \tag{2.14}$$

at point $\{\xi,\eta\}$ the value of the shape function for node $\{1,1\}$ is $\xi\,\eta$. The parametrized coordinates can be written in this form, following from equation 4.8:

$$\begin{aligned}\langle x,y\rangle &= \xi\,\eta\{x_a-x_b+x_c-x_d, y_a-y_b+y_c-y_d\} \\ &\quad +\xi\{x_b-x_a, y_b-y_a\}+\eta\{x_d-x_a, y_d-y_a\}+\{x_a,y_a\}\end{aligned} \tag{2.15}$$

$$\begin{aligned}\langle x,y,\phi_c,1\rangle &= \\ &\langle\xi,\eta,\xi\eta,1\rangle\begin{pmatrix} x_b-x_a & y_b-y_a & 0 & 0\\ x_d-x_a & y_d-y_a & 0 & 0\\ x_a-x_b+x_c-x_d & y_a-y_b+y_c-y_d & 1 & 0\\ x_a & y_a & 0 & 1\end{pmatrix} \\ &= \langle\xi,\eta,\xi\eta,1\rangle\,[\mathbf{A}]\end{aligned} \tag{2.16}$$

The result is equivalent to the transformation of a unit square into a quadrilateral (a,b,c,d) according to the following calculation (note: $h=1$ see equation 2.4):

$$[\mathbf{A}] = \begin{pmatrix}0&0&0&1\\1&0&0&1\\1&1&1&1\\0&1&0&1\end{pmatrix}^{-1}\cdot\begin{pmatrix}x_a&y_a&0&1\\x_b&y_b&0&1\\x_c&y_c&1&1\\x_d&y_d&0&1\end{pmatrix} \tag{2.17}$$

The transformation is affine.

Similarly, the projective geometry representation can be derived by setting a different set of constants to zero. The result is equivalent to that from the Wachspress formulation see equation B.27:

$$
\begin{aligned}
&\langle x^*, y^*, \phi_a^*, h\rangle \quad = \\
&\langle \xi, \eta, \eta\xi, 1\rangle \cdot \\
&\begin{pmatrix}
x_b\triangle(d,a,c) - x_a\triangle(b,c,d) & y_b\triangle(d,a,c) - y_a\triangle(b,c,d) & 0 & \triangle(d,a,c) - \triangle(b,c,d) \\
x_d\triangle(a,b,c) - x_a\triangle(b,c,d) & y_d\triangle(a,b,c) - y_a\triangle(b,c,d) & 0 & \triangle(a,b,c) - \triangle(b,c,d) \\
0 & 0 & 1 & 0 \\
x_a\triangle(b,c,d) & y_a\triangle(b,c,d) & 0 & \triangle(b,c,d)
\end{pmatrix} \\
&\qquad = \quad \langle \xi, \eta, \eta\xi, 1\rangle \begin{pmatrix}
a_{11} & a_{12} & 0 & a_{13} \\
a_{21} & a_{22} & 0 & a_{23} \\
0 & 0 & 1 & 0 \\
a_{31} & a_{32} & 0 & a_{33}
\end{pmatrix} \\
&\text{where :} \qquad x = \frac{x^*}{h}, \quad y = \frac{y^*}{h}, \quad \text{and} \quad \phi_a = \frac{\phi_a^*}{h}.
\end{aligned}
\tag{2.18}
$$

If the quadrilateral is a parallelogram then the transformations are equivalent.

2.2.3 Jacobian of the perspective transformation

Interpolations within any convex quadrilateral can be derived by planar perspective transformation of any other convex quadrilateral. Integration can be performed in convenient coordinates and transformed to the global coordinates. The method is the same as for isoparametric transformation. The

validity of the transformation is tested using the Jacobian [30]. Given a set of shape functions on a unit square, see equation 2.2. If the transformation from $\{s,t\}$ to $\{x,y\}$ coordinates is a perspective transformation in the $\{x,y\}$ plane then:

$$\langle x^*, y^*, h\rangle = \langle s,t,1\rangle \begin{pmatrix} a_{11} & a_{12} & a_{13} \\ a_{21} & a_{22} & a_{23} \\ a_{31} & a_{32} & a_{33} \end{pmatrix} = \langle s,t,1\rangle \,[\mathbf{A}] \tag{2.19}$$

Where the constants a_{ij} are defined in equation 2.18, then:

$$x = \frac{x^*}{h} = \frac{a_{11}s + a_{21}t + a_{31}}{a_{13}s + a_{23}t + a_{33}} \quad \text{and} \quad y = \frac{y^*}{h} = \frac{a_{12}s + a_{22}t + a_{32}}{a_{13}s + a_{23}t + a_{33}} \tag{2.20}$$

solving for the parameters s and t,

$$s = \begin{vmatrix} x & y & 1 \\ a_{21} & a_{22} & a_{23} \\ a_{31} & a_{32} & a_{33} \end{vmatrix} \Big/ \begin{vmatrix} x & y & 1 \\ a_{11} & a_{12} & a_{13} \\ a_{21} & a_{22} & a_{23} \end{vmatrix} \tag{2.21}$$

and

$$t = \begin{vmatrix} x & y & 1 \\ a_{31} & a_{32} & a_{33} \\ a_{11} & a_{12} & a_{13} \end{vmatrix} \Big/ \begin{vmatrix} x & y & 1 \\ a_{11} & a_{12} & a_{13} \\ a_{21} & a_{22} & a_{23} \end{vmatrix}. \tag{2.22}$$

The transformation of the infinitesimal area becomes:

$$\mathrm{d}x\mathrm{d}y \;=\; \frac{|\mathbf{A}|}{(a_{13}s + a_{23}t + a_{33})^3}\mathrm{d}s\mathrm{d}t = |J(s,t)|\mathrm{d}s\mathrm{d}t \tag{2.23}$$

Using these relations the integration can be performed in the normed coordinates. Notice that the Jacobian is a function of $\{s,t\}$ (or $\{x,y\}$) and the solution requires the integration of a simple rational polynomial even in the normed coordinates. A function $f(x,y)$ defined on a convex quadrilateral domain can be integrated in normed coordinates if the perspective transformation is known.

$$\int\int f(x,y)\mathrm{d}x\mathrm{d}y = \int_0^1\int_0^1 f(s,t)|J(s,t)|\mathrm{d}s\mathrm{d}t \tag{2.24}$$

The functions defined in the normed domain $\phi(s,t)$ must also be transformed. The weightings are functions of the perspective vanishing points. For example:

$$s\,t \;\;\rightarrow\;\; \frac{a_{13}+a_{23}+a_{33}}{a_{13}s+a_{23}t+a_{33}}s\,t, \quad \text{in general} \quad \phi(s,t)\rightarrow\frac{\phi(s,t)}{c_1s+c_2t+c_3}. \tag{2.25}$$

Accordingly the rational polynomial formulation is valid everywhere except where the denominator is zero. According to the tenants of projective geometry, the singular portion necessarily lies outside the convex domain [61].

2.2.4 General integration in cartesian coordinates

In general, integration within any polygon can be performed without a coordinate transformation. Instead the divergence therorem is applied as follows:

$$\int_{\lceil} f(x,y)\mathrm{d}x\mathrm{d}y = \int_\Gamma \vec{\phi}\cdot\hat{n}\mathrm{d}\Gamma \tag{2.26}$$

Where:

$$\vec{\phi} = \phi_1 \hat{i} + \phi_2 \hat{j} \quad \text{and} \quad \hat{n} = n_1 \hat{i} + n_2 \hat{j} \tag{2.27}$$

Let:

$$\phi_1(x, y) = \int f(x, y) \mathrm{d}x \quad \text{and} \quad \phi_2(x, y) = 0 \tag{2.28}$$

Along the boundary Γ the polygon is linear. Let each section be parametrized by t:

$$x = x_i + t(x_j - x_i) \quad \text{and} \quad y = y_i + t(y_j - y_i) \tag{2.29}$$

Since ϕ_2 is zero, only the component of $\hat{n}$ in the x direction n_1 contributes to the solution. Finally:

$$\int_{\mathcal{D}} f(x, y) \mathrm{d}x\mathrm{d}y = \sum_{i=1}^{n} \int_0^1 (y_{i+1} - y_i) \phi_1(x_i + t(x_{i+1} - x_i), y_i + t(y_{i+1} - y_i)) \mathrm{d}t \tag{2.30}$$

The proposed rational and irrational shape functions are analytically integrable. The integration along the boundary segments can be performed numerically [16].

2.3 Testing applicability of a transformation by deriving the elliptic field equation

The shape function $\phi(x, y)$ for a triangle is linear since three points uniquely define a planar surface. This necessarily satisfies all second order elliptic

equations following the maximum principle. The shape function within a rectangle satisfies Laplace's equation (Taig's quadrilateral):

$$\frac{\partial^2\phi(x,y)}{\partial x^2}+\frac{\partial^2\phi(x,y)}{\partial y^2}=0 \quad \text{where } \{x,y\} \text{ are cartesian coordinates.} \tag{2.31}$$

Similarly, Laplace's equation is satisfied with respect to the normed coordinates $\{s,t\}$.

If $\{s,t\}$ are functions of $\{x,y\}$ then the elliptic function which is satisfied in cartesian coordinates can be found by chain rule. The second order equation becomes:

$$\begin{Bmatrix} \frac{\partial^2\cdot}{\partial s^2} \\ \frac{\partial^2\cdot}{\partial t^2} \end{Bmatrix} = \begin{bmatrix} \frac{\partial^2 x}{\partial s^2} & \frac{\partial^2 y}{\partial s^2} \\ \frac{\partial^2 x}{\partial t^2} & \frac{\partial^2 y}{\partial t^2} \end{bmatrix} \begin{Bmatrix} \frac{\partial\cdot}{\partial x} \\ \frac{\partial\cdot}{\partial y} \end{Bmatrix} + \begin{vmatrix} \frac{\partial x}{\partial t} & -\frac{\partial x}{\partial s} \\ \frac{\partial y}{\partial s} & \frac{\partial y}{\partial t} \end{vmatrix} \begin{Bmatrix} \frac{\partial^2\cdot}{\partial x\partial y} \\ \frac{\partial^2\cdot}{\partial x\partial y} \end{Bmatrix} + \begin{bmatrix} \left(\frac{\partial x}{\partial s}\right)^2 & \left(\frac{\partial y}{\partial s}\right)^2 \\ \left(\frac{\partial x}{\partial t}\right)^2 & \left(\frac{\partial y}{\partial t}\right)^2 \end{bmatrix} \begin{Bmatrix} \frac{\partial^2\cdot}{\partial x^2} \\ \frac{\partial^2\cdot}{\partial y^2} \end{Bmatrix} \tag{2.32}$$

Following the definition of an elliptic operator (see reference [24, pg.1]); equation 2.32 is elliptic in $\{x,y\}$ if:

$$0 < \left(\frac{\partial x}{\partial t}\frac{\partial y}{\partial s}-\frac{\partial x}{\partial s}\frac{\partial y}{\partial t}\right)^2 \quad \text{or} \quad \det\begin{vmatrix} \frac{\partial x}{\partial s} & \frac{\partial y}{\partial s} \\ \frac{\partial x}{\partial t} & \frac{\partial y}{\partial t} \end{vmatrix} = |J| \neq 0 \tag{2.33}$$

For a real valued transformation throughout the domain: $\left\{\frac{\partial x}{\partial s}, \frac{\partial x}{\partial t}, \frac{\partial y}{\partial s}, \frac{\partial y}{\partial t}\right\} \in \Re$. The transformation must exist at every point. The condition that the Jacobian be non-zero is also a coordinate transformation requirement. In mechanical terms it is related to the conservation of mass:

$$\rho_0 V_o = \rho V \quad \text{and} \quad V = |J| V_o \tag{2.34}$$

if the Jacobian were zero the initial mass, with density ρ_0, would be destroyed by the transformation. This condition similarity applies to conformal mapping. Consequently, if a first order interpolation is constructed on

a representative geometry then an interpolation resulting from a compliant transformation of that geometry also satisfies the boundedness requirements.

According to the general shape function derivations and the perspective transformations the form of the simplest interpolation function need not be limited to the polynomial form even within the normed coordinate system $\{s,t\}$. Within a convex quadrilateral, if the shape function is a rational polynomial Laplace's equation is not automatically satisfied. An elliptic function can be derived as a coordinate transformation from $\{s,t\}$ to $\{x,y\}$ coordinates using equation 2.21.

2.3.1 Non-uniqueness of a smooth linear interpolation

Transformation from the normed coordinates s and t can be found according to the chain rule, see equation 2.32. Within a skew quadrilateral (no parallel sides) two different shape functions which satisfy constancy and linearity conditions while remaining bounded in the domain can be derived in terms of two different field equations. For example, given nodes located at points $\{\{0,0\},\{1,0\},\{2,2\},\{0,1\}\}$ the elliptic functions can be derived as a coordinate transformation from Laplace's equation according to equation 2.32:

$$\begin{aligned}\mathcal{L}_{\text{iso}}(\cdot) \;\rightarrow\; & \left(1+(x-y)^2+2\,y\right)\frac{\partial^2\cdot}{\partial x^2} \\ & +2\,\left(x+x^2+y-2\,x\,y+y^2\right)\frac{\partial^2\cdot}{\partial x\partial y} \\ & +\left((1+x)^2-2\,x\,y+y^2\right)\frac{\partial^2\cdot}{\partial y^2}\end{aligned}$$

$$\begin{aligned}\mathcal{L}_{\mathrm{rat}}(\cdot) \;\rightarrow\; & (2+x\;(2+x))\,\frac{\partial^2\cdot}{\partial x^2} + 2\;(x+y+x\,y)\;\frac{\partial^2\cdot}{\partial x\partial y} \\ & +(2+y\;(2+y))\;\frac{\partial^2\cdot}{\partial y^2} \\ & +2\;(1+x)\;\frac{\partial\cdot}{\partial x} + 2\;(1+y)\,\frac{\partial\cdot}{\partial y} \end{aligned} \tag{2.35}$$

Both operators are elliptic. Consequently both representations are smooth and bounded within the domain. Accordingly either representation can be used as a kinematic test function to approximate the behavior of the domain with respect to any other elliptic operator [46, pp. 237–238].

Chapter 3

Approximating concavity: describing the singularity associated with a reentrant corner

The shape functions for a concave quadrilateral can not be derived in terms of a perspective transformation of another shape. A more general method for finding interpolations is required. The classical finite element references and summary volumes make no reference of a kinematic concave element [67, 32]. Nor is there any concave element available in commercial finite element packages [64, 34]. Conventionally, a concave domain is approximated

using separate convex elements.[1] The divided domain is neither smooth nor bounded. Instead, a linear interpolation can be constructed as the solution to a specific field equation, without violating the ellipticity requirements. Unlike for the convex domain the approximate shape function is not necessarily of lowest order; the path-lines of the interpolation can not be linear, see §2.2. The solution to any linear second order elliptic boundary value problem would satisfy the linear and constancy requirements exactly, see §1.2.1. For a four noded element only one solution need be derived explicitly, see appendix B.3.

3.1 Available methods for concave element construction

Using finite element meshes composed of triangular and convex quadrilateral elements, the analysis of a physical body whose behavior is governed by a concavity requires either a meshing of the domain using very small elements or special elements which exhibit singular behavior around the reentrant corner. For fracture mechanics applications, singular elements have been constructed such that the stress field exhibits a $\frac{1}{\sqrt{r}}$ singularity at the reentrant vertex [27]. The order of the singularity is chosen according to the behavior of an linearly elastic isotropic material. The singularity, derived from kinetic conditions, does not apply to fully plastic, non-hardening material for which

[1] A concave domain can be tesselated into non-concave sub domains [11]. Efficient domain decomposition algorithms can be constructed using the tenants of Computational Geometry [21, pp. 45–61].

a $1/r$ stress singularity is more appropriate. Energy methods, such as the J integral method, can be formulated to avoid the singularity entirely. Such methods are dependent on the material properties of the domain.[2]

Alternatively, if the solution to the field equation is known, the peak in the gradient field at the reentrant corner can be derived exactly and the boundary element method can be used to describe the behavior of the domain.[3] The method is applicable to convex and concave domains. The direct boundary integral method, for example, can be used to solve unknown boundary displacements or stresses directly in terms of specified boundary conditions.

3.1.1 Conformal mapping

A field equation independent concave element can be constructed from the solution to a specific elliptic field equation if the boundary conditions are sufficiently described. Many methods for approximating the kinematic impact of the geometry of the domain are constructed as solutions to elliptic functions [66]. For a concave quadrilateral only one test function need be derived numerically, the remaining three test functions can be calculated simply from the first, see appendix B.3. An exact, but impractical, solution can be derived using conformal mapping.

A closed form solution could be found using the Schwartz-Christoffel

[2]Various methods are described in a general fracture reference [2, pp. 595–598, 101–116, 586 & 577–591]

[3]The application of the boundary element method to fracture mechanics is outlined [2, pp. 569–571]. Alternatively, combined boundary and finite element methods or mesh-less methods have been employed [5, 52]

Transformation. Using this transformation any polygon can be transformed into a semi-infinite domain, see figure 3.1.

$$\Omega = \mathcal{M} \int_0^t \frac{\mathrm{d}t}{(t-a_1)^{\frac{\alpha}{\pi}}(t-a_2)^{\frac{\beta}{\pi}}(t-a_3)^{\frac{\gamma}{\pi}}\ldots} + \mathcal{N} \tag{3.1}$$

Three of the $n+2$ constants, usually not $\mathcal{M}$ or $\mathcal{N}$, are chosen arbitrarily. $n-1$ of the n image points a_i, located on the linear boundary of a semi-infinte domain, are determined according to the location of the vertices of the polygon. $\alpha, \beta, \gamma \ldots$ are the angles, in the positive direction, from one line

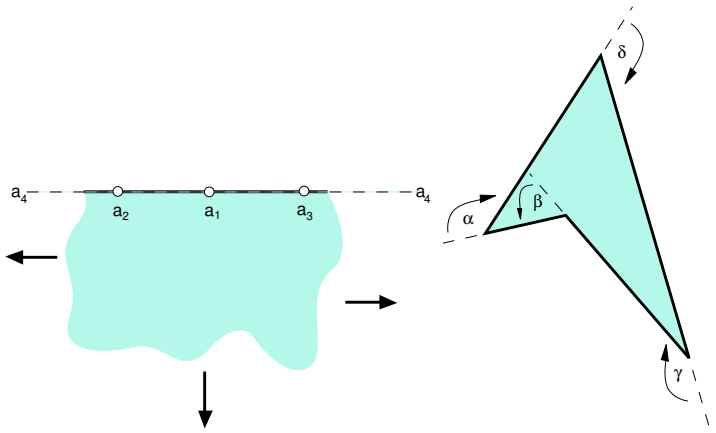


Figure 3.1: Semi-infinite → polygonal

of the polygon to the next. If the polygon is closed:

$$\alpha + \beta + \gamma + \delta + \cdots = 2\pi. \tag{3.2}$$

Also, if any of the vertices (k) are located at infinity the factor $(t-k)^{\frac{\kappa}{\pi}}$ is set to one, i.e. dropped from the equation. For the sum (equation 3.2) to be accurate the angles must be selected from a 2π range, it is convenient

to choose the range $-\pi$ to π. Within the range the concave nodes have negative angles. Consequently, if the angle (e.g. μ) is negative then the point u in $(t-u)^{\frac{\mu}{\pi}}$ does not exhibit singular behavior, this is convenient for the numerical computation. Still, the peak in gradient associated with the concavity is not lost. The solution to Poisson's equation in a concave domain at the re-entrant corner is a function of geometry, the singularity of the derivative is proportional to $r^{\frac{\pi}{b}-1}$ where b is the interior obtuse angle $\pi < b < 2\pi$. The degree of singularity $\alpha = \frac{\pi}{b} - 1$ ranges from zero to negative one half. The variable singularity encountered with respect to Poisson's distribution has been observed experimentally in problems of heat conduction, potential flow and transverse electromagnetic lines [1, pp. 280–285].

3.1.2 Application to the concave quadrilateral

For any four noded quadrilateral $\{\{x_1, y_1\}, \{x_2, y_2\}, \{x_3, y_3\}, \{x_4, y_4\}\}$ with one image point a_4 arbitrarily placed at infinity. α, β and γ are the external angles, $\delta = 2\pi - (\alpha + \beta + \gamma)$. a_1, a_2, a_3 and a_4 are the image points. The closed form mapping is[4]:

$$\mathbf{f}(z) = M_2 + M_1 \left((z - a_1)^{1-\frac{\alpha}{\pi}} \mathbf{F_1} \left(1 - \frac{\alpha}{\pi}, \frac{\beta}{\pi}, \frac{\gamma}{\pi}; 2 - \frac{\alpha}{\pi}; \frac{a_1 - z}{a_1 - a_2}, \frac{a_1 - z}{a_1 - a_3} \right) \right) \quad (3.3)$$

[4]Equation solved using *Mathematica* 4.0

$\mathbf{F_1}(\cdot)$ is the Appell hypergeometric function of two variables $\mathbf{F_1}(a, b_1, b_2; c; \mathbf{r}, \mathbf{s})$ where a, b_1, b_2 and c are constants.[5] It has the series expansion

$$\begin{aligned} \mathbf{F_1}(a, b_1, b_2; c; \mathbf{r}, \mathbf{s}) &= \sum_{m=0}^{\infty} \sum_{n=0}^{\infty} \frac{a^{\overline{m+n}} b_1^{\overline{m}} b_2^{\overline{n}}}{m! n! c^{\overline{m+n}}} \mathbf{r}^m \mathbf{s}^n \\ r^{\overline{k}} &= r(r-1)\ldots(r-k+1) \quad \forall \text{ Integer } k \geq 0 \\ &= \frac{\Gamma(r+k)}{\Gamma(r)} \end{aligned} \tag{3.5}$$

If a numerator constant is negative the series becomes finite since $(-a)^{\underline{k}} = 0$ when $k > a \geq 0$. Thus if angles β or γ are concave then the summation is bounded. The function can be evaluated if $c \geq 0$ [33, pp. 11-30].

Two examples of this transformation include the symmetric and asymmetric concave quadrilateral elements. The former is significantly more well-behaved than the latter. The symmetric element, in figure 3.2, has sources in the semi-infinite plane at -1, 0 and 1, and corresponding angles of $\frac{9\pi}{10}$, $-\frac{\pi}{3}$, and $\frac{9\pi}{10}$. The transforming equation $\mathbf{F_1}(\cdot)$ reduces to the apparently more numerically stable hypergeometric ${}_{\mathbf{p}}\mathbf{F}_{\mathbf{q}}(\cdot)$ function. The asymmetric, in figure 3.3, element has sources in the semi-infinite plane at -1, 0 and 1, and corresponding angles of $\frac{5\pi}{6}$, $-\frac{\pi}{3}$, and $\frac{9\pi}{10}$. The transforming equation $\mathbf{F_1}(\cdot)$ does not reduce and the numerical approximation required to plot output does not appear to be very stable. This transformation should be used with

[5] symmetric equation and consequently

$$\frac{\left((z-a_1)^{1-\frac{\alpha}{\pi}} \mathbf{F_1}\left(1-\frac{\alpha}{\pi}, \frac{\beta}{\pi}, \frac{\gamma}{\pi}; 2-\frac{\alpha}{\pi}; \frac{a_1-z}{a_1-a_2}, \frac{a_1-z}{a_1-a_3}\right)\right)}{\left((z-a_2)^{1-\frac{\beta}{\pi}} \mathbf{F_1}\left(1-\frac{\beta}{\pi}, \frac{\alpha}{\pi}, \frac{\gamma}{\pi}; 2-\frac{\beta}{\pi}; \frac{a_2-z}{a_2-a_1}, \frac{a_2-z}{a_2-a_3}\right)\right)} = \mathbf{C}, \tag{3.4}$$

where $\mathbf{C}$ is a constant.

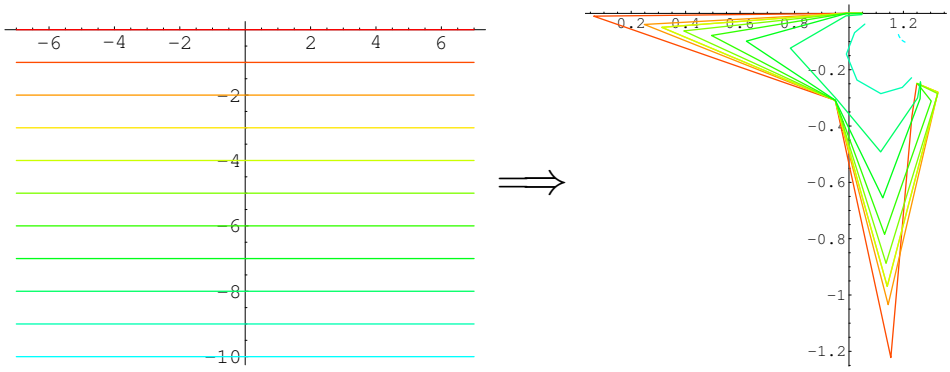


Figure 3.2: Symmetric element

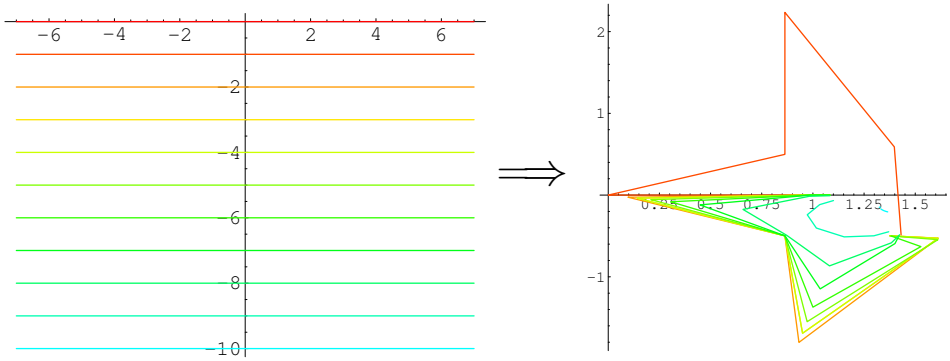


Figure 3.3: Asymmetric element

caution.

Following this method a closed form analytic solution can be found on any polygonal domain. Consequently, any elliptic function can be evaluated even in a concave domain, see appendix B.2. If the elliptic function which corresponds with the test function approximation is known, it can be evaluated in this manner. Accordingly, a first order interpolation then can be approximated by the solution to an elliptic function with appropriate boundary conditions [18].

3.2 Concave element construction from path-lines

Alternatively, a bounded shape function for any polygonal element can be constructed from path-lines, whose endpoints are defined, which do not travel outside the domain and can not overlap, see §2.2. Tessellating a concave domain results in path-lines whose behavior is given in each sub-region and connected by some continuity requirement. If only $\mathtt{C}^0$ continuity is enforced, the shapes constructed using tessellation do not preserve the geometrical features of concavity. For example, a peak in strain at the reentrant node is not captured.[6]

For example, a concave quadrilateral divided into two convex triangles is forced to behave linearly along the diagonal line, see figure 3.4. A smooth concave element would not necessarily behave linearly along the diagonal. As a result, the behavior of the gradient field at the concave node may even be singular, see figure 3.5.

3.2.1 Satisfying the first order continuity requirement

A combination of two triangular elements who share a boundary with $\mathtt{C}^1$ continuity can approximate a concave shape and a singularity at the concave node. The interpolation is constructed by assuming a linear behavior along

[6]There are methods for formulating a shape function such that it is forced to have a singularity. For such methods the degree of singularity must be known before element construction and is not derived from kinetic considerations [27].

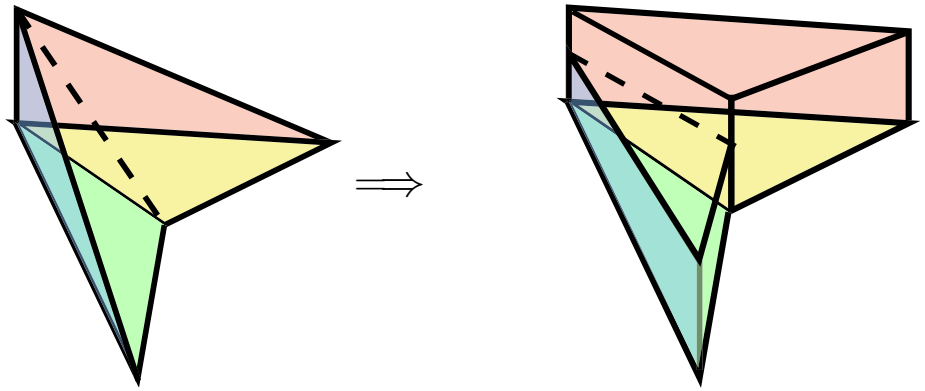


Figure 3.4: Concave quadrilateral element approximated by triangles and the associated gradient.

the oblique coordinates parallel to the boundary adjacent to a magnitude-one node. If the assumption applies, then the behavior of the shape function in the domain can be described in terms of a general function $f(\cdot)$ which is defined by the smooth connection at the interface between the sub-triangles.

The nodes are numbered counter clockwise and a convenient coordinate system is chosen. Set the origin at node-2 and let the y-axis cross through node-4. Let the general function then be only a function of y and connect node-2 and node-4 see figure 3.6.

Given such a coordinate system and node numbering the shape functions in terms of the function $f(y)$ from node-2 to node-3 is:

$$\begin{aligned} \phi_{left}(x,y) &= \frac{(x_1\,y - x\,y_1)\;f(y + \frac{x\,(-y_1+y_4)}{x_1})}{x_1\,y + x\;(-y_3+y_4)} \\ \phi_{right}(x,y) &= \frac{(x_3\,y - x\,y_3)\;f(y + \frac{x\,(-y_3+y_4)}{x_3})}{x_3\,y + x\;(-y_3+y_4)} \end{aligned} \tag{3.6}$$

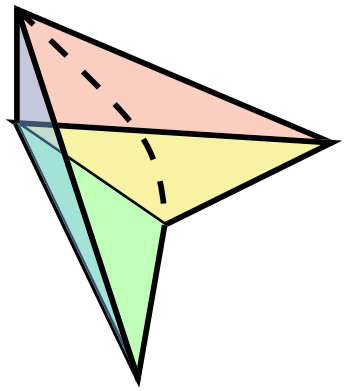


Figure 3.5: Smooth concave element sketch.

Notice that the values of these shape functions are zero valued along node-1 to node-2 and along node-2 to node-3, and linear from node-1 and node-3 to node-4 respectively. Also, the shape functions are linear within the left and right triangles separated by the line connecting node-2 and node-4, with respect to the oblique coordinate system parallel to the node-1, 4, 3 line.

Along the node-2, 4 line the first derivative must exist. Therefore, the derivatives in x,y for the left and right domain shape functions must be equal. The derivatives along that line are:

$$\begin{aligned} \frac{\partial}{\partial x}\phi_{left}(x,y) &= \frac{-\left(y_4\, f(y)\right) + y\ \left(-y_1 + y_4\right)\ f'(y)}{x_1\, y} \\ \frac{\partial}{\partial x}\phi_{right}(x,y) &= \frac{-\left(y_4\, f(y)\right) + y\ \left(-y_3 + y_4\right)\ f'(y)}{x_3\, y} \end{aligned} \tag{3.7}$$

The derivatives must be equal, so solve the resulting first order differential

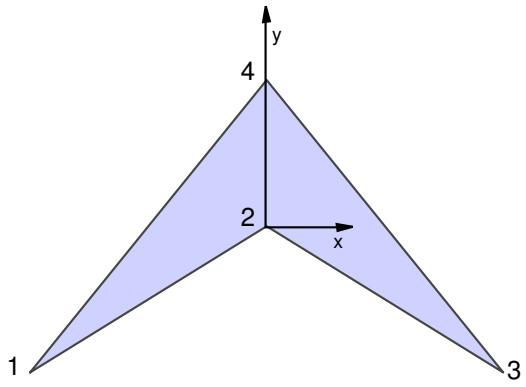


Figure 3.6: Coordinate system for quadrilateral analysis

equations for $f(y)$.

$$f(y) = C y^{\frac{x_1\, y_4 - x_3\, y_4}{x_3\, y_1 - x_1\, y_3 + x_1\, y_4 - x_3\, y_4}} \tag{3.8}$$

The constant C should be set such that the value of the function at node-4 is one.

The left and right portions of the shape function can then be written in closed form:

$$\begin{aligned} \phi_{left}(x,y) &= \frac{(x_1\, y - x\, y_1)\left(\frac{y + \frac{x\,(-y_1+y_4)}{x_1}}{y_4}\right)^{\frac{(x_1-x_3)\,y_4}{x_3\,(y_1-y_4)+x_1\,(-y_3+y_4)}}}{x_1\, y + x\,(-y_1 + y_4)} \\ \phi_{right}(x,y) &= \frac{(x_3\, y - x\, y_3)\left(\frac{x_3\, y - x\, y_3 + x\, y_4}{x_3\, y_4}\right)^{\frac{(x_1-x_3)\,y_4}{x_3\,(y_1-y_4)+x_1\,(-y_3+y_4)}}}{x_3\, y + x\,(-y_3 + y_4)} \end{aligned} \tag{3.9}$$

Even though the shape function is described separately for each convex part of the concave domain it is differentiable and continuous over the entire

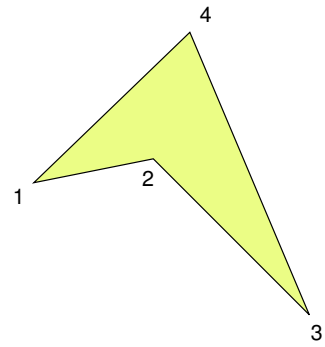


Figure 3.7: Skew concave element

domain. The shape functions for the remaining nodes are prescribed by the patch test requirements, see appendix B.3.

The shape functions can be rewritten in general barycentric coordinates. Accordingly, for any concave quadrilateral the set of shape functions is necessarily positive. The ratios of the areas of the triangles must be positive in either the left or right sub-domain respectively:

$$\frac{\triangle(\vec{x},1,2)}{\triangle(1,2,4)}\left(1-\frac{\triangle(\vec{x},4,1)}{\triangle(1,2,4)}\right)^{\frac{\triangle(1,2,3)}{\triangle(1,3,4)}} \quad \text{and} \quad \frac{\triangle(\vec{x},2,3)}{\triangle(2,3,4)}\left(1-\frac{\triangle(\vec{x},3,4)}{\triangle(2,3,4)}\right)^{\frac{\triangle(1,2,3)}{\triangle(1,3,4)}} \tag{3.10}$$

The shape function for node c in triangle $\triangle(a,b,c)$ is necessarily bounded.

$$0 \leq \frac{\triangle(\vec{x},a,b)}{\triangle(a,b,c)} \leq 1 \tag{3.11}$$

Using the patch test requirements, the remaining three shape functions are in domains $\triangle(1,2,4)$ and $\triangle(3,4,2)$ respectively (figure 3.8):

node-1**:**

$$\frac{\triangle(\vec{x},2,3)}{\triangle(1,2,3)} - \frac{\triangle(2,3,4)\,\triangle\,(\vec{x},1,2)}{\triangle(1,2,3)\,\triangle\,(1,2,4)}\left(1-\frac{\triangle(\vec{x},1,4)}{\triangle(2,1,4)}\right)^{\frac{\triangle(1,2,3)}{\triangle(1,3,4)}}$$

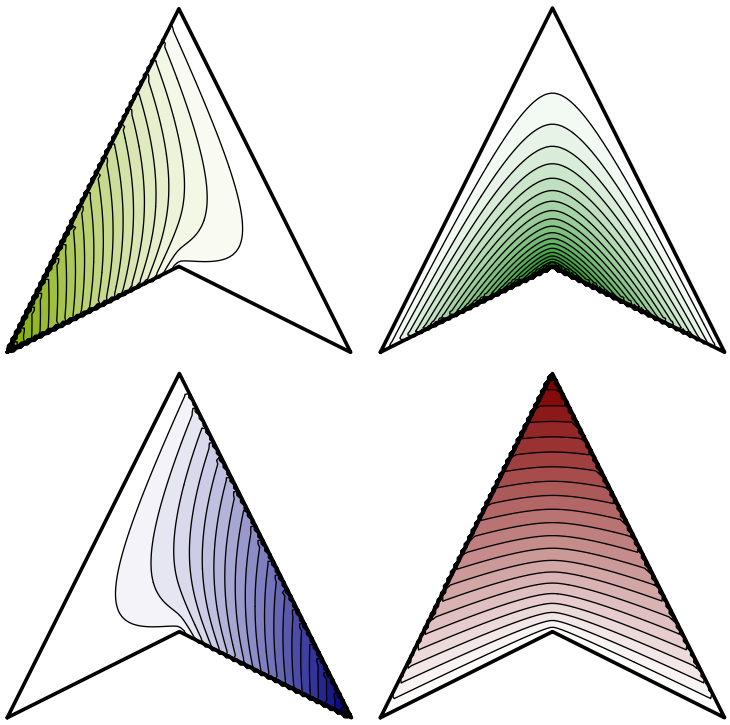


Figure 3.8: Remaining shape functions from patch test

and

$$\frac{\triangle(\vec{x},3,2)}{\triangle(1,3,2)}\left(1-\left(1-\frac{\triangle(\vec{x},3,4)}{\triangle(2,3,4)}\right)^{\frac{\triangle(1,2,3)}{\triangle(1,3,4)}}\right)$$

node-2:

$$\frac{\triangle(\vec{x},1,3)}{\triangle(1,3,2)}-\frac{\triangle(1,3,4)\triangle(\vec{x},1,2)}{\triangle(1,3,2)\triangle(1,2,4)}\left(1-\frac{\triangle(\vec{x},1,4)}{\triangle(2,1,4)}\right)^{\frac{\triangle(1,2,3)}{\triangle(1,3,4)}}$$

and

$$\frac{\triangle(\vec{x},1,3)}{\triangle(1,3,2)}-\frac{\triangle(1,3,4)\triangle(\vec{x},3,2)}{\triangle(1,3,2)\triangle(3,2,4)}\left(1-\frac{\triangle(\vec{x},3,4)}{\triangle(2,3,4)}\right)^{\frac{\triangle(1,2,3)}{\triangle(1,3,4)}}$$

node-3:

$$\frac{\triangle(\vec{x},1,2)}{\triangle(1,2,3)}\left(1-\left(1-\frac{\triangle(\vec{x},1,4)}{\triangle(1,4,2)}\right)^{\frac{\triangle(1,2,3)}{\triangle(1,3,4)}}\right)$$

and $$\frac{\triangle(\vec{x},1,2)}{\triangle(1,2,3)}-\frac{\triangle(4,1,2)\triangle(\vec{x},3,2)}{\triangle(1,2,3)\triangle(3,2,4)}\left(1-\frac{\triangle(\vec{x},3,4)}{\triangle(2,3,4)}\right)^{\frac{\triangle(1,2,3)}{\triangle(1,3,4)}}$$

node-4:

$$\frac{\triangle(\vec{x},1,2)}{\triangle(1,2,4)}\left(1-\frac{\triangle(\vec{x},4,1)}{\triangle(1,2,4)}\right)^{\frac{\triangle(1,2,3)}{\triangle(1,3,4)}} \text{ and } \frac{\triangle(\vec{x},2,3)}{\triangle(2,3,4)}\left(1-\frac{\triangle(\vec{x},3,4)}{\triangle(2,3,4)}\right)^{\frac{\triangle(1,2,3)}{\triangle(1,3,4)}}$$

The resulting shape functions are similarly bounded and exhibit singular behavior only at the concave node.

The degree of the singularity is a function of the domain geometry. The exponent $\frac{\triangle(1,2,3)}{\triangle(1,3,4)}$ is a measure of the degree of concavity. If the triangle $\triangle(1,2,3)$ is not concave, the exponent remains positive and no singularity occurs in the derivative. Furthermore, the greater the concavity the closer

the exponent is to negative one. Consequently in polar coordinates, r^{α}, for a concave quadrilateral the measure of singularity $\alpha = \frac{\triangle(1,2,3)}{\triangle(1,3,4)}$ ranges from zero to negative one.

3.3 General methods for all polygons

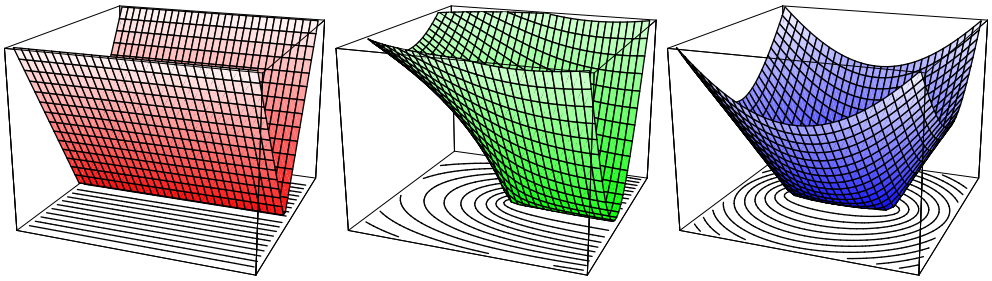


Figure 3.9: Functions which are minimum along a line

Shape functions for any simple non-intersecting polygonal shape with any number of vertices, side nodes and concavities can be constructed as the quotient of irrational polynomial functions. The shape function requirements form a guideline for shape function construction, see §1.2.1. Any smooth and bounded interpolation can be constructed from the combination of functions which are minimum and zero along a given line such as line $\bar{ab}$, see figure 3.9. For the Wachspress rational polynomial construction such functions are lin-

ear[7] [17].

$$r_{ab}(x,y) = \left| \det \begin{pmatrix} x & y & 1 \\ x_a & y_a & 1 \\ x_b & y_b & 1 \end{pmatrix} \right| \tag{3.12}$$

For a concave element the representation $r_{ab}(x,y)$ must be nonlinear. A linear description would prescribe a minimum value within the interior of the domain and violate the ellipticity requirement. Instead, a function $r_{ab}(x,y)$ with conical contours can be used to describe the boundary of any polygonal domain.

3.3.1 Smooth zeroth order concave shape

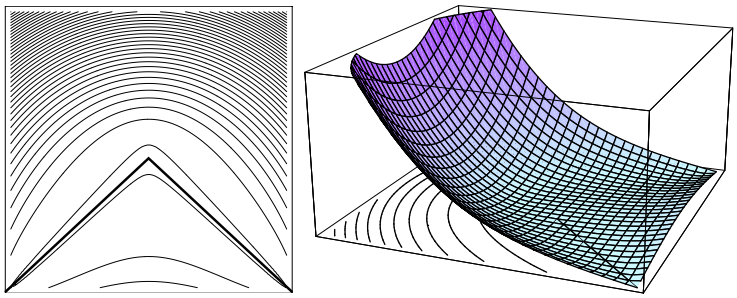


Figure 3.10: Behavior of finite lines at a reentrant corner.

In a concave shape the bounding lines do not lie exterior to the domain and thus if they continue to be zero valued beyond the nodes a and b then

[7]To assure that the line upon which the function is zero valued is a minimum the representation is described as an absolute value, in practical application the negative portion of the plane lies strictly outside the convex domain and the absolute value is not required.

the values inside the domain are corrupted, see figure 3.10. Assume a zero line $r_{ab}(x, y)$ function can be constructed such that it is zero valued, and minimum along the line connecting points a to b. Define a product of minimum functions accordingly:

$$s_i(x, y) = \prod_{\text{non-adj. sides}} r_{ab}(x, y) \quad \text{and} \quad \phi_i(x, y) = \frac{k_i(s_i(x, y))}{\sum_{\text{all}} k_j(s_j(x, y))}. \tag{3.13}$$

where the k_i are arbitrary positive constants. For the smooth zeroth order case all the k_i are set to one. The function $s_i(x, y)$ is zero along all the boundaries except those adjacent to node i. Also, the constancy condition is satisfied.

$$\sum_{i=1}^{n} \phi_i(x, y) = 1 \tag{3.14}$$

The boundary is not necessarily linear and the linearity requirement is not necessarily satisfied.

Nevertheless, unlike p element formulations (§1.1.2), the boundedness of the interpolation is preserved. At the named node $\{x_i, y_i\}$ the value of the shape function ϕ_i is one, at all other nodes the value is zero. The behavior along the boundary is bounded by the behavior at the nodes.

Examples of zeroth order bounded interpolations

A function which is zero valued and minimum only along the line connecting nodes a to b describes the length of the perimeter of the triangle between the points $\{x, y\}$, $\{x_a, y_a\}$ and $\{x_b, y_b\}$.

$$\sqrt{(x - x_a)^2 + (y - y_a)^2} + \sqrt{(x - x_b)^2 + (y - y_b)^2} - \sqrt{(x_a - x_b)^2 + (y_a - y_b)^2} \tag{3.15}$$

The contour lines of this function $r_{a,b}(x, y)$ are ellipses with foci located at nodes a and b.

The shape functions constructed using such zero valued lines are not linear along the boundary, but do satisfy the constancy requirement. Since $r_{ab}(x, y)$ is necessarily positive and has no minima other than along the line point a to point b, the constructed functions are also bounded within the domain.

Given a quadrilateral defined by the following vertex nodes

$$\{\{0, 0\}, \{\frac{3}{5}, \frac{1}{4}\}, \{1, 0\}, \{\frac{2}{3}, 1\}\}$$

smooth and bounded shape functions can be constructed, see figure 3.11.

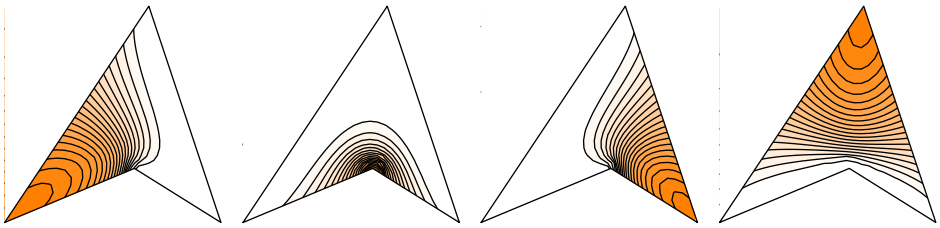


Figure 3.11: Concave quadrilateral element with smooth interpolation contours

Given a pentagon defined by the following vertex nodes

$$\{\{0, 0\}, \{\frac{3}{5}, \frac{1}{4}\}, \{1, 0\}, \{\frac{4}{5}, \frac{2}{3}\}, \{\frac{1}{3}, 1\}\}$$

the resulting shape functions are smooth and bounded, see figure 3.12. Even

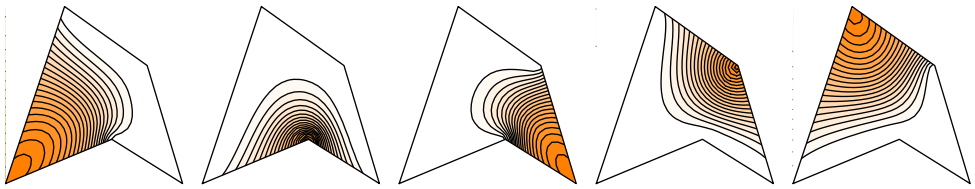


Figure 3.12: Concave pentagonal element with smooth interpolation contours

quite complicated shapes can be described. For example the eighteen noded shape in figure 3.13.

3.3.2 Construction of a linear edged interpolation

The linear boundary condition can be captured using equation 3.13 provided the functions $r_{ab}(x, y)$ satisfy additional linearity conditions. Along any given edge $j\bar{k}$ the shape function should be linear:

$$\phi_i(x_{j\bar{k}}, y_{j\bar{k}}) = 0 \quad \text{if} \quad i \neq j \text{ or } i \neq k. \tag{3.16}$$

Along any edge $i\bar{j}$ only the functions $s_k(x, y)$ with $k = i$ or $k = j$ are non-zero, see equation 3.13.

$$\phi_i(x_{i\bar{j}}, y_{i\bar{j}}) = \frac{k_i\, s_i(x_{i\bar{j}}, y_{i\bar{j}})}{k_i\, s_i(x_{i\bar{j}}, y_{i\bar{j}}) + k_j\, s_j(x_{i\bar{j}}, y_{i\bar{j}})} = \frac{k_i r_{jl}(x_{i\bar{j}}, y_{i\bar{j}})}{k_i\, r_{jl}(x_{i\bar{j}}, y_{i\bar{j}}) + k_j\, r_{hi}(x_{i\bar{j}}, y_{i\bar{j}})}. \tag{3.17}$$

If the function $r_{ij}(x, y)$ it is linear along the edges $\bar{h}i$ and $\bar{j}l$ the boundary will be linear as well. Cancelling, the common $r_{kl}(x, y)$ term:

$$\phi_i(x_{i\bar{j}}, y_{i\bar{j}}) = \frac{k_i\,(r_{jl}(x_i, y_i)(1-t))}{k_i r_{jl}(x_i, y_i)(1-t) + k_j r_{hi}(x_j, y_j)t} \tag{3.18}$$

Solving for the constants:

$$k_i = r_{hi}(x_j, y_j) \quad \text{and} \quad k_j = r_{jl}(x_i, y_i). \tag{3.19}$$

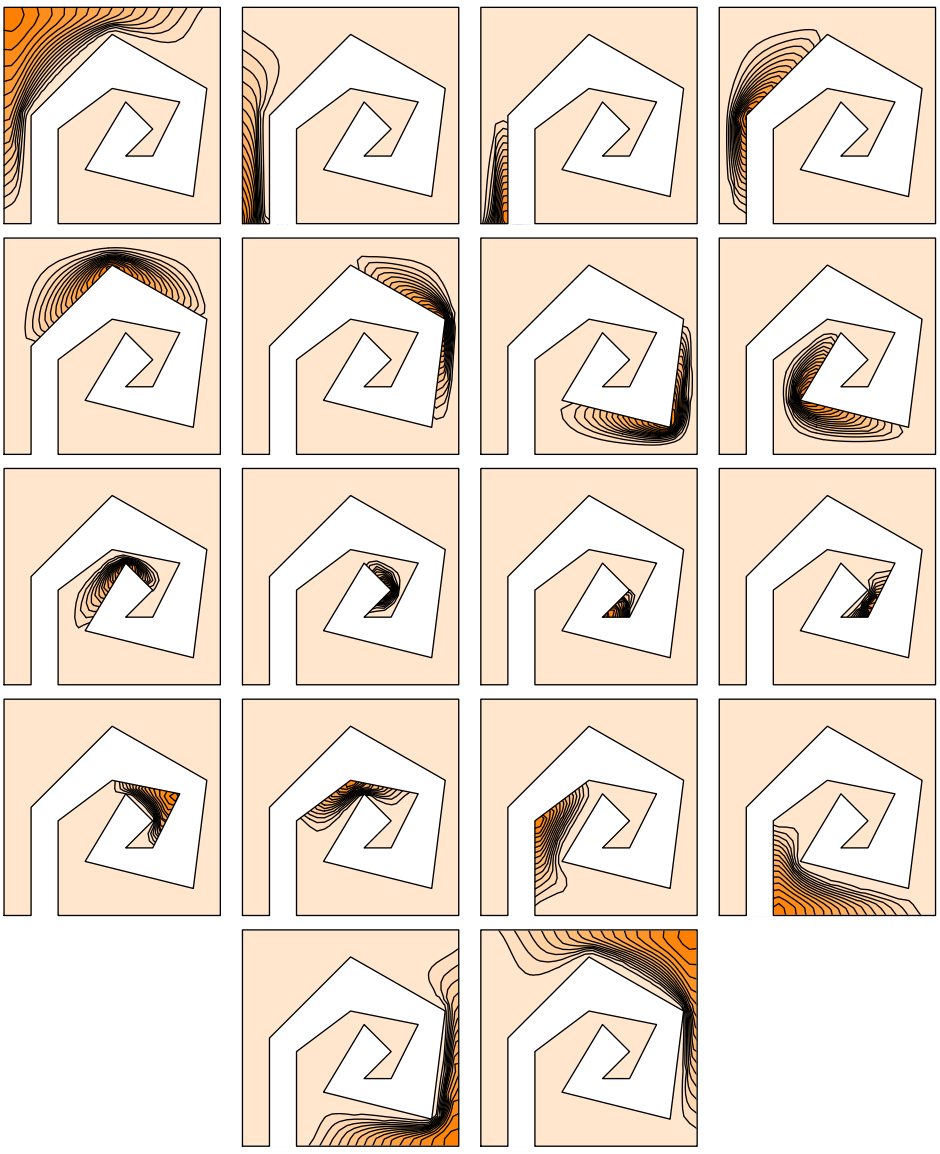


Figure 3.13: Smooth interpolation on a concave element with eighteen nodes

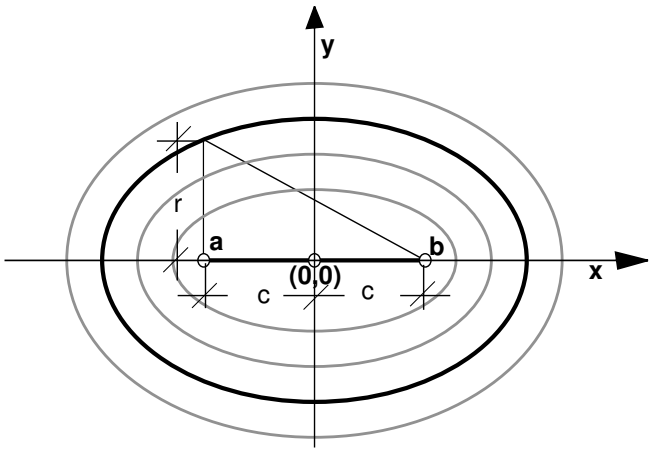


Figure 3.14: Elliptical contours.

Consequently, it is convenient to scale $r_{ij}(x, y)$ such that:

$$r_{ij}(x_l, y_l) = r_{jl}(x_i, y_i) = |\triangle(i, j, l)|. \tag{3.20}$$

A function $\hat{r}_{ij}(x, y)$ can be constructed such that it is zero valued and minimum along the line $\bar{ij}$ and linear on the paths normal to $\bar{ij}$ through nodes i and j.

$$\hat{r}_{ij}(x, y) = \frac{(l_{\vec{x}a}(x, y) + l_{\vec{x}b}(x, y))^2 - l_{ab}^2}{2(l_{\vec{x}a}(x, y) + l_{\vec{x}b}(x, y))/l_{ab}} \tag{3.21}$$

Where $l_{\vec{x}k}$ is the length of a line betweeen points $\{x, y\}$ and k, and l_{ab} is the length of the line between points a and b, see figure 3.14.

$$l_{ml} = \sqrt{(x_m - x_l)^2 + (y_m - y_l)^2} \quad \text{and} \quad l_{\vec{x}l}(x, y) = \sqrt{(x - x_l)^2 + (y - y_l)^2}.$$

Using equation 3.21 a interpolation on any shape with only normal angles can be constructed such that the edge behavior is linear, and the constant

field is captured exactly. The linear fields are not necessarily captured.

Example of normal angled linear edged elements

A square domain can more easily be described by the concave element formulation. Nevertheless, the general formulation can be applied. Given a square with nodes at:

$$\{\{0,0\},\{2,0\},\{2,2\},\{0,2\}\} \tag{3.22}$$

the shape functions for node one is quite complicated. Nevertheless, the boundary is linear, and the domain behavior is bounded, see figure 3.15. A normal angled concave element can be described with the same method.

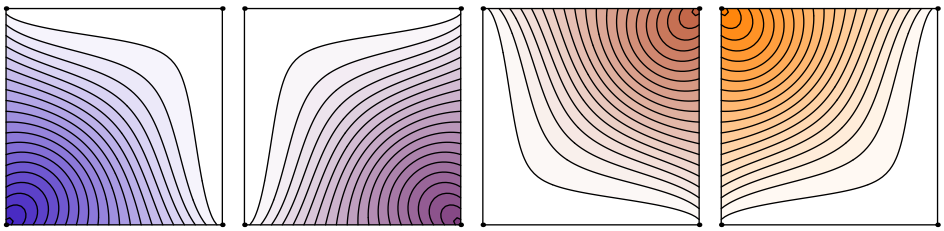


Figure 3.15: General linear edged interpolation within a square.

Given a six noded reentrant figure:

$$\{\{0,0\},\{2,0\},\{2,1\},\{1,1\},\{1,2\},\{0,2\}\} \tag{3.23}$$

The resulting shape functions are linear along the edges and bounded and smooth within the domain, see figure 3.16.

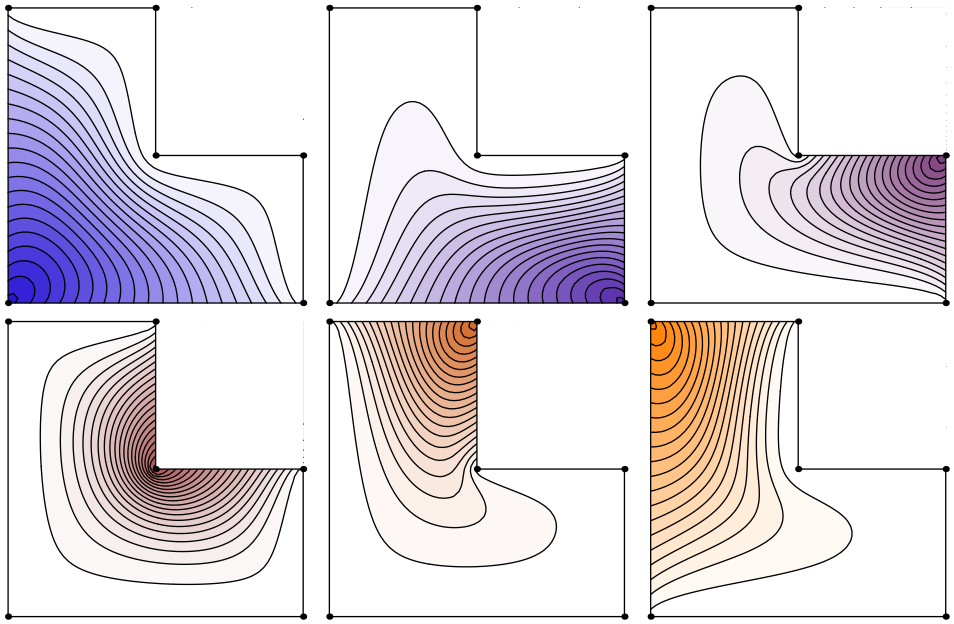


Figure 3.16: Smooth linear edged interpolation within a concave domain.

3.3.3 A general linear edged interpolation

Leaving away (x, y) for convenience, a general function which is linear along incoming angle α and exiting angle β is:

$$\bar{r}_{ab} = \frac{(A\sin(\alpha) + B\sin(\beta))((l_{b\vec{x}} + l_{a\vec{x}})^2 - l_{ab}^2)(l_{ab}/2)}{(l_{b\vec{x}} + l_{a\vec{x}})(A + B) - l_{ab}(A\cos(\alpha) + B\cos(\beta))} \tag{3.24}$$

where:

$$A = \left(l_{b\vec{x}}^2 + l_{ab}^2 - 2l_{ab}l_{b\vec{x}}\cos\beta\right) - l_{a\vec{x}}^2$$

and

$$B = \left(l_{a\vec{x}}^2 + l_{ab}^2 - 2l_{ab}l_{a\vec{x}}\cos\alpha\right) - l_{b\vec{x}}^2.$$

The angles can be defined in terms of the boundary nodes:

$$\cos(\alpha) = \frac{l_{ab}^2 + l_{da}^2 - l_{bd}^2}{2 l_{ab} l_{da}}, \quad \sin(\alpha) = \frac{2|\triangle(d,a,b)|}{l_{da} l_{ab}},$$

$$\cos(\beta) = \frac{l_{ab}^2 + l_{bc}^2 - l_{ca}^2}{2 l_{ab} l_{bc}} \quad \text{and} \quad \sin(\beta) = \frac{2|\triangle(a,b,c)|}{l_{bc} l_{ab}}$$

Where, the nodes along the boundary, in order, are (d, a, b, c) and the function r_{ab} is zero valued along $\bar{ab}$, and linear along $\bar{da}$ and $\bar{bc}$. Consequently, it can be used to describe the boundary of a reentrant portion or inclusion in the polygon.

Select convex polygon interpolations with linear edge behavior

A concave element with any angles can be described with this method. Given a reentrant quadrilateral with the following nodes:

$$\{\{-1,-1\},\{0,0\},\{1,-1\},\{0,1\}\},$$

a reentrant pentagon with nodes:

$$\{\{0,1/2\},\{1,0\},\{3/2,1/2\},\{-1/4,1\},\{-1/2,1/4\}\},$$

A reentrant hexagon with nodes:

$$\{\{1,1\},\{0,1\},\{0,0\},\{7/8,0\},\{1/2,1/2\},\{1,1/8\}\}$$

and a star shaped octagon:

$$\{\{0, 1/2\}, \{1, 0\}, \{1/4, 1/2\}, \{3/2, 1\},$$
$$\{1/5, 5/8\}, \{-1/4, 1\}, \{0, 11/20\}, \{-1/2, 1/4\}\}$$

the resulting geometric test function is linear along the edges and smooth and bounded within the domain, see figure 3.18. The behavior of the boundary edges is linear, see figure 3.17.

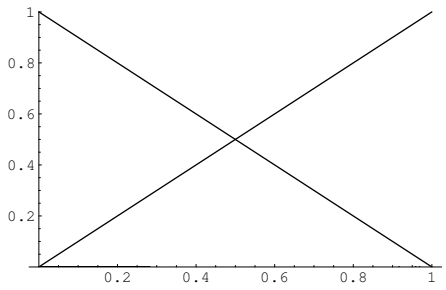


Figure 3.17: Linear boundary behavior, even along reentrant boundaries.

3.3.4 Smooth first order bounded interpolations

A linear edged element with a smooth interpolation can be forced to satisfy the constancy and linearity requirements, see appendix B.3. For the four-noded element one shape function can be used to determine the remaining three, see figure 3.15. For the six node element, similarly, three shape functions are not independent. Some care must be given in choosing the appropriate independent functions such that the derived functions are bounded, see figure 3.20.

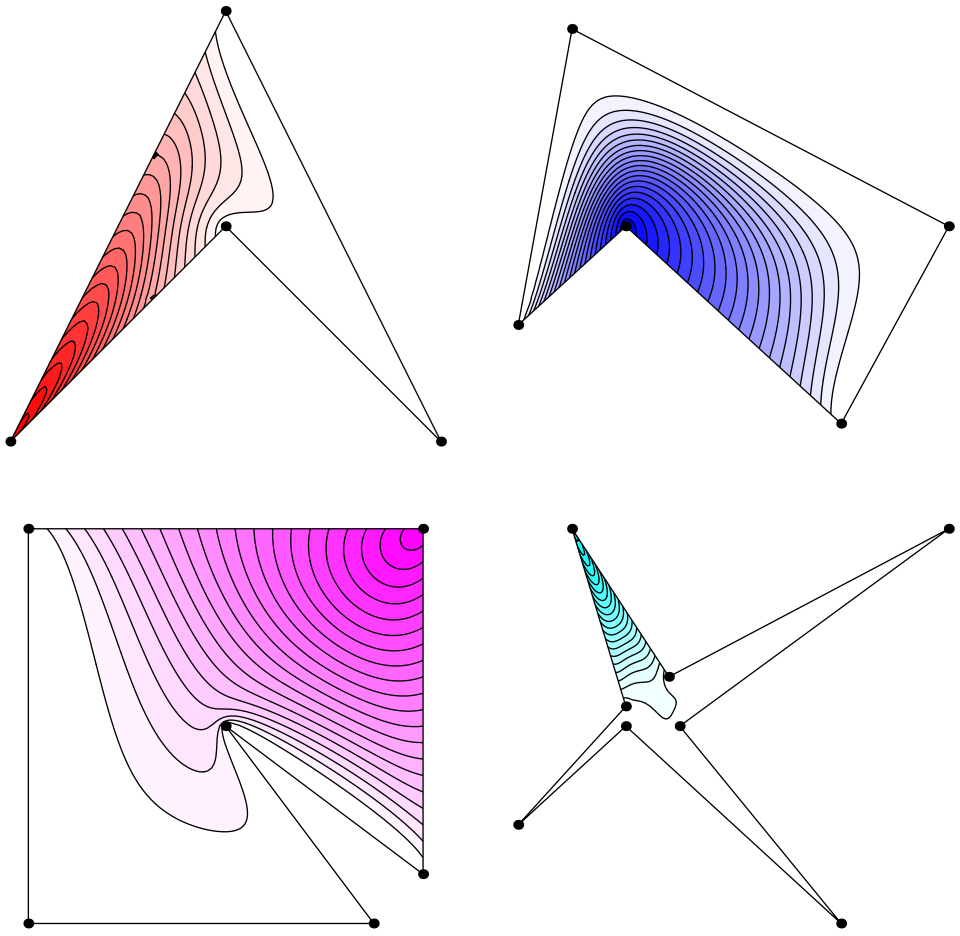


Figure 3.18: Smooth, bounded interpolation contours within reentrant shapes.

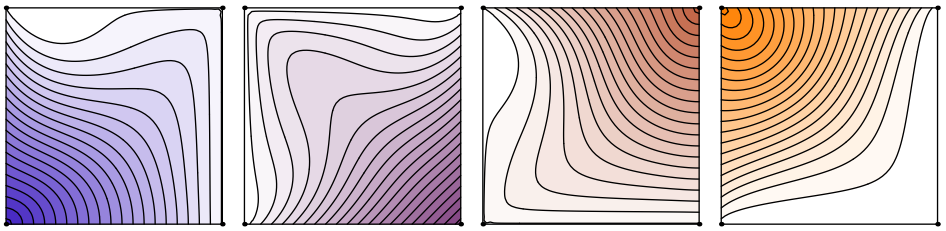


Figure 3.19: Smooth first order interpolation within a square.

3.4 Comparison of concave representations

For a concave quadrilateral with the following nodes:

$$\{\{-1,-1\},\{0,0\},\{1,-1\},\{0,1\}\} \tag{3.25}$$

For each linear representation the behavior along the boundary is linear. The behavior along the diagonal from point $\{0,0\}$ to point $\{0,1\}$ varies for each representation. For the approximate shape function, with $\mathtt{C}^1$ pathlines, the representation is $\frac{1}{2\sqrt{y}}$, the derivative at the concave node exhibits a $r^{-1/2}$ discontinuity, see figure 3.22. In general the behavior along the boundary is a function of the geometry $\tau^{1+\frac{\triangle(1,2,3)}{\triangle(1,3,4)}}$. The singularity obtained using conformal mapping of a domain governed by Poisson's equation is $r^{\pi/\beta}$. In this example the interior obtuse angle is $\beta = \frac{3\pi}{2}$ and the associated singularity of the gradient field at the concave node is of the order $r^{-1/3}$.

For the smooth zeroth order representation, the behavior along the diagonal is nonlinear, see figure 3.24. The linearized functions exhibit a similar behavior. A sharper peak occurs at sharper concavities. Figure 3.23 compares the behavior along the diagonal connecting the concave and opposite

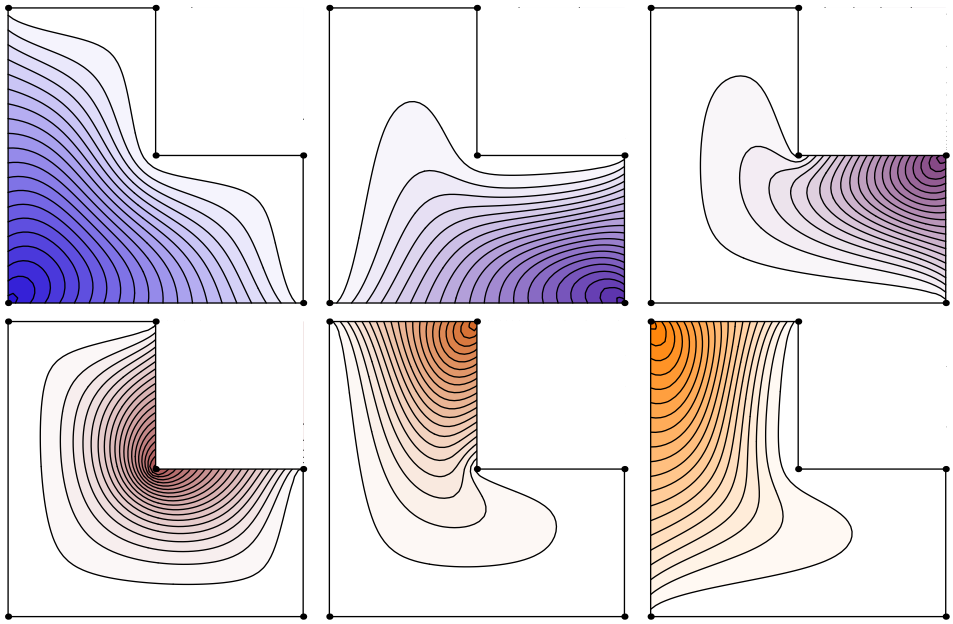


Figure 3.20: Smooth first order interpolation within a concave domain.

concave node for the concave quadrilateral and concave hexagon examples. The behavior in the five noded reentrant figure also exhibits a peak at the concave node, see figure 3.25.

Unlike the solution to Poisson's equation and the smoothed pathline construction, the singularity at the concave node is removable. In the limit the

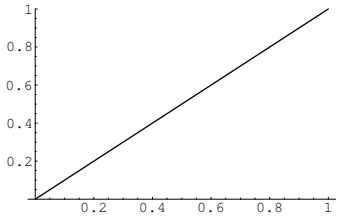


Figure 3.21: C^0 Tessellated model

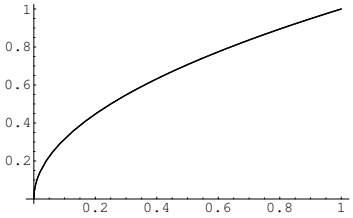


Figure 3.22: C^1 Smooth model

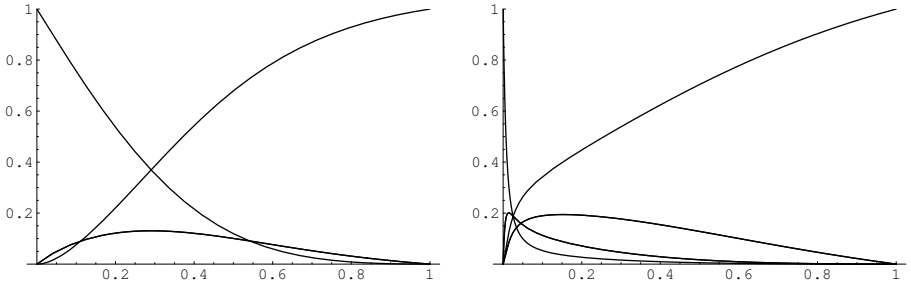


Figure 3.23: Liner edged test function behavior along the diagonal from the concave and opposite concave nodes for the reentrant quadrilateral (left) and hexagon (right). The hexagon in this example (right) has a more sharp concave node than the quadrilateral (left).

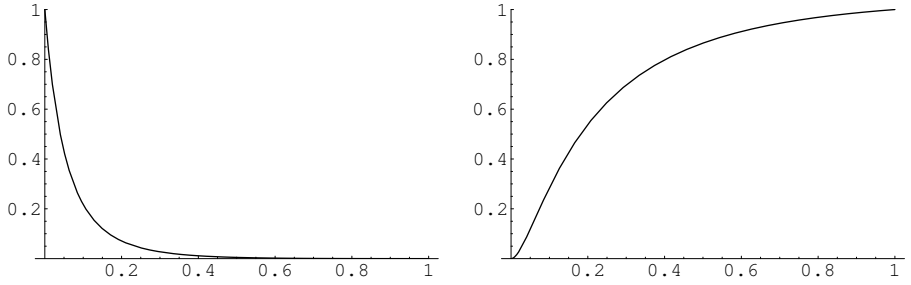


Figure 3.24: Zeroth order test function behavior along the diagonal from the concave and opposite concave nodes.

magnitude of the gradient along the diagonal—for the concave node shape function, at the concave node—is 19.16. Similarly, the behavior of the smooth linear edged shape functions and linear order interpolations along the diagonal from concave to opposite concave node have a removable singularity at the concave node, see figure 3.26. Nevertheless, each representation captures the general characteristics of the behavior of an interpolation inside a concave shape. These characteristics are not captured by the C^0 tesselated

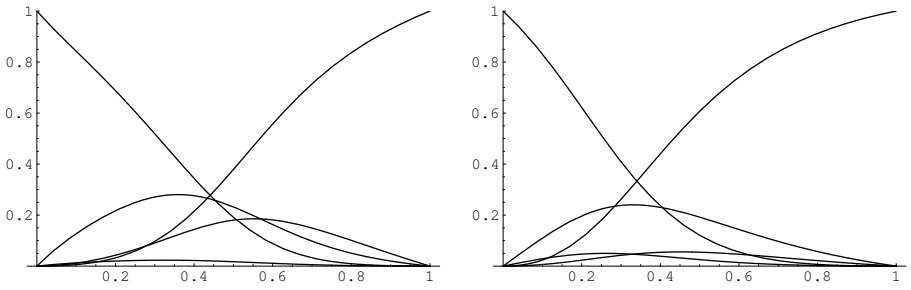


Figure 3.25: Linear edged test function behavior along the diagonal of the shape on paths from the concave node to the non-concave nodes. The behavior of all the functions are drawn one graph. The peak occurs at the concave node.

model, see figure 3.21. The functions for the opposite concave node are generally concave down and gradient is maximum at the concave node. The shape functions for the concave node generally peak around the concavity.

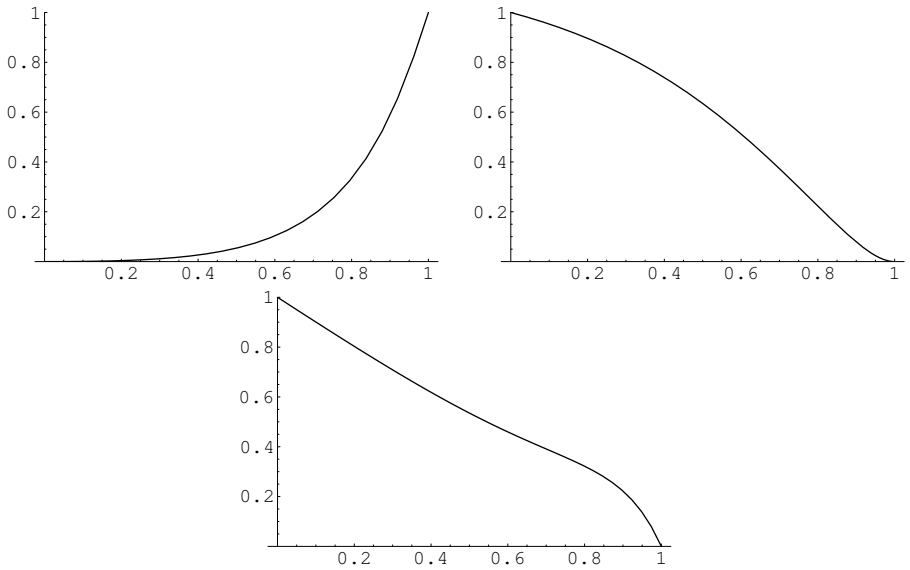


Figure 3.26: Behavior from the concave node $\{0, 0\}$ to the opposite concave node $\{1, 1\}$. The plots are for the linear edged shape functions for nodes-1 and 4 and the linear interpolation for node-1 respectively.

Chapter 4

Order of approximation

Conventionally, the ability to derive any convex quadrilateral element from a normed square element is central to the efficiency and simplicity of finite element mesh construction. The integration over an element can be performed in fixed computational, as opposed to variable geometric, coordinates. The transformation is especially convenient if all the integration must be performed numerically [67]. As a result finite element meshes composed of rectangles and skew quadrilaterals are commonly available in finite element programs [34, 64]. As a side effect, the analysis of the element properties has also been performed in computational coordinates [57]. The effect of changing the functional domain for the finite element analysis from polynomial to rational and even irrational polynomials has not been studied directly, except for the Wachspress rational polynomial formulation [9, pp. 87], [32, pp.], [61].

As a result, the impact to the accuracy of a given mathematical model with respect to the increasing the number of nodes in an element has only been described in a qualitative manner [38]. Generally Lagrange type elements which model quadratic and higher order fields exactly are termed high order elements [67]. The effect of adding the additional nodes, and associated kinematic modes, has not been studied *per se*.

One measure of a shape function is its ability to interpolate a given function [30, 57]. The goal of the shape function representation is not only to represent the interaction between force and displacement, see §1.1.1, but also to show the displaced shape and the state of stress. The more closely the shape function approximates the actual solution the better calculated displacement reflects the actual [57]. Interpolations over a collection of nodes can be categorized by their order of approximation.

Given a polygonal domain $\mathcal{D}$ with n number of nodes, a shape function distributes a known collection of boundary values $f^i = f(x_i, y_i)$ at each given node-(i) such that the final representation $N_i(x, y)$ is smooth and bounded over the domain. Evaluating the shape function at vertices of the polygon and boundary points, nodes-(j):

$$N_i(x_j, y_j) = \delta_{ij} \quad \text{and} \quad \begin{array}{l} N_i(x_{i+1} + t(x_i - x_{i+1}), y_{i+1} + t(y_i - y_{i+1})) = t \\ N_i(x_{i-1} + s(x_i - x_{i-1}), y_{i-1} + s(y_i - y_{i-1})) = s. \end{array} \tag{4.1}$$

Consequently, the interpolation is defined as linear, even though the behavior in the domain is non-linear. A smooth function defined within the domain

$\mathcal{D}$ can be approximated by a linear combination of the interpolations:

$$f(x,y) \approx \sum_{i=1}^{n} N_i(x,y) f^i \quad \forall \{x,y\} \ \in \mathcal{D} \tag{4.2}$$

The error of approximation with respect to the smooth function which satisfies the constancy and linearity requirements, equation 1.7, and the Chebyshev condition, equation 1.6, can be determined using a two dimensional Taylor Series expansion.

4.1 Taylor Expansion

Two dimensional Taylor Series expansion:

$$\begin{aligned} f(x,y) \ &= \ f^0 + f^0{}_{,x}\,(x-x_0) + f^0{}_{,y}\,(y-y_0) + f^0{}_{,xx}\,\frac{(x-x_0)^2}{2} + \\ &\quad f^0{}_{,xy}\,(x-x_0)(y-y_0) + f^0{}_{,yy}\,\frac{(x-x_0)^2}{2} + \cdots + \\ &\quad \frac{(x-x_0)^{n+1}(y-y_0)^{m+1}}{(n+1)!(m+1)!} f_{,x^{(n+1)}y^{(m+1)}}\,(\eta,\zeta) \\ \text{where :} \quad &\quad f^0 = f(x_0,y_0), \quad f^0{}_{,x} = \left.\frac{\partial f(x,y)}{\partial x}\right|_{\{x_0,y_0\}}, \quad \ldots \end{aligned} \tag{4.3}$$

If $\{x_0, y_0\}$ is a point within the polygonal domain and the function $f(x,y)$ is continuous around the point then the series should converge. The point $\{\eta, \zeta\}$ is in the domain $\eta \in [x_0, x]$ and $\zeta \in [y_0, y]$. The values of the nodal points-(i) in terms of the expansion about the same point $\{x_0, y_0\}$:

$$f^i \ = \ f^0 + f^0{}_{,x}\,(x_i - x_0) + f^0{}_{,y}\,(y_i - y_0) + \cdots \tag{4.4}$$

Multiplying this result by the shape functions $N_i(x, y)$:

$$\begin{aligned} f(x,y) &= \sum_{i=1}^{n} N_i(x,y) f^i + \frac{f^{0},_{xx}(\eta,\zeta)}{2} \sum_{i=1}^{n} (x^2 - N_i(x,y) x_i^2) + \\ & \quad f^{0},_{xy}(\eta,\zeta) \sum_{i=1}^{n} (xy - N_i(x,y) x_i y_i) + \frac{f^{0},_{yy}(\eta,\zeta)}{2} \sum_{i=1}^{n} (y^2 - N_i(x,y) y_i^2) \\ &= \sum_{i=1}^{n} N_i(x,y) f^i + \mathcal{E}(x,y) \end{aligned} \tag{4.5}$$

Since the shape function is bounded the truncation error is governed either by the distances $(x - x_i)$ and $(y - y_i)$ or the curvature:

$$\begin{aligned} \mathcal{E}(x,y) &= \sum_{i=1}^{n} N_i(x,y) \left((x - x_i) \left(\frac{f^{0},_{xx}(\eta,\zeta)}{2} x_i + \frac{f^{0},_{xy}(\eta,\zeta)}{2} y_i \right) + \right. \\ & \quad \left. (y - y_i) \left(\frac{f^{0},_{yy}(\eta,\zeta)}{2} y_i + \frac{f^{0},_{xy}(\eta,\zeta)}{2} x_i \right) \right). \end{aligned} \tag{4.6}$$

This result corresponds with the established result that displacement based elements with linear elements are order h^2 where h is linear measure of the dimension of the element [57].

The minimum number of nodes required to satisfy the linear and constancy requirements (equations 1.7) is three and increasing the number of nodes in an element does not, by the Taylor series calculation, increase the order of convergence. Despite the conclusion that three nodes is sufficient for an order h^2 approximation, a three sided element performs less well than a parallelogram [38, pp. 203–259]. The kinematic degrees of freedom of an element also have an impact on the efficacy of the model.

Finite element methods constructed according to polynomial basis func-

tions are order h^2 approximations as predicted by the Taylor Series expansion, equation 4.5.[1] A higher order approximation then would require a minimum of six nodes and the shape functions should satisfy the constancy and linearity requirements along with the quadratic requirements

$$\sum_{i=1}^{n} N_i(x,y)x_i^2 = x^2, \quad \sum_{i=1}^{n} N_i(x,y)y_i^2 = y^2 \quad \text{and} \quad \sum_{i=1}^{n} N_i(x,y)x_iy_i = xy. \quad (4.7)$$

Following this argument, an p order approximation would require at minimum a $p(p+1)/2$ noded element. In the global frame such higher order elements would not necessarily provide a higher order approximation [38, pp. 72, 93–100]. The boundary of any higher order element is not necessarily linear, nor is its behavior is not strictly defined by the location and values of the two adjacent boundary nodes. Consequently the boundary of such a a higher order element would not necessarily be bounded and any assumption with respect to continuity across element boundaries depends on the location of the nodes. The convergence of such an approximation is not necessarily uniform, see §1.1.2.

4.2 Form of the shape function

The polynomial form is insufficient for representing any polygonal element with linear sides. The restrictions of the representation were first presented by Wachspress in 1975 [61, p.247]. Rational polynomial and even irrational

[1] A series of more rigorous derivations applicable also to piecewise continuous functions is given in the reference [57]

polynomial representations are required, see equation 2.13. For example, the shape functions for the skew quadrilateral are only polynomial in a computational coordinate frame. Let $\{s,t\}$ parametrize the cartesian $\{x,y\}$ coordinates.

$$\{x,y\} = (1-s)\,(1-t)\{x_a,y_a\}+s(1-t)\{x_b,y_b\}+st\{x_c,y_c\}+t(1-s)\{x_d,y_d\} \quad (4.8)$$

The shape functions for nodes a, b, c, and d are respectively: $\phi_a = s\,t$, $\phi_b = s(1-t)$, $\phi_c = (1-s)(1-t)$ and $\phi_d = (1-s)t$. Solving for the shape function ϕ_a in terms of x and y, the resulting equation is a quadratic in terms of the shape function ϕ_a, see also equation 2.13:

$$\alpha\,\phi_a^2 - \beta(x,y)\phi_a + \gamma(x,y) = 0 \quad (4.9)$$

where the coefficients are polynomials in (x,y):

$$\begin{aligned} \alpha &= (\triangle(b,c,d) - \triangle(a,b,c))\,(\triangle(b,c,d) - \triangle(a,c,d)) \\ \beta(x,y) &= (\triangle(b,c,d))^2 - (\triangle(\vec{x},c,d)\,(\triangle(b,c,d) - \triangle(a,b,c)) + \\ &\qquad \triangle(\vec{x},b,c)\,(\triangle(b,c,d) - \triangle(a,c,d))) \\ \gamma(x,y) &= \triangle(\vec{x},b,c)\triangle(\vec{x},c,d) \end{aligned} \quad (4.10)$$

The coefficient α is zero if the transformed element is trapezoidal. The resulting shape functions satisfy the patch test requirements and perform well in numerical applications [38]. If the coefficient α is not zero then the inverse function has two solutions.

The coefficients are polynomials in terms of the global cartesian coordinate system $\{x, y\}$: α is constant, $\beta(x, y)$ is linear and $\gamma(x, y)$ is quadratic. If α is zero the shape function is a rational polynomial:

$$\phi_a|_{\alpha=0} = \frac{\gamma(x, y)}{\beta(x, y)}. \tag{4.11}$$

If α not zero then the branch which satisfies the boundary conditions is:

$$\phi_a = \frac{\beta(x, y) - \sqrt{\beta(x, y)^2 - 4\alpha\gamma(x, y)}}{2\alpha}. \tag{4.12}$$

In $\{x, y\}$ coordinates the quadrilateral representation must be analyzed as a rational or even irrational polynomial.

The type of equation is related to the geometry. A polynomial shape function can only represent a polygon whose opposite boundaries are parallel. Similarly a rational polynomial formulation applies to a trapezoid. And the irrational polynomial formulation applies to any other skew non-concave quadrilateral.

4.3 Padé approximation

The order of approximation can be increased without disturbing the linearity conditions. A higher order approximation can be constructed as a rational polynomial or Padé approximation. In one dimension:

$$f(x) + \epsilon f'(x) + \frac{\epsilon^2}{2} f''(x) + \frac{\epsilon^3}{6} f'''(x) + \frac{\epsilon^4}{24} f^{IV}(x) \approx \frac{f(x) + \alpha\epsilon + \beta\epsilon^2}{1 + \gamma\epsilon + \delta\epsilon^2} \tag{4.13}$$

Ignoring terms of order $O(\epsilon^5)$ the constants of the rational polynomial can be evaluated. If the evaluation is not close to the zeros of the approximation then the representation is valid [55].[2]

The degree of higher order representation then is dependent on the number of nodes n. The linear boundary, and the constancy and linearity requirements are not violated by the addition of a node to the Wachspress test function formulation. The basis functions for the convex polygon with n number of sides, are Padé approximations $\frac{p(x)}{q(x)}$ of order $(n-2)$ over $(n-3)$. In one dimension the Taylor series approximation of the function $f(x)q(x)-p(x)$ is of order $(2n-4)$. The denominator $q(x)$ is, by construction, non-zero within the domain.

Rational polynomial basis functions can be constructed according to the tenants of projective geometry. The shape function for an n sided convex

[2]Solving for the derivatives in terms of the constants:

$$\begin{aligned}
f(x) &\approx \sum_{i=1}^{n} N_i(x) f_i \\
f'(x) &\approx \alpha - \gamma \sum_{i=1}^{n} N_i(x) f_i \\
f''(x) &\approx 2(\beta - \alpha\gamma + (\gamma^2 - \delta) \sum_{i=1}^{n} N_i(x) f_i) \\
f'''(x) &\approx -6(\gamma(\beta - \alpha\gamma) + \alpha\delta + (\gamma^3 - 2\gamma\delta) \sum_{i=1}^{n} N_i(x) f_i) \\
f^{IV}(x) &\approx 24(\beta\gamma^2 - \alpha\gamma^3 - \beta\delta + 2\alpha\gamma\delta + (\gamma^4 - 3\gamma^2\delta + \delta^2) \sum_{i=1}^{n} N_i(x) f_i)
\end{aligned} \tag{4.14}$$

Accordingly approximations of higher order derivatives are constructed. The order of error with respect to the Taylor expansion is $O(\epsilon^5)$.

polygon can be constructed as a $n-2$ over $n-3$ order rational polynomial, see appendix B.4. Increasing the order of approximation requires an additional node. The node must be located such that the shape remains strictly convex. The denominator of the polynomial is determined from geometry, consequently only $n-2$ constants are minimized in the variational setting [61].

4.4 Quadratic Shafer (Hermite-Padé)

Higher order methods can further increase the order of approximation. Quadratic Shafer or Hermite-Padé approximates are an extension of the Padé form:

$$f(x)^2 \sum_{i=0}^{l} \alpha_i x^i - f(x) \sum_{i=0}^{k} \beta_i x_i + \sum_{i=0}^{j} \gamma_i x^i = O(x^{j+k+l+2}) \tag{4.15}$$

If the $\alpha_i \to 0$ then the rational polynomial form is recaptured. The singularity associated with the approximation is captured in the coefficient of the highest order $f(x)$ term. Consequently, for the quadratic interpolation, evaluation near the zeros of the α polynomial ($\sum_{i=0}^{l} \alpha_i x^i = 0$) must be avoided. Similarly, two branching approximations are formed using the quadratic representation. The appropriate branch must be chosen for the interpolation to be valid [55].[3]

The shape function for an element with a side node must be able to represent discontinuous linear boundary conditions. The polynomial and

[3]The interpolation can be constructed for any order: $\sum_{k=0}^{N} f^k(x) \sum_{n=0}^{m_k} A_{k,n} x^n = 0\left(x^{(\Sigma m_k + N)}\right)$ [55, pp. 449].

rational polynomial representations are necessarily smooth (or undefined) along a given line. Both can only represent the discontinuous hat function approximately. Quadratic Shafer representation, on the other hand, can be used to represent the boundary condition and the smooth domain with a limited number of terms. Similar boundary discontinuities are required for the representation of a concave domain.

Edge nodes have also been used to construct uniquely shaped elements. Wachspress derives an element interpolation as a projection of a three dimensional curved shape onto the two dimensional plane. The shape function for a side node is derived in terms of the other shape functions. Curved non-convex elements are constructed from the derivation [61, p. 245–253].

Irrational functions have been applied to degenerate elements in other contexts. Singularity elements have been applied to fracture mechanics problems for the analysis of stresses near a crack tip or a crack edge[4]. For such elements displacements and stresses are proportional to $r^{\frac{1}{2}}$ and $r^{-\frac{1}{2}}$ respectively, where r is the distance from the singular point. The singularities are introduced into the element by transformation. The singularity is captured in the Jacobian. In global cartesian $\{x, y\}$ coordinates the solution is an irrational polynomial.[5] The singularity elements applied to fracture mechanics

[4]The method of creating a singular element by displacing mid-side nodes was first introduced by Henshell and Shaw in 1975 [27]

[5]For example the coordinate transformation of a standard unit element with $0 \leq \rho \leq 1$ with an interior node at ah is [1, p. 282]:

$$x(\rho) = h(4a-1)\rho + 2h(1-2a)\rho^2 \quad \text{and} \quad J = \frac{\partial x}{\partial \rho} h(4a-1) + 4h(1-2a)\rho \qquad (4.16)$$

are generally restricted to quadratic and higher order isoparametric elements – where the edge behavior is not linear [63].

4.4.1 Degenerate side-node element

Singular behaviors related to point forces occurring along boundaries or at the vertex of a reentrant corner are well documented. The shape function representation can capture the peak at the concave point in the kinematic representation of a shape using a Quadratic Shafer representation. The representation of any element with a side node on a straight edge can be constructed according to the shape functions for the adjacent vertex nodes. Let the vertex shape functions for the element without a side node be denoted with an asterisk:

$$\phi_k = \frac{(1-(1-u)\phi_i^* - u\,\phi_{i-1}^*) - \sqrt{(1-(1-u)\phi_i^* - u\phi_{i-1}^*)^2 - 4u\,\phi_{i-1}^*(1-u)\phi_i^*}}{2u(1-u)} \quad (4.18)$$

The new shape functions for the parent nodes are updated to with respect to the side node:

$$\phi_i = \phi_i^* - (1-u)\phi_k \quad \text{and} \quad \phi_{i-1} = \phi_{i-1}^* - u\,\phi_k. \quad (4.19)$$

The function can be applied iteratively to describe any side noded element.[6]

If $a = \frac{1}{4}$ then the side node is located at $\frac{h}{4}$, also $x = h\rho^2$ and $\rho = \left(\frac{x}{h}\right)^{1/2}$. The inverse Jacobian captures the singularity:

$$J^{-1} = \frac{\partial \rho}{\partial x} = \frac{1}{2}(hx)^{\frac{1}{2}} \quad (4.17)$$

[6]Details of the derivation are described in a journal paper [41].

4.5 Numerical test: impact of the number of element nodes to the approximation

A test of the approximation is constructed by comparing linear edged shape functions to a function which is not necessarily linear along the boundary. All of the presented linear edged shape functions satisfy the constant and linear fields. Consequently the error in the shape functions with respect to a constant field, a linear field in x, or a linear field in y is zero, see figure 4.1. The matching of the shape functions to the field xy is better than

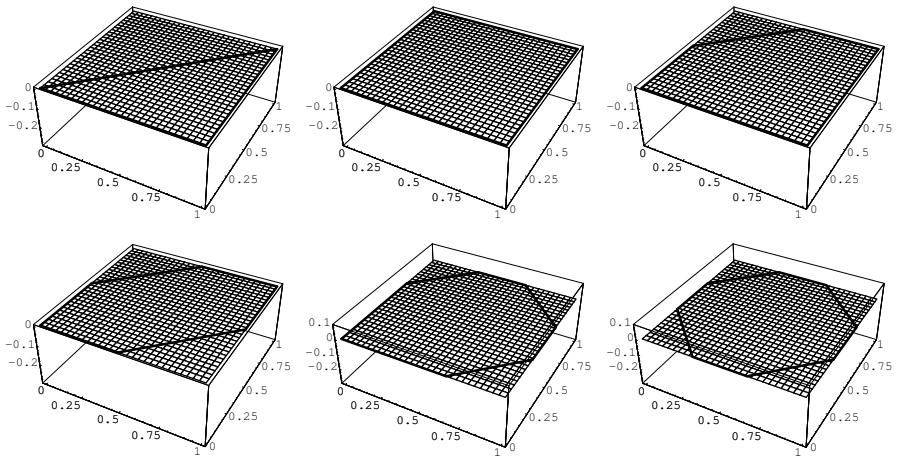


Figure 4.1: Error for constant and linear fields is zero

for the higher order terms because the function xy is linear along most of the boundary of the elements, see figure 4.2. The maximum error for each interpolation is 25% for the triangular element, the square is exact, 6.4% for the pentagon, 8.3% for the hexagon, 2.9% for the septagon and 2.9% for

the octagon. The other quadratic fields x^2 and y^2 are not approximated as exactly. Increasing the number of nodes only slightly increases the quality of the approximation, see figures 4.3 and 4.4. The error with respect to the x^2 field is: 25% for the triangle, quadrilateral and pentagon; 21% for the hexagon; and 20% for the septagon and octagon. The error with respect to the y^2 field is similarly high: 25% for the triangle, quadrilateral, pentagon, hexagon and septagon; and 20% for the octagon. Most of the error is related to the inability to capture the boundary behavior.

By increasing the number of side nodes without changing the shape of element the error is reduced more significantly, see figures 4.5 and figures 4.6. The error with respect to the x^2 field is 25% for the quadrilateral with four or five nodes; 17% for the six noded case, 16% for for the seven noded case and 14% for the eight noded case. For the eight noded element the largest error no longer occurs on the boundary, but rather in the interior of the domain.

Unlike the Lagrange element, the linear edged interpolations do not necessarily model polynomial fields exactly. Instead higher order behaviors are captured according to the Padé and Quadratic Shafer approximations.

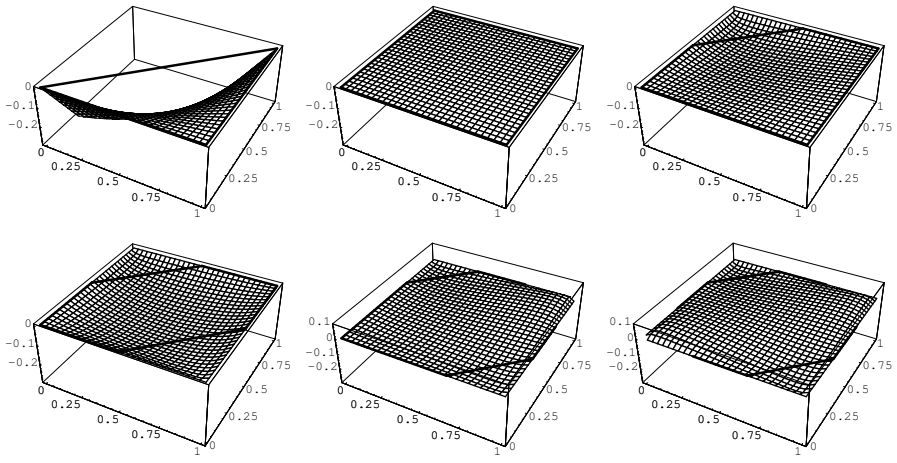


Figure 4.2: Error with respect to the field xy for a convex triangle, quadrilateral, pentagon, hexagon, septagon and octagon respectively

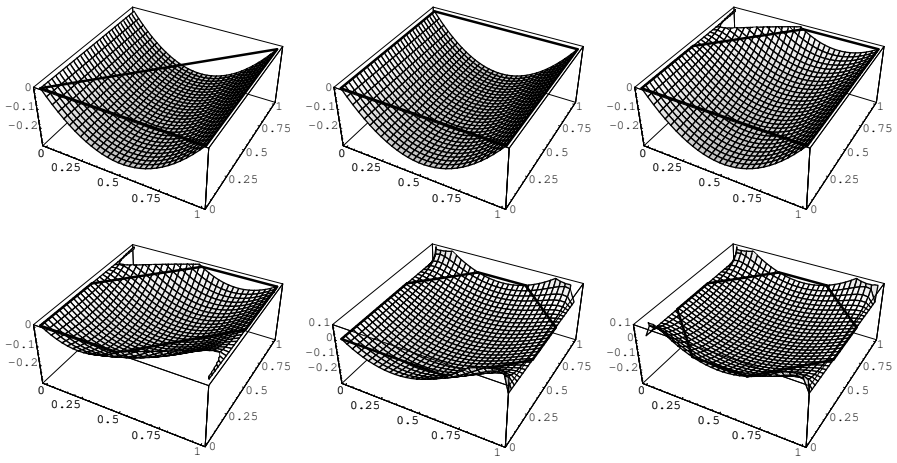


Figure 4.3: Error with respect to the field x^2 for a convex triangle, quadrilateral, pentagon, hexagon, septagon and octagon respectively

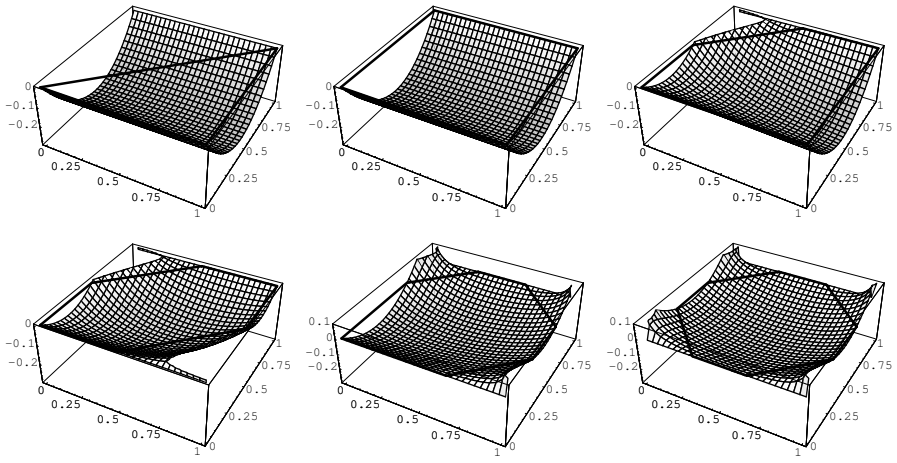


Figure 4.4: Error with respect to the field y^2 for a convex triangle, quadrilateral, pentagon, hexagon, septagon and octagon respectively

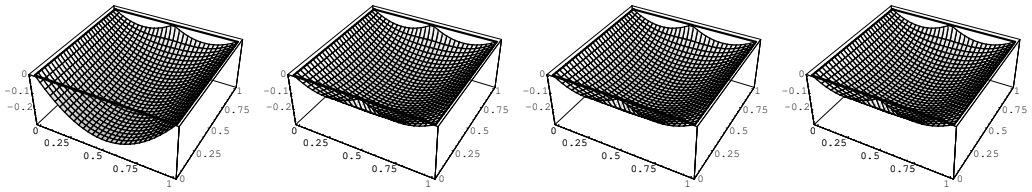


Figure 4.5: Error with respect to the quadratic x^2 field for a quadrilateral with five, six, seven and eight nodes

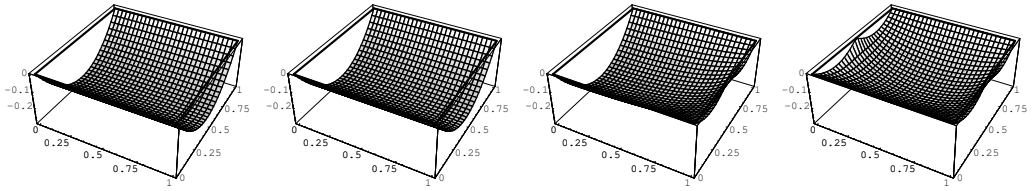


Figure 4.6: Error with respect to the quadratic y^2 field for a quadrilateral with five, six, seven and eight nodes

Shape	x^2	xy	y^2	x^3	x^2y	y^2x	y^3
triangle	0.25	0.25	0.25	0.38	0.38	0.38	0.38
quadrilateral	0.25	0.	0.25	0.38	0.25	0.25	0.38
pentagon	0.25	0.064	0.25	0.38	0.14	0.25	0.38
hexagon	0.17	0.083	0.17	0.264	0.17	0.17	0.264
septagon	0.16	0.029	0.16	0.245	0.08	0.08	0.245
octagon	0.14	0.029	0.14	0.22	0.075	0.075	0.22

The approximation with respect to some of the higher order fields is better than the approximation to the lower order fields.

The side node elements similarly capture some of the higher order fields:

Number of Nodes	x^2	xy	y^2	x^3	x^2y	y^2x	y^3
4	0.25	0.	0.25	0.38	0.25	0.25	0.38
5	0.25	0.	0.25	0.38	0.13	0.25	0.38
6	0.21	0.	0.25	0.32	0.13	0.25	0.38
7	0.20	0.	0.25	0.32	0.13	0.13	0.38
8	0.20	0.	0.20	0.32	0.13	0.13	0.322

These side node elements capture the lower order quadratic modes better than the convex polygonal element but are less equipped to represent the higher order modes. As predicted by the Padé and Quadratic Shafer approximations, the impact of adding an additional node is spread out over a range of higher order modes.

Consequently, using linear edged elements allows for the exact modeling of lower order constant and linear modes while capturing some of the higher

order effects of the function being modeled.

4.5.1 Comparison of the general methods

The general zeroth order and first order methods, from section §3.3, can be applied as interpolations. The zeroth order method represents the constant field exactly, but not linear fields. It can be applied to any shape:

Shape	x	y	x^2	xy	y^2
triangle	0.29	0.29	0.32	0.38	0.53
quadrilateral	0.12	0.12	0.32	0.17	0.32
pentagon	0.33	0.087	0.33	0.27	0.25
hexagon	0.33	0.33	0.22	0.28	0.22
septagon	0.23	0.23	0.20	0.20	0.20
octagon	0.23	0.23	0.20	0.19	0.20

The zeroth order method can also be applied to elements with side nodes:

Number of Nodes	x	y	x^2	xy	y^2
4	0.12	0.12	0.32	0.17	0.32
5	0.12	0.08	0.31	0.17	0.26
6	0.12	0.09	0.28	0.17	0.30
7	0.098	0.098	0.25	0.17	0.29
8	0.098	0.098	0.25	0.17	0.25

The error in the lower order fields x and y is of the same magnitude as the error of the rational polynomial elements to the higher order fields x^2, y^2 and

xy. Generally, as the number of nodes increase, the approximation better matches both the lower order and higher order solutions. Unlike the rational polynomial element example, the convergence is not monotonic.

The general linear method applies only to domains defined by boundary lines meeting at right angles. It can be used to describe convex and concave domains. Two such domains are defined by the following sets of nodes:

$$\{\{0,0\},\{2,0\},\{2,2\},\{0,2\}\}, \tag{4.20}$$

and

$$\{\{0,0\},\{2,0\},\{2,1\},\{1,1\},\{1,2\},\{0,2\}\}. \tag{4.21}$$

Comparing approximations for the zeroth order, linear edged and first order interpolations:

Number of Nodes	x	y	x^2	xy	y^2
4: zeroth order	0.24	0.24	1.29	0.68	1.28
6: zeroth order	0.16	0.16	0.96	0.30	0.96
4: linear edged right angled	0.20	0.26	1.18	0.51	1.18
6: linear edged right angled	0.16	0.16	1.0	0.26	1.0
4: linear edged general	.090	.090	.27	0.14	0.25
6: linear edged general	0.13	0.13	0.27	0.18	0.30
4: first order	0	0	1.0	0.51	1.0
6: first order	0	0	1.0	0.26	1.0

The error should be considered with respect to the area of the element; for example the 2×2 elements should be less acurate than the 1×1 sized elements.

The general linear edged concave elements are on the 1×1 scale with the following nodal positions, for the quadrilateral:

$$\{\{1,1\},\{0,1\},\{0,0\},\{1/4,3/4\}\}$$

and

$$\{\{1,1\},\{0,1\},\{0,0\},\{7/8,0\},\{1/2,1/2\},\{1,1/8\}\}$$

The method applies to any shape with any edge angles. The approximations compare well to the zeroth order approximations on non-concave shapes, see figure 4.7. The pointiness of the reentrant corner does not seem to adversly affect the test function performance, see figure 4.8.

Accordingly, the error is similar to that for convex shapes. Elements with more nodes capture higher order fields. The linear interpolations can capture linear fields exactly, while the linear edged interpolations cannot. The concavity in the domain does not hinder the interpolation.

4.5.2 Counter example to closure

The examples suggest that linear interpolations would converge monotonically to any order field if enough nodes are used. Unfortunately that is not the case. A linear interpolation alone can not be used to represent the be-

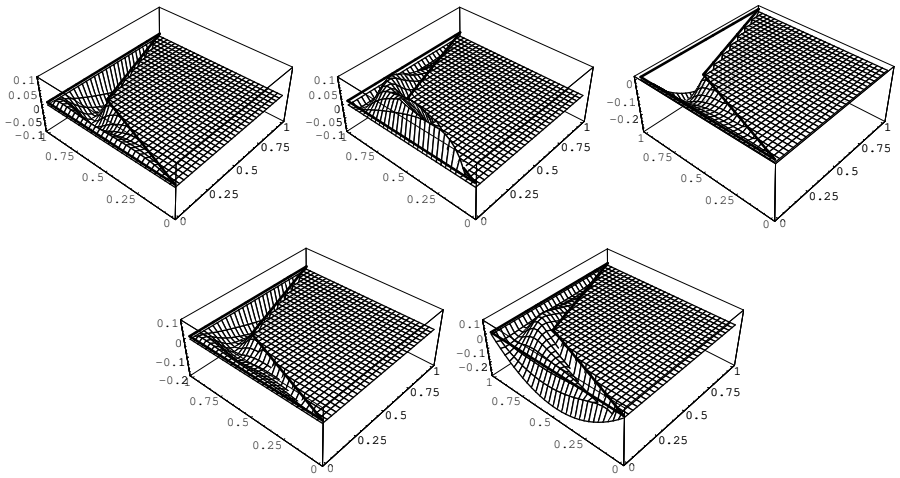


Figure 4.7: Error with respect to the field x, y, x^2, xy and y^2 for a reentrant quadrilateral

havior of any domain governed by Dirichlet boundary conditions. A linear edged interpolation is not unique with respect to a given set of boundary data. For example, a skew quadrilateral can be represented either by a rational polynomial or an irrational polynomial formulation, see §2.2.2. Neither formulation will approach the other as the number of side nodes increases.

For example, given a skew quadrilateral with the following vertex nodes:

$$\{\{0,0\},\{1,0\},\{2,2\},\{0,1\}\} \tag{4.22}$$

The rational polynomial interpolation for the third node is:

$$\frac{3\,x\,y}{2\,(2+x+y)} \tag{4.23}$$

The isoparametric interpolation is:

$$\frac{1+x+y-\sqrt{4\,x+(1-x+y)^2}}{2} \tag{4.24}$$

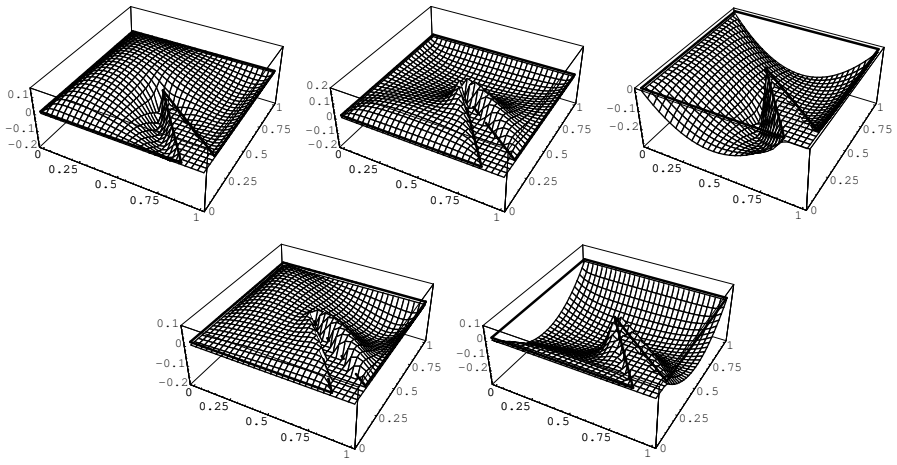


Figure 4.8: Error with respect to the field x, y, x^2, xy and y^2 for a reentrant hexagon

Both representations are smooth and bounded within the domain and satisfy the same boundary conditions. The maximum error between the two representations is 1.3%, see figure 4.9. Since the boundary conditions are satisfied exactly, adding side nodes will not decrease the relative differences between the approximations, see §4.4.1.

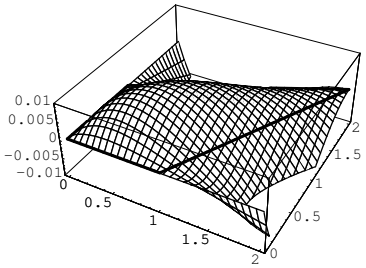


Figure 4.9: Error between two linear skew quadrilateral representations

4.6 Interior behavior and convergence

A boundary dependent geometric test function will never converge to the exact solution unless an interior variables are added to the formulation. If only boundary data is given the field equation has no effect on a solution described only by boundary interpolations. To capture the effect, an interior point representation must be used. The influence of the exterior displacements $u_b(\vec{x})$ described by the geometric test functions, can be separated from the influence of interior displacements $u_i(\vec{x})$:

$$u(\vec{x}) = u_b(\vec{x}) + u_i(\vec{x}) \quad \text{and} \quad \mathcal{L}[u(\vec{x})] = f(\vec{x}) \tag{4.25}$$

$$\mathcal{L}[u_i(\vec{x})] = f(\vec{x}) - \mathcal{L}[u_b(\vec{x})] \tag{4.26}$$

Describing interior points without discretization is the subject of ongoing research.

If the object of interpolation is a functional operator, and not a specific field behavior, a very close solution can be constructed. Adding nodal points, even along the boundary, increases the number of degrees of freedom available to represent the continuous operator as a linear operator. Each additional node can capture a higher order behavior.

Chapter 5

Elliptic operator solution approximation using a variational form

A test function used to approximate an elliptic operator need only be analytic and bounded inside the domain. Consequently, the singularities associated with a rational or irrational polynomial need not be detrimental to the efficacy of an approximation, provided they do not occur in the interior of the domain. Interpolations constructed to satisfy terms of a general Hermite-Padé Approximation can describe more complicated geometric regions while introducing singular points only along the boundary.

The applicability of such interpolations to finite elements is limited by integration and algebraic simplicity requirements. When a singularity is

confined to the boundary of the finite element the domain remains integrable in a distributional sense. The shape functions are locally integrable at every point except where the singularity occurs [56, pp. 31–34][1]. When evaluating such a function numerically care must be given around the singular points.

5.1 The potential problem

An approximate solution to Laplace's equation on any given domain $\mathcal{D}$ is constructed by replacing the partial differential equation with a variational representation:[2]

$$\nabla^2 u(x,y) \quad \text{becomes} \quad \int_{\mathcal{D}} \frac{\partial u(x,y)}{\partial x}^2 + \frac{\partial u(x,y)}{\partial y}^2 \mathrm{d}A. \tag{5.1}$$

and conditions for the boundary of the domain Γ. The solution state $u(x,y)$ is assumed such that either the essential boundary conditions are satisfied or the field equation is satisfied. The shape functions which satisfy linear interpolation requirements also satisfy linear geometric boundary conditions, see equations 1.1, 1.2, B.26 and 4.18. Accordingly the displacement based approximation is constructed from the polynomial, rational polynomial, or irrational polynomial interpolations:

$$u(x,y) = \sum_{i=1}^{N} u_i N_i(x,y) \tag{5.2}$$

Where $N_i(x,y)$ satisfies only the Dirichlet —prescribed temperature— boundary conditions on Γ for $u(x,y)$. The variational form then can be minimized

[1] A specific example is given in the reference see example 2 pp. 38–39 [56].
[2] Variational calculus or Weighted Residual

according to the nodal values. The conductivity matrix becomes:

$$S_{ij} = \int_{\mathcal{D}} \frac{\partial N_i(x,y)}{\partial x}\frac{\partial N_j(x,y)}{\partial x} + \frac{\partial N_i(x,y)}{\partial y}\frac{\partial N_j(x,y)}{\partial y}\mathrm{d}A \tag{5.3}$$

If the shape functions satisfy the linear interpolation conditions, then they also satisfy the rigid body conditions. Accordingly, the conductivity matrix $S_{ij}(x,y)$ is singular. All of its eigenvalues, save one, are strictly positive. The matrix S_{ij} relates the prescribed temperature to the temperature flux along the boundary:

$$Q_j = S_{ij}u_j \tag{5.4}$$

The approximate solution can be constructed according to Courant Triangulation. While the solution is not smooth within the domain it does approach the actual at a rate of $O(h^2)$ where h is a linear measure of the size of triangulation [57, pp. 105–116]. The solution converges if the set of shape functions is closed with respect to the actual solution. The boundary test function formulation is not closed. It does however, provide an ever better approximation to the solution as the number of points increases [46, 57]. An interior point formulation is the subject of further research [39].

5.1.1 Test case: triangulation vs. side nodes

Solving Laplace's equation on a unit square with nodal coordinates located at $\{\{0,0\},\{1,0\},\{1,1\},\{0,1\}\}$, the eigenfunction solution is given in §1.2.1:

$$\frac{\partial^2 u(x,y)}{\partial x^2} + \frac{\partial^2 u(x,y)}{\partial y^2} = 0 \tag{5.5}$$

Either heat or heat flux conditions are given for every point along the boundary. Three approaches to solving the boundary value problem approximately using the finite element method are: triangulation, higher order Lagrange elements and irrational shape functions which accommodate side nodes.

Triangulation

Dividing the domain into two triangles with nodes $\{\{0,0\},\{1,0\},\{0,1\}\}$ and $\{\{1,0\},\{1,1\},\{0,1\}\}$ and applying linear shape functions results in the following conductivity matrix:

$$S_4^{\triangle} = \begin{pmatrix} 2 & -1 & -1 & 0 \\ -1 & 2 & 0 & -1 \\ -1 & -1 & 2 & -1 \\ 0 & -1 & -1 & 2 \end{pmatrix} \tag{5.6}$$

The conductivity matrix relates heat sources at $\{\{0,0\},\{1,0\},\{0,1\},\{1,1\}\}$ to heat fluxes at the same locations.

Dividing the domain into three triangles with nodes $\{\{0,0\},\{1,0\},\{1/2,1\}\}$, $\{\{1/2,1\},\{1,0\},\{1,1\}\}$ and $\{\{0,0\},\{1/2,1\},\{0,1\}\}$ and applying linear shape functions results in the following conductivity matrix:

$$S_5^{\triangle} = \begin{pmatrix} 7/4 & -3/4 & -1/2 & 0 & -1/2 \\ -3/4 & 13/4 & -1/2 & -2 & 0 \\ -1/2 & -1/2 & 7/2 & -1/2 & 2 \\ 0 & -2 & -1/2 & 5/2 & 0 \\ -1/2 & 0 & -2 & 0 & 5/2 \end{pmatrix} \tag{5.7}$$

The conductivity matrix relates heat sources at
$\{\{0,0\},\{1,0\},\{1/2,1\},\{1,1\},\{0,1\}\}$ to heat fluxes at the same location.

Dividing the domain into four triangles with nodes
$\{\{0,0\},\{1,0\},\{1/2,1/2\}\},\{\{1/2,1/2\},\{1,0\},\{1,1\}\},\{\{1,1\},\{0,1\},\{1/2,1/2\}\}$
and $\{\{0,1\},\{0,0\},\{1/2,1/2\}\}$ and applying linear shape functions results in
the following conductivity matrix:

$$S_{5'}^{\triangle} = \begin{pmatrix} 2 & 0 & -2 & 0 & 0 \\ 0 & 2 & -2 & 0 & 0 \\ -2 & -2 & 8 & -2 & -2 \\ 0 & 0 & -2 & 2 & 0 \\ 0 & 0 & -2 & 0 & 2 \end{pmatrix} \tag{5.8}$$

The conductivity matrix relates heat sources at
$\{\{0,0\},\{1,0\},\{1/2,1/2\},\{1,1\},\{0,1\}\}$ to heat fluxes at the same location.

Dividing the domain into six triangles with nodes
$\{\{0,0\},\{1/2,0\},\{0,1/2\}\},\{\{1/2,0\},\{1,0\},\{1,1/2\}\},\{\{1,1/2\},\{1/2,0\},\{1,1/2\}\}$,
$\{\{0,1/2\},\{1,1/2\},\{1/2,1\}\},\{\{1/2,1\},\{1,1/2\},\{1,1\}\}and\{\{0,1/2\},\{1/2,1\},\{0,1\}\}$
and applying linear shape functions results in the following conductivity ma-

trix:

$$S_8^{\triangle} = \begin{pmatrix} 2 & -1 & -1 & 0 & 0 & 0 & 0 & 0 \\ -1 & 4 & -1 & -1 & -1 & 0 & 0 & 0 \\ -1 & -1 & 4 & 0 & 0 & -1 & 0 & -1 \\ 0 & -1 & 0 & 2 & -1 & 0 & 0 & 0 \\ 0 & -1 & 0 & -1 & 4 & -1 & -1 & 0 \\ 0 & 0 & -1 & 0 & -1 & 4 & -1 & -1 \\ 0 & 0 & 0 & 0 & -1 & -1 & 2 & 0 \\ 0 & 0 & -1 & 0 & 0 & -1 & 0 & 2 \end{pmatrix} \tag{5.9}$$

The conductivity matrix relates heat sources at
$\{\{0,0\},\{1/2,0\},\{0,1/2\},\{1,0\},\{1,1/2\},\{1/2,1\},\{1,1\},\{0,1\}\}$ to heat fluxes at the same location.

Lagrange Interpolation

Lagrange interpolation over the same domain for similar edge conditions results in the following matrices for a square elements with nodes at $\{\{0,0\},\{1,0\},\{1,1\},\{0,1\}\}$, $\{\{0,0\},\{1,0\},\{1,1\},\{1/2,1\},\{0,1\}\}$ and
$\{\{0,0\},\{1/2,0\},\{1,0\},\{1,1/2\},\{1,1\},\{1/2,1\},\{0,1\},\{0,1/2\}\}$ respectively:

$$S_4^{\diamond} = \begin{pmatrix} 1 & -1 & 0 & -1 \\ 1 & 1 & -1 & 0 \\ 1 & -1 & 0 & 1 \\ 1 & 1 & 1 & 0 \end{pmatrix}, \tag{5.10}$$

$$S_5^{\diamond} = \begin{pmatrix} 4/3 & -1/3 & -1/3 & 2/3 & 0 \\ -1/3 & 4/3 & 0 & -2/3 & -1/3 \\ -1/3 & 0 & 82/45 & -74/45 & 7/45 \\ -2/3 & -2/3 & -74/45 & 208/45 & -74/45 \\ 0 & -1/3 & 7/45 & -74/45 & 82/45 \end{pmatrix} \tag{5.11}$$

and

$$S_8^{\diamond} = \begin{pmatrix} 56/45 & -2/5 & -1/15 & 2/9 & -2/45 & 2/9 & -1/15 & -2/5 \\ -2/5 & 176/45 & -2/5 & -32/45 & 2/9 & 0 & 2/9 & -32/45 \\ -1/15 & -2/5 & 56/45 & -2/5 & -1/15 & 2/9 & -2/45 & 2/9 \\ 2/9 & -32/45 & -2/5 & 176/45 & -2/5 & -32/45 & 2/9 & 0 \\ -2/45 & 2/9 & -1/15 & -2/5 & 56/45 & -2/5 & -1/15 & 2/9 \\ 2/9 & 0 & 2/9 & -32/45 & -2/5 & 176/45 & -2/5 & -32/45 \\ -1/15 & 2/9 & -2/45 & 2/9 & -1/15 & -2/5 & 56/45 & -2/5 \\ -2/5 & -32/45 & 2/9 & 0 & 2/9 & -32/45 & -2/5 & 176/45 \end{pmatrix} . \tag{5.12}$$

The conductivity matrices relates heat sources located at node $\{0, 0\}$ and following counter clockwise around the square to heat fluxes at the same locations.

Linear edged irrational shape function

The irrational linear edged shape functions are algebraically more complicated. Consequently the integration of the conductivity matrices is evaluated numerically. The four noded approximation is equal to the Lagrange

formulation. The conductivity matrices for five and eight noded elements:

$$\hat{S}_5 = \begin{pmatrix} 1.33 & -0.333 & -0.417 & -0.500 & -0.0833 \\ -0.333 & 1.33 & -0.0833 & -0.500 & -0.417 \\ -0.417 & -0.0833 & 1.57 & -0.980 & -0.0933 \\ -0.500 & -0.500 & -0.980 & 2.96 & -0.980 \\ -0.0833 & -0.417 & -0.0933 & -0.980 & 1.57 \end{pmatrix} \tag{5.13}$$

and

$$\hat{S}_8 = \begin{pmatrix} 1.6 & -0.72 & 0.12 & -0.19 & -0.021 & -0.19 & 0.12 & -0.72 \\ -0.72 & 3.0 & -0.72 & -0.53 & -0.19 & -0.099 & -0.19 & -0.53 \\ 0.12 & -0.72 & 1.5 & -0.72 & 0.12 & -0.19 & 0.021 & -0.19 \\ -0.18 & -0.53 & -0.71 & 3.0 & -0.72 & -0.53 & -0.19 & -0.099 \\ 0.021 & -0.19 & 0.12 & -0.72 & 1.55 & -0.72 & 0.12 & -0.19 \\ -0.19 & -0.099 & -0.19 & -0.53 & -0.72 & 3.0 & -0.72 & -0.53 \\ 0.12 & -0.19 & 0.021 & -0.19 & 0.12 & -0.72 & 1.55 & -0.72 \\ -0.72 & -0.53 & -0.19 & -0.099 & -0.19 & -0.53 & -0.72 & 2.96 \end{pmatrix} \tag{5.14}$$

The nodes and edge sources for the five noded element are located at

$\{\{0,0\},\{1,0\},\{1,1\},\{1/2,1\},\{0,1\}\}$

and the eight noded element's nodes are located at

$\{\{0,0\},\{1/2,0\},\{1,0\},\{1,1/2\},\{1,1\},\{1/2,1\},\{0,1\},\{0,1/2\}\}$.

5.2 Interpolation and stability

All of the interpolations which satisfy the constancy and linearity requirements and are conformal on the domain should converge to the solution

according to the patch test condition [30, 57]. The shape functions applied to a domain tessellated into triangles satisfy the constancy and linearity conditions by construction. Similarly the Lagrange interpolation does not necessarily satisfy the condition. Satisfaction of the constancy condition is reflected in the singularity of the conductivity matrix. One eigenvalue is zero. The conductivity matrix is positive, and accordingly all the non-zero eigenvalues are positive.

The eigenvalues for the conductivity matrices in the given examples are:

Shape function type:	Number of nodes :	Eigenvalues:	condition number
2 triangles	4	$\{0, 2, 2, 4\}$	2
3 triangles	5	$\{0, 1.2, 2.1, 5, 5.1\}$	4.25
4 triangles	5	$\{0, 2, 2, 10\}$	5
6 triangles	8	$\{0, 1.3, 1.3, 4.2, 4.7, 4.7\}$	3.62
Linear Lagrange	4	$\{0, 4/3, 2, 2\}$	1.5
Asymmetric Lagrange	5	$\{0, 1.3, 1.5, 2, 6.1\}$	4.69
Quadratic Lagrange	8	$\{1.0, 1.0, 1.0, 1.3,$ $2.6, 4.2, 4.2, 5.3\}$	5.4
Linear^3	4	$\{0, 4/3, 2, 2\}$	1.5
Linear with one side node	5	$\{0, 1.33, 1.60, 1, 3.85\}$	3.16
Linear with symmetric side nodes	8	$\{0, 1.22, 1.22, 1.33,$ $3.36, 3.36, 3.62, 3.91\}$	3.20

All of the examples except the Quadratic Lagrange element for an eight noded square can reproduce a constant field.

Accordingly, an approximate solution constructed for such an element contains spurious modes. If an additional node is included in the center of the element, like it was for the four triangle example, the constancy condition would be recaptured. Such an additional shape function which is zero along the boundary and single valued somewhere in the domain is termed a bubble function. This example fails because the bubble function is missing, others fail because it is added to an otherwise compliant element. The inability to capture the constant and linear fields is a pathology associated with bubble function construction [38, pp. 486–492].

Additionally, the shape functions for the non-linear Lagrange elements are not necessarily bounded according to the Chebyshev condition. An unbounded assumption is especially troublesome if a bounded value, such as temperature in Kelvin, is being distributed [41]. Slowly convergent oscillatory solutions are a pathology associated with Lagrange elements [50].

The range of the eigenvalues also has an impact on the efficacy of the approximation. For a general Ritz approximation to converge the eigenvalues of the stiffness or conductivity matrix $[K]$ (of $[K]\{u\} = \{f\}$) are all positive and bounded. The speed and stability of the approximation is dependent on the maximum and minimum eigenvalue. The eigenvalues associated with the increasing the degrees of freedom, and consequently order of approximation, can not exhibit an unbounded increase, or decrease. [46, pp. 158–159]:

$$0 \leq C_1 \leq \lambda_k^{(n)} \leq C_2 \leq \infty \tag{5.15}$$

Where λ_k are the eigenvalues which are not associated with eigenvectors

which do not produce energy (non-zero eigenvalues). The Ritz approximation in general finds only the minimum eigenvalues, not the best eigenvector solution of a given variational problem [56].

In the simple examples given in the previous section all of the eigenvalues are positive and none apper to be unreasonably large or small. Only the eigenvalue for the bubble-function-like mode in the four node triangle approximation, with a value of 10, is significantly larger than the others in that group, which vary between 1.2 and 5.1. The domain tessellation introduces an additional uncertainty to the approximation. The continuity of the domain is not preserved and the eigenvalues are not directly functions of the number of nodes. The choice of how the domain is tessellated also effects the computation [21, 67].

The addition of any data point irrespective of location, improves the approximate solution [46, p.159]. Consequently it is more convenient to add solution points on the boundary then in the domain. This avoids tessellation and preserves smoothness. Furthermore, the order of approximation within the element is increased if the elements contain more data, see §4.

In this example, the linear edged elements are the most well behaved. The zero eigenvalues are preserved and the range of positive eigenvalues is bounded between one and four. The singularity associated with the mid-side node did not add spurious data into the computation. The smoothness of the domain is not compromised. The formulation is integrable, although algebraically more complicated than the others. The representation preserves

the boundedness and smoothness over the domain.

5.2.1 Single element properties

The linear edged shape functions satisfy constant and linear fields by construction, see equation 1.7. Accordingly, the constant gradient patch tests should be satisfied automatically. However, some losses in precision are incurred using numerical integration. The numerical integration is performed using a five point gaussian quadrature scheme, a more sophisticated method would render better results. An algebraic method would render exact results.

If a constant heat source $\bar{u}(x, y)$ is applied along the entire boundary of an element, the corresponding heat flux should be zero. If the linear heat source is $\bar{u}(x, y) = x$ the heat flux: along the left boundary, between nodes $\{0, 1\}$ and $\{0, 0\}$ is negative one; along the right boundary, between nodes $\{1, 0\}$ and $\{1, 1\}$ is one; and the top and bottom boundaries exhibit zero flux. If the linear heat source is $\bar{u}(x, y) = y$ the heat flux: along the bottom boundary, between nodes $\{0, 0\}$ and $\{1, 0\}$ is negative one; along the top boundary, between nodes $\{1, 1\}$ and $\{0, 1\}$ is one; and the right and left boundaries exhibit zero flux.

Shape function type	heat flux at nodes caused by linear field (in x)	heat flux at nodes caused by linear field (in y)
Lagrange 4	$\{-1, 1, 1, -1\}$	$\{-1, -1, 1, 1\}$
Lagrange 8	$\{\frac{1}{45}, \frac{16}{15}, \frac{31}{45}, \frac{12}{5}, \frac{31}{45}, \frac{16}{15}, \frac{1}{45}, -\frac{4}{15}\}$	$\{\frac{1}{45}, -\frac{4}{15}, \frac{1}{45}, \frac{16}{15}, \frac{31}{45}, \frac{12}{5}, \frac{31}{45}, \frac{16}{15}\}$
Linear Edge 5	$\{-1, 1, 1, 0, -1\}$	$\{-1, 1, \frac{1}{2}, 1, \frac{1}{2}\}$
Linear Edge 8	$\{-\frac{1}{2}, 0, \frac{1}{2}, 1, \frac{1}{2}, 0, -\frac{1}{2}, 1\}$	$\{-\frac{1}{2}, -1, -\frac{1}{2}, 0, \frac{1}{2}, 1, \frac{1}{2}, 0\}$

Heat flux is a value per unit length. The result at the nodes is the linear combination of the total heat flux over each adjacent boundary. The integration error for the five and eight node linear edged element was on the order of 10^{-7} and 10^{-6} respectively. The integration over the Lagrange element is exact. The constant flux patch test condition is satisfied by all of the linear edged elements. Since the linear edged elements are conformal, the general many element patch test is also satisfied [38, pp. 193–194]. The eight noded Lagrange element does not pass the test. This result is similar to that found by the eigenvalue test.

5.2.2 Closure test for the skew quadrilateral

The rational polynomial and isoparametric skew quadrilateral formulations both satisfy the eigenvalue test and the constant strain patch test. As linear interpolations one formulation can not be used to approximate the other, see §4.5.2. As test functions both formulations can be used to approximate the solution to a boundary value problem. The conductivity matrix from the

isoparametric formulation is:

$$\tilde{S}_{iso} = \begin{pmatrix} 1.47 & -0.648 & -0.175 & -0.648 \\ -0.648 & 2.43 & -0.216 & -1.56 \\ -0.175 & -0.216 & 0.608 & -0.216 \\ -0.64 & -1.57 & -0.216 & 2.43 \end{pmatrix} \tag{5.16}$$

The conductivity matrix for the rational polynomial formulation is:

$$\tilde{S}_{rat} = \begin{pmatrix} 1.38 & -0.588 & -0.206 & -0.558 \\ -0.588 & 2.39 & -0.196 & -1.61 \\ -0.206 & -0.196 & 0.598 & -0.196 \\ -0.588 & -1.61 & -0.196 & 2.39 \end{pmatrix} \tag{5.17}$$

The eigenvalues are:

$$\text{eig}_{iso} = \{0., .810, 2.14, 4.\} \quad \text{and} \quad \text{eig}_{rat} = \{0., .797, 1.96, 4.\}. \tag{5.18}$$

The difference between the eigenvalues of the two formulations is on the order of .1. The rational polynomial formulation is slightly more flexible than the isoparametric formulation and consequently closer to the actual solution [44, 46].

Also, the rational polynomial element can be used to approximate the solution to the elliptic function which the isoparametric element satisfies, equation 2.35. Rewriting in variational form:

$$(1 + (x-y)^2 + 2y)\left(\frac{\partial \phi}{\partial x}\right)^2 + 2(x + x^2 + y - 2xy + y^2)\left(\frac{\partial \phi}{\partial y}\frac{\partial \phi}{\partial x}\right)$$
$$+((1+x)^2 - 2xy + y^2)\left(\frac{\partial \phi}{\partial y}\right)^2$$

The result derived using the isoparametric element is the minimum result possible:

$$\mathbf{S}_{iso} = \begin{pmatrix} 7/3 & -1/2 & -4/3 & -1/2 \\ -1/2 & 8/3 & -5/6 & -4/3 \\ -4/3 & -5.6 & 3 & -5/6 \\ -1/2 & -4/3 & -8/3 & 8/3 \end{pmatrix} \tag{5.19}$$

The approximate result derived using the rational polynomial interpolation:

$$\mathbf{S}_{rat} = \begin{pmatrix} 2.298 & -.492 & -1.31 & -.492 \\ -0.492 & 2.67 & -0.85 & -1.323 \\ -1.31 & -0.85 & 3.02 & -0.852 \\ -0.492 & -1.323 & -.852 & 2.672 \end{pmatrix} \tag{5.20}$$

The associated eigenvalues are:

$$\text{eig}_{iso} = \{4.149, 4, 2.516, 0\} \quad \text{and} \quad \text{eig}_{rat} = \{4.148, 4, 2.512, 0\} \tag{5.21}$$

The error in the interpolations is close to 10%, the error in the approximation of the eigenvalue is closer to 0.1%. The Rayleigh Ritz method effectively finds eigenvalues if the assumed function satisfies the essential boundary conditions, and the smoothness requirements. If in addition, the combination of functions satisfy the constant and linear fields exactly and boundary conditions in the interior are known; then a convergent finite element solution can be used to find the eigenfunction behavior in the domain.

5.2.3 Test case: concavity

The zeroth order linear edged shape function can be also be used to approximate the solution of this boundary value problem. The constant temperature

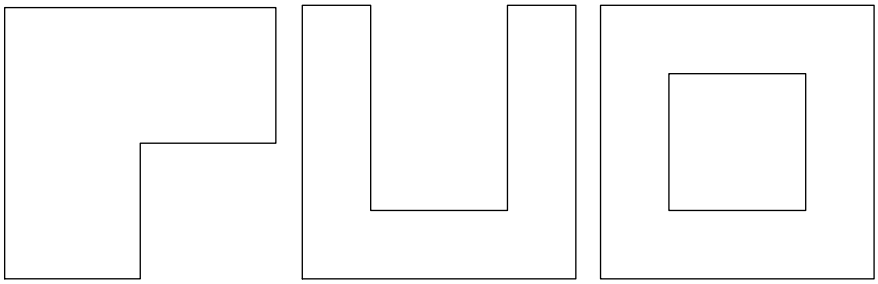


Figure 5.1: **L**, **U** and **O** shaped concave domains.

case is captured. Given a six node **L**, **U** and **0** shaped elements with nodes:
$\{\{0,0\},\{1/2,0\},\{1/2,1/2\},\{1,1/2\},\{1,1\},\{0,1\}\}$,
$\{\{0,0\},\{1,0\},\{1,1\},\{3/4,1\},\{3/4,1/4\},\{1/4,1/4\},\{1/4,1\},\{0,1\}\}$ and
$\{\{0,0\},\{1,0\},\{1,1\},\{0,1\},\{1/4,1/4\},\{3/4,1/4\},\{3/4,3/4\},\{1/4,3/4\}\}$. The following conductivity matrices result:

$$S_6^{\mathbf{L}} = \begin{pmatrix} 2.1 & -1.1 & -0.96 & -0.10 & -0.13 & 0.15 \\ -1.1 & 2.8 & -0.68 & -0.44 & -0.075 & -0.55 \\ -0.96 & -0.68 & 3.3 & -0.52 & -0.208563 & -0.95 \\ -0.10 & -0.44 & -0.52 & 1.3 & -0.0177575 & -0.17 \\ -0.13 & -0.075 & -0.21 & -0.018 & 0.444222 & -0.020 \\ 0.15 & -0.55 & -0.95 & -0.17 & -0.020 & 1.6 \end{pmatrix},$$

$$S_8^{\mathbf{U}} = \begin{pmatrix} 4.9 & 1.2 & -0.016 & -0.039 & -1.4 & -4.8 & -1.21 & 1.4 \\ 1.2 & 4.8 & 1.4 & -1.2 & -4.8 & -1.4 & -0.039 & -0.016 \\ -0.016 & 1.4 & 3.8 & -3.08 & -2.0 & -0.054 & -0.11 & 0.016 \\ -0.039 & -1.2 & -3.08 & 4.0 & 1.2 & -0.22 & -0.51 & -0.11 \\ -1.4 & -4.8 & -2.0 & 1.2 & 6.6 & 0.72 & -0.22 & -0.054 \\ -4.8 & -1.4 & -0.054 & -0.22 & 0.72 & 6.6 & 1.2 & -2.0 \\ -1.2 & -0.039 & -0.11 & -0.51 & -0.22 & 1.2 & 4.0 & -3.1 \\ 1.4 & -0.016 & 0.016 & -0.11 & -0.054 & -2.0 & -3.1 & 3.8 \end{pmatrix}$$

and

$$S_8^{\mathbf{O}} = \begin{pmatrix} 4.8 & 1.6 & 0.21 & 1.6 & -4.4 & -1.75 & -0.28 & -1.7 \\ 1.6 & 4.8 & 1.6 & 0.21 & -1.7 & -4.4 & -1.7 & -0.28 \\ 0.21 & 1.6 & 4.8 & 1.6 & -0.28 & -1.7 & -4.4 & -1.7 \\ 1.6 & 0.21 & 1.6 & 4.8 & -1.75 & -0.28 & -1.7 & -4.4 \\ -4.4 & -1.7 & -0.28 & -1.74 & 6.0 & 1.0 & 0.05 & 1.0 \\ -1.7 & -4.4 & -1.7 & -0.3 & 1.0 & 6.0 & 1.0 & 0.05 \\ -0.28 & -1.7 & -4.4 & -1.7 & 0.055 & 1.0 & 6.0 & 1.0 \\ -1.7 & -0.28 & -1.7 & -4.4 & 1.0 & 0.055 & 1.0 & 6.0 \end{pmatrix}.$$

Constructing shape functions for an element with a concavity can be achieved using the same algorithms, see §3.3.2. Consequently, while the **U** and **O** shapes have different conductivity matrices, they have very similar eigenvalues. The peaks in the concave shape functions at the concave nodes make integration somewhat more difficult than for non-concave shapes. Care in integration must be taken around the concave node. Nevertheless, the

conductivity matricies can be found. The condition numbers of the resulting matrices are larger than for the non-concave cases. The concavity reduces the stability of the system, but can be evaluated without tessellation.

Shape function type:	Number of nodes :	Eigenvalues:	condition number
Concave **L**	6	$\{0, 0.52, 1.5, 1.6, 3.6, 4.2\}$	8.08
Concave **U**	8	$\{0, 1.1, 1.1, 1.3,$ $4.6, 9.5, 9.5, 16\}$	14.5
Inclusion **O**	8	$\{0, 1.1, 1.1, 1.3,$ $4.6, 9.5, 9.5, 16\}$	14.5

Chapter 6

Summary and applications

The presented general linear interpolations satisfy the boundedness and smoothness conditions on any two dimensional polygonal domain. Unlike the conventional parametric representation the interpolation functions are described in global coordinates, for example cartesian $\{x, y\}$. The interpolations are rational or even irrational polynomial functions. As such the degree of approximation cannot be calculated directly using the Taylor Series, instead a Padé Approximation or the Quadratic Hermite Approximation is employed. Unlike a polynomial interpolant, the rational and irrational forms can capture higher order behaviors without violating the constant and linear field requirements and geometric boundary conditions.

Displacement based concave element formulations have not yet been employed in the solution of any practical problem. No displacement based shape functions for concave elements are discussed in the finite element literature.

Only specific concavities have been addressed within the context of stress based, mixed or hybrid methods.

The derived general method for linear shape function construction applies to any polygonal domain convex or concave, even simply connected domains. The nonlinear behavior which must occur along the diagonal connecting the concave and opposite concave node is captured using the geometric test function. Linearizing the diagonal by tessellation results in a model which does not capture the increased gradient at the concave node; for example, increased stress intensity at a crack tip.

Consequently, an application of the derived shape function method is to model how a material's microstructure effects its macro behavior, see figure 6.1. For example, how the degree of stress concentration captured by the concave element formulation effects the behavior of the element. Further research is required to discern which length scales can effect the macro behavior of a material. For example, if a test function model which faithfully reproduces hexagonal inclusions can predict the behavior of a material built up from nano-tubes with the same structure [42, 36]. Using the developed test functions the effect of local inclusions and stress concentrations on the macro behavior of a column under plane torsion can be studied without imposing an additional local structure associated with a mesh, see figure 6.2. An approximate solution to the plane torsion problem was the first application of a tessellation [13].

The boundedness of the solution is similarly preserved. The general geo-

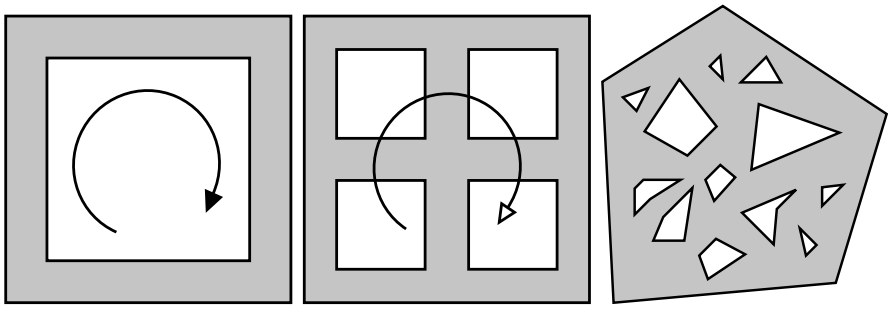


Figure 6.1: Modeling the structure of material, the torsion problem.

metric test function satisfies the Chebyshev condition. In a heat conduction problem, for example, a temperature value given in Kelvin can never physically be less than zero. A bounded interpolation respects such physical restrictions. Furthermore, it tends monotonically to the actual solution. Oscillatory convergence is avoided. Elements with side nodes have been aplied to the study of bounded temperature distributions [41].

The linear edge condition assures that any collection of elements with any geometry and any number of side nodes is conformal. Abutting elements necessarily have the same boundary behavior. Consequently, the global geometric test function may act as a local shape function. Even on concave domains the zero eigenvalues associated with the rigid body conditions are captured exactly. Elements can be used in conjunction with one another to describe, for example, the radiation properties of an unbounded media, see figure 6.3. Concave cells do not exhibit the same degree of spurious inter-element waves as tesselated cells incur, see figure 6.4.

When applied as test functions, the polygonal interpolants serve as the

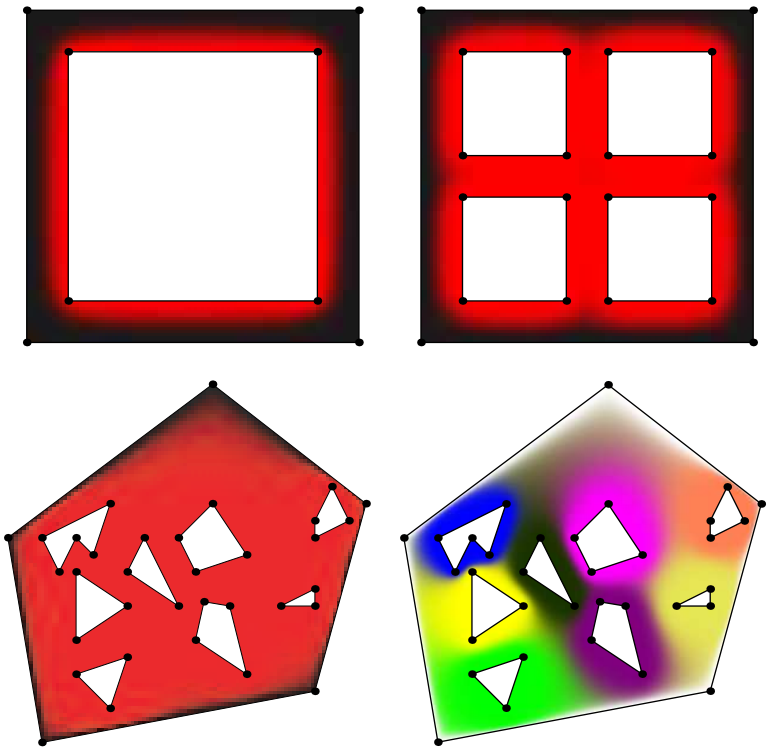


Figure 6.2: Interpolants for modeling planar torsion.

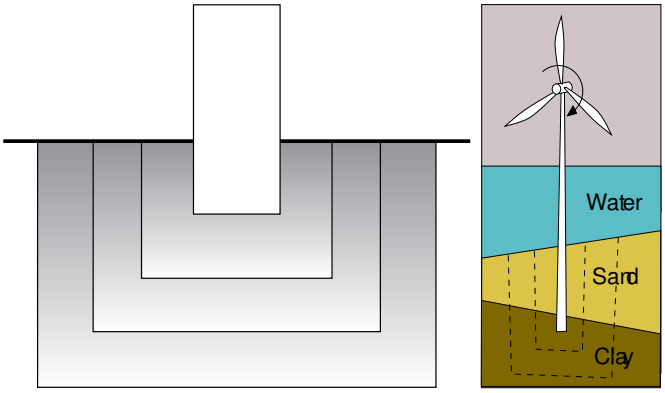


Figure 6.3: Soil structure interaction with concave cells.

kinematic analog to the domain independent Green's function employed in the boundary element formulation. The nodal data need only be given along the boundary. The addition of any data improves the behavior of the finite degree-of-freedom model with respect to the infinite degree-of-freedom domain it is describing. Inversely to the boundary element formulation, the geometric test functions satisfy the geometric boundary conditions but not the governing field equation.

Another first application of rational and irrational polynomial test functions is the modeling of a domain described by limited boundary data. For example, analysis of the growth of biological systems from Magnetic Resonance Imaging measurements. Nondestructive testing of living organs furnishes only a small number of data points, see figure 6.5. Rational polynomial shape functions have been applied to the study of the eye and skull growth. The higher order kinematic behavior of the many sided polygons is captured with the Padé approximation [19, 43]. Similarly, for the analyses of bio-

logical systems where concavity is germane to performance, a test function formulation applicable to reentrant domains is required.

Other applications include those not governed by any specific field equation. In computer graphics, for example, the coloring on a smooth domain is not prescribed by a specific elliptic functional. Using the developed test functions, a smooth color gradient governed by boundary data can be constructed over any polygon. Convex polygons have been described using Wachspress' rational polynomials [18, 45]. The additional memory consumption and computation time required for the discretization of the domain is avoided. The smoothness of the resulting picture depends only on the resolution of the image, see figure 6.6. Inversely, if a domain is described with a computer graphics model, for example a Computer Aided Drafting plan, the stiffness of the domain can be approximated without additional meshing.

This research extends the class of two dimensional polygons which can be described using geometric test functions. Concave and degenerate domains with side nodes can now be described. The applications including interpolation, finite element analysis and elliptic operator approximation would be best served by extending the class even farther. Three and more dimensional elements and curved element boundaries require an equally consistent representation.

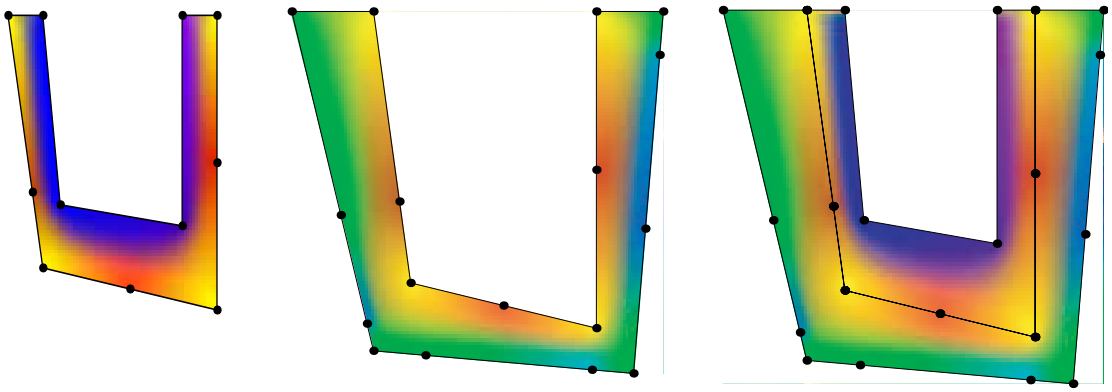


Figure 6.4: Concave cell interpolation.

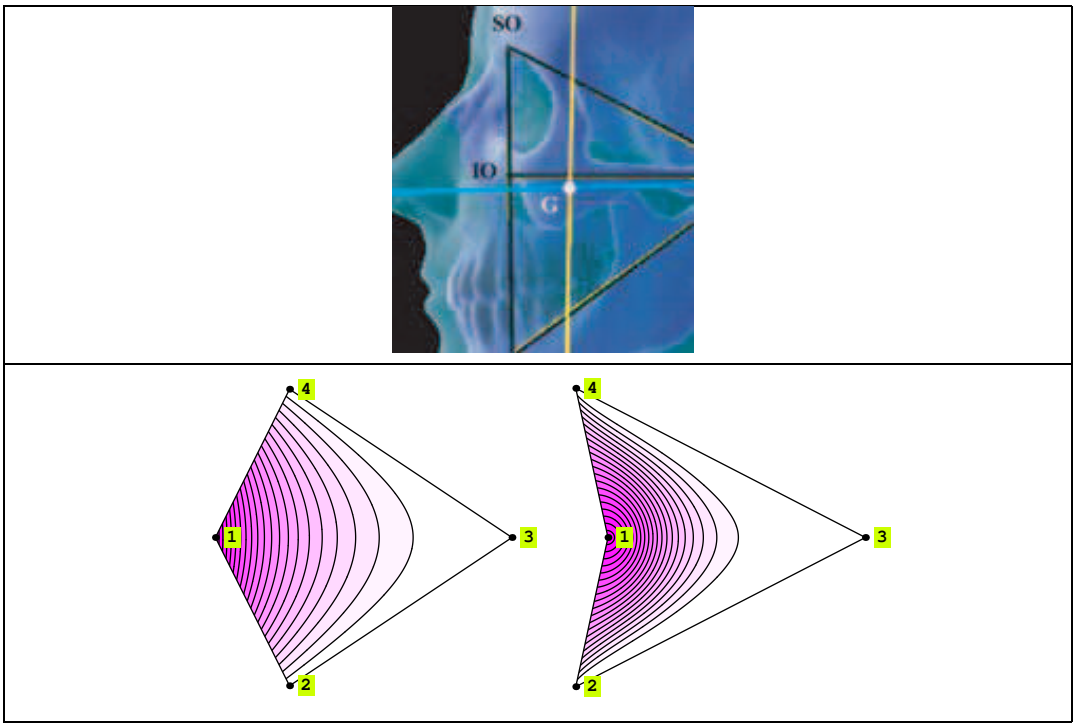


Figure 6.5: Analysis of biological structures defined by a limited number of data points. (Maxiofacial frame picture from Jaques Treil [60])

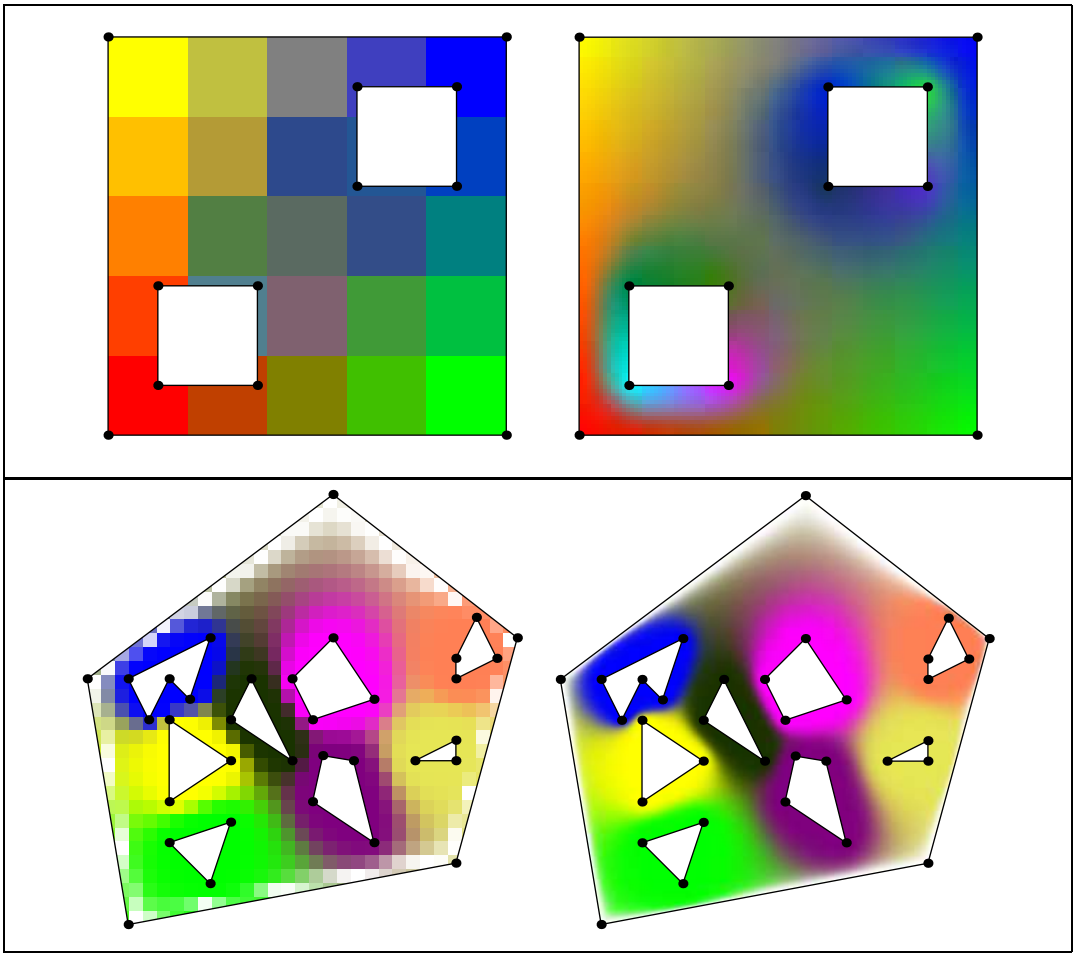


Figure 6.6: Smooth gradient colorings can be generated at any desired resolution without tessellation.

Bibliography

[1] J. E. Akin. *Finite Elements for Analysis and Design*. Computational Mathematics and Applications. Academic Press, San Diego, CA, 1994. Second printing 1995.

[2] T. L. Anderson. *Fracture Mechanics: Fundamentals and Applications*. CRC Press, 2nd edition, 1995.

[3] John Barlow. A different view of the assumed stress hybrid method. *International Journal for Numerical Methods in Engineering*, 22:11–16, 1986.

[4] K. J. Bathe. The inf-sup condition and its evaluation for mixed finite element methods. *Computers and Structures*, 79:243–252, 2001.

[5] T. Belytschko and T. Black. Elastic crack growth in finite elements with minimal remeshing. *International Journal for Numerical Methods in Engineering*, 45(5):601–620, 1999.

[6] Jean-Daniel Boissonnat and Mariette Yvinec. *Géométrie Algorithmique*. Edisciences International, Paris, 1995. (English edition: Algorithmic Geometry, Cambridge University Press 1998).

[7] C. A. Brebbia. *The Boundary Element Method for Engineers*. John Wiley and Sons, 1978.

[8] C. A. Brebbia and J. Dominguez. *Boundary Elements - An Introductory Course*. McGraw-Hill, 1992.

[9] Susanne C. Brenner and L. Ridgeway Scott. *The Mathematical Theory of Finite Element Methods*. Number 15 in Text in Applied Mathematics. Springer, 1994.

[10] U. Brink and E. Stein. On some mixed finite element methods for incompressible and nearly incompressible finite elasticity. *Computational Mechanics*, 19:105–119, 1996.

[11] Bernard Chazelle and David P. Dobkin. Optimal convex decompositions. Elsevier Science, 1985.

[12] R. W. Clough. The finite element in plane stress analysis. *Proceedings of the 2nd ASCE Conference on Electronic Computation*, September 1960.

[13] R. Courant. Variational methods for the solution of problems of equilibrium and vibrations. *Bulletin of the American Mathematical Society*, 49:1–23, 1943.

[14] R. Courant and D. Hilbert. *Methoden der Mathematischen Physik*. Springer Verlag, Berlin, 2nd edition, 1931.

[15] Gautam Dasgupta. Tessellica: a defect-free finite element paradigm. *International Conference on Logic, History and Educational Computing, Computer Science*, pages 230–242, 1996. (The metod was submitted by Columbia University, New York, NY, for patent protection under Columbia Innovative Enterprise in May 1996).

[16] Gautam Dasgupta. Integration within polygonal finite elements. *ASCE Journal of Aerospace engineering*, 16(1):9–18, 2003.

[17] Gautam Dasgupta. Interpolants within convex polygons: Wachspress' shape functions. *ASCE*, 16(1):1–8, January 2003.

[18] Gautam Dasgupta and Elisabeth Anna Malsch. Boundary element color interpolation for instrumentation, imaging and internet graphics industry. *International Journal for Engineering Analysis with Boundary Elements*, 26(5):379–389, 2002.

[19] Gautam Dasgupta, Mona E. McAlarney, C. Goodall, L. Moss-Salentijn, and M. Moss. Form comparison without anatomical landmarks. *International Journal for Engineering Analysis with Boundary Elements*, pages 972—975, 1992.

[20] Philip J. Davis. *Interpolation and Approximation*. Dover, 1975. First edition printed 1963.

[21] Mark de Berg, Marc van Krevald, Mark Overmars, and Otfried Schwartzkopf. *Computational Geometry, Algorithms and Applications*. Springer Verlag, 2nd edition, 2000.

[22] C. A. Felippa. A historical outline of matrix structural analysis: a play in three acts. *Computers and Structures*, 79(14):1313–1324, 2001.

[23] Curtis F. Gerald and Patrick O. Wheatly. *Applied Numerical Analysis*. Addison-Wesley, New York, 6th edition, 1999.

[24] David Gilbarg and Neil S. Trudinger. *Elliptic Partial Differential Equations of Second Order*, volume 224 of *Grundleheren der Mathematischen Wissenschaften*. Springer Verlag, 2001. Reprint of the 1998 Edition.

[25] C. Gout. C^k Surface approximation from surface patches. *Computers and Mathematics with Applications*, pages 389–406, 2002.

[26] Richard Haberman. *Elementary Applied Partial Differential Equations*. Prentice Hall, New York, 3rd edition, 1998.

[27] R. D. Henshell and K. G. Shaw. Crack tip finite elements are unnecessary. *International Journal for Numerical Methods in Engineering*, 9:495–507, 1975.

[28] David Hilbert. *Foundations of Geometry*. Open Court, 1971. Translated by Leo Unger.

[29] Thomas J. R. Hughes. *The Finite Element Method: Linear Static and Dynamic Finite Element Analysis*. Prentice-Hall, 1987.

[30] Bruce Irons and Sohrab Ahmad. *Techniques of Finite Elements*. John Wiley and Sons, 1980.

[31] J. Jirousek and P. Teodorescu. Large finite elements method for the solution of problems in the theory of elasticity. *Computers and Structures*, 15(5), 1982.

[32] H. Kardestuncer and D. H. Norrie, editors. *Finite Element Handbook*. McGraw-Hill, 1987.

[33] Wolfram Koepf. *Hypergeometric Summation*. Advanced Lectures in Mathematics. Vieweg, Braunschweig, Germany, 1998.

[34] Peter Kohnke, editor. *Ansys Theory Reference*. SAS IP Inc, 11th edition, 1994.

[35] M. Laydi and P. Lesaint. *Sur les elements finis rationnels de Serendip de degre quelconque*, volume 47 of *Numerische Mathematik*. Springer Verlag, 1985.

[36] A. P. Li, F. Müller, A. Birner, K Nielsch, and U. Gösele. Hexagonal pore arrays with a 50–420 nm interpore distance formed by self-organization in anodic alumina. *Journal of Applied Physics*, 84(11):6023–6026, 12 1998.

[37] Richard H. MacNeal. On the limits of finite element perfectability. *International Journal for Numerical Methods in Engineering*, 35:1589–1601, 1992.

[38] Richard H. MacNeal. *Finite Elements: Their Design and Performance*. Mechanical Engineering. Marcel Dekker, Inc., 1993. TA347.f5M36 1993.

[39] Elisabeth Malsch and Gautam Dasgupta. Shape functions for polygonal domains with interior nodes. *International Journal for Numerical Methods in Engineering*, (Submitted), 2003.

[40] Elisabeth A. Malsch. Four-noded triangular finite elements. In *15th ASCE Engineering Mechanics Conference*, Columbia University, New York, NY, June 2002. ASCE.

[41] Elisabeth A. Malsch. Interpolation constraints and thermal distributions: a method for all non-concave polygons. *International Journal of Solids and Structures*, 2003. Accepted.

[42] Hideki Masuda and Kenji Fukuda. Ordered metal nanohole arrays made of two-step replication of honeycomb structures of anodic alumina. *Science*, 268(5216):1466–1468, 1995.

[43] Mona E. McAlarney, Gautam Dasgupta, M. L. Moss, and L. Moss-Salentijn. Anatomical macro element in the study of cranial facial rat growth. *Journal of Cranial Facial Growth and Developmental Biology*, 12:3–12, 1992.

[44] Robert J. Melosh. *Structural engineering analysis by finite elements*. Number 12 in Prentice-Hall International Series in Civil Engineering and Engineering Mechanics. Prentice-Hall, 1990.

[45] M. Meyer. Generalized barycentric coordinates on irregular polygons. *Journal of Graphics Tools*, 7:1086–7651, 2002.

[46] S. G. Mikhlin and K. L. Smolitskiy. *Approximate methods for solution of differential integral equations*. American Elsevier, New York, 1967.

[47] N. Nikuchi and J. T. Oden. Problems with constraints. *Finite Element Handbook*, 2(9):2.321–2.337, 1987.

[48] Theodore H. H. Pian. Derivation of element stiffness matrices by assumed stress distributions. *American Institute of Aeronautics and Astronautics*, 2:1333–1336, 1964. TL501.A33.

[49] L. Prandtl and O. G. Tietjens. *Fundamentals of Hydro- and Aeromechanics*. Engineering Societies Monographs. Dover, 1957. First edition printed 1934.

[50] G. Prathap. The displacement-type finite element approach–from art to science. *Progress in Aerospace Sciences*, 30:295–405, 1994.

[51] Ch. Provatidis and A. Kanarachos. Performance of macro-FEM approach using global interpolation (Coons') functions in axisymmetric potential problems. *Computers and Structures*, 79:1769–1779, 2001.

[52] B. N. Rao and S. Rahman. An efficient meshless method for fracture analysis of cracks. *Computational Mechanics*, pages 398–408, 2000.

[53] D. F. Rogers and J. A. Adams. *Mathematical Elements of Computer Graphics*. McGraw-Hill, 1990.

[54] A. Schwartz and C. Stanton. Analyzing surfaces: the truth about elimination theory. *ACM*, 87(6):348–353, 1987.

[55] R.E. Shafer. On quadratic approximation. *SIAM Journal on Numerical Analysis*, 11(2):447–460, April 1974.

[56] Ivar Stakgold. *Boundary Value Problems of Mathematical Physics*, volume 1 of *Macmillian Series in Advanced Mathematics and Theoretical Physics*. Macmillian, 1967.

[57] Gilbert Strang and George J. Fix. *An Analysis of the Finite Element Method*. Automatic Computation. Prentice-Hall, 1973.

[58] Victor L. Streeter. *Fluid Dynamics*. McGraw-Hill, 1948.

[59] R. L. Taylor, J. C. Simo, O. C. Zienkiewicz, and A. C. H. Chan. The patch test – a condition for assessing FEM convergence. *International Journal for Numerical Methods in Engineering*, 22:39–62, 1986.

[60] Jaques Treil, C. Madrid, M. Jaeger, J. Casteit, and P. Borianne. Biometrie tridimensionnelle maxillo-faciale. *Biom. Hum. et Anthropol.*, 15(1.2):65–73, 1997.

[61] E. L. Wachspress. *A Rational Finite Element Basis*. Academic Press, 1975.

[62] Joe Warren. Barycentric coordinates for convex polytopes. Technical report, Department of Computer Science, Rice University, 1996.

[63] J. R. Whiteman. Finite-element method with singularities. *Finite Element Handbook*, pages 2.203–2.214, 1987. McGraw-Hill.

[64] Wilson. *Sap2000*. Ceanet, 2000.

[65] Chia-Shun Yih. *Fluid Mechanics*. McGraw-Hill, New York, 1969.

[66] Z. Yosibash. Numerical analysis on singular solutions of the Poisson equation in two-dimensions. *Computational Mechanics*, 20:320–330, 1997.

[67] O. C. Zienkiewicz and R. L. Taylor. *The Finite Element Method*, volume 1. McGraw-Hill, New York, 4th edition, 1989.

Appendix A

Code examples

A.1 Lagrange polynomial from Taylor Series

Using the Taylor series expansion and the Richarson's extrapolation and weights, set n to the number of known points other than z_0. The *Mathematica* code below finds the coefficients of $f(z_0), f(z_1), \ldots, f(z_n)$:

```
Coefficient[
 Simplify[
  Series[f[z], {z, zn[0], n}] /.
    Solve[
     Table[
      (f[z] == (Series[f[z], {z, zn[0], n}] // Normal)
        /. z -> zn[i]), {i, n}],
   NestList[D[#, zn[0]] &, D[f[zn[0]], zn[0]], n - 1]
              ] // Normal][[1]],
    Table[f[zn[i]], {i, 0, n}]
    ]
```

Test, for $n = 1$:

$$f(z) \approx f(z_0)\frac{z - z_1}{z_0 - z_1} + f(z_1)\frac{z - z_0}{z_1 - z_0}.$$

Notice, that solutions follow pattern which can be followed directly instead of rederiving for each new value of n (proof by induction not included).

```
f[z_][pts_, ptVals_] :=
  Sum[ptVals[[i]]*(Times @@ ((z - #) & /@
```

```
    Drop[pts, {i, i}]))/(Times @@ ((pts[[i]] - #) & /@
    Drop[pts, {i, i}])), {i, Length[pts]}]
```

For test input:

```
pts = {z1, z2, z3};
ptVals = {f[z1], f[z2], f[z3]};
```

The output is:

$$f(z) \approx f(z_0)\frac{(z-z_1)(z-z_2)}{(z_0-z_1)(z_0-z_2)} + f(z_1)\frac{(z-z_0)(z-z_2)}{(z_1-z_0)(z_1-z_2)} + f(z_2)\frac{(z-z_0)(z-z_1)}{(z_2-z_0)(z_2-z_1)}.$$

Deriving the function following the pattern for a given n nodes is an $O(n)$ operation. Evaluating the function is $O(1)$.

A.2 Shape function routine for convex polygons

The `i`$^{\text{th}}$ shape function in cartesian (x, y) coordinates, for any `n` sided convex polygon with nodal points {`xn[i],yn[i]`} can be found in closed form using the following *Mathematica* code.

```
convexSF[i_, n_, {xn_, yn_}][x_, y_] :=
   (#[[i]]/Plus @@ # &[((
      Det[({xn[#], yn[#],1} & /@ {#1, #2, #3})]/
         (Times @@ (Det[
```

```
            Flatten[{{{x, y, 1}}, ({xn[#], yn[#], 1} & /@ #)}, 1]]&
               /@ {{#1, #2}, {#2, #3}}))) & @@@ #)&
               [Thread[{RotateRight[#], #, RotateLeft[#]}]
      &[Range[n]]]];
```

Test with generic nodal values, e.g. triangle:

```
Array[xn,3]; Array[yn,3];
convexSF[1, 3, {xn, yn}][x, y] // Simplify
```

The resulting shape function for node-1 is:

```
(y(xn[3]-xn[2]) - xn[3] yn[2] + x(yn[2]-yn[3]) + xn[2] yn[3])/
   (xn[3] (yn[1]-yn[2]) + xn[1](yn[2]-yn[3]) + xn[2](yn[3]-yn[1]))
```

The result is equal to $\triangle(\vec{x}, 2, 3)/\triangle(1, 2, 3)$, the expected shape function. Test with specific nodal values, e.g. unit square $\{0, 0\}, \{1, 0\}, \{1, 1\}, \{0, 1\}$:

```
{{xn[1], yn[1]}, {xn[2], yn[2]}, {xn[3], yn[3]}, {xn[4], yn[4]}} =
{{0, 0}, {1, 0}, {1, 1}, {0, 1}};
Table[convexSF[i, 4, {xn, yn}][x, y], {i, 4}] // Simplify
```

The resulting shape functions, for nodes-$1, 2, 3, 4$ respectively, are the expected:

$$\{(x-1)(y-1), (x-1)y, xy, (y-1)x\} \tag{A.1}$$

For an arbitrary septagon:

$$\{\{0,0\}, \{\frac{1}{2}, -1\}, \{1,0\}, \{1, \frac{1}{2}\}, \{\frac{2}{3}, 2\}, \{\frac{1}{2}, 2.5\}, \{\frac{1}{4}, 3\}, \{0,1\}\}$$

The shape function for node-1 is

$$\frac{14\ (x-1)\ (9\,x+2\ (y-5))\ (2\,x-y-2)\ \left(0.875-0.5\,x-\frac{y}{4}\right)\ \left(0.667-0.5\,x-\frac{y}{6}\right)}{25.3\,x^4+0.0417\ (y-86.6)\ (y-4.63)\ (y-3.86)\ (y+2.54)}$$

The order of the shape function is as expected. A polynomial of the order $(n-2)$ over a polynomial of the order $(n-3)$. Deriving the shape function for an element with n nodes is an $O(n)$ operation. Evaluating the resulting function is $O(1)$.

A.3 Shape function for an element with side nodes

Given shape functions `phi` and `theta` at the nodes which are at the ends of a straight line, any side-node's influence can be calculated:

```
u[threePts_] := Divide @@ ((Sqrt[#.#] &[#[[2]] - #[[1]]
                &[Drop[threePts, {#}]]]) & /@{3, 2})
nk[0 | 1][phi_, theta_] := 0 /; theta == phi
nk[0 | 1][phi_, theta_] := (phi*theta)/(1-(1-u)*phi-theta *u)
nk[u_][phi_, theta_] := (#2-Sqrt[#2^2 - 4* #1*#3])/(2 *#1)
             &[u(1 - u), 1-(1-u)*phi - theta *u, phi*theta]
npkt[u_][phi_, theta_] := {phi-(1-u)*#, #, theta - u*#}
                              &[nk[u][phi,theta]]
```

The shape functions for a triangle with a midside node:

$$\text{pts} = \{\{0,0\},\{1,0\},\{\frac{1}{2},\frac{1}{2}\},\{0,1\}\} \tag{A.2}$$

Shape functions for the vertices of the triangle are:

$$N_1^*(x,y) = 1-x-y, \quad N_2^*(x,y) = x \quad \text{and} \quad N_4^*(x,y) = y. \tag{A.3}$$

The shape function for the midside node then can be found by evaluating:

```
npkt[u[{{1,0},{1/2,1/2},{0,1}}]][Ni[2][{x,y}],Ni[4][{x,y}]]
```

The shape function for node-1 is unaffected. The shape functions for node-2 and node-4 are updated with respect to the midside node:

$$\begin{aligned}
N_1^*(x,y) &= 1-x-y \\
N_2^*(x,y) &= \frac{-2+3\,x+y+2\sqrt{-(x\,y)+\frac{(-2+x+y)^2}{4}}}{2} \\
N_3^*(x,y) &= 2-x-y-2\sqrt{-(x\,y)+\frac{(-2+x+y)^2}{4}} \\
N_4^*(x,y) &= \frac{-2+x+3\,y+2\sqrt{-(x\,y)+\frac{(-2+x+y)^2}{4}}}{2}
\end{aligned} \tag{A.4}$$

A.4 Concave quadrilateral shape function routine

The approximate shape functions for a four noded convex or concave quadrilateral where only node-4 can be the reentrant node can be found

using the following *Mathematica* code pieces. Given the values at the vertex points (`xn[i], yn[i]`), Define sub-triangle areas and zero lines:

```
twotri[a_, b_, c_] := Det[{xn[#], yn[#], 1} & /@ {a, b, c}]
zerolin[{x _,y_}, b_, c_] :=
   Det[{{x, y, 1}, {xn[b], yn[b], 1}, {xn[c], yn[c], 1}}]
```

Select the convex, triangular, portions of the quadrilateral domain:

```
right[x_, y_] := (1/8)((1 + Sign[zerolin[{x, y}, 2, 3]])
 (1+Sign[zerolin[{x,y},3,4]]) (1+Sign[zerolin[{x,y},4,2]]))
left[x_, y_] := (1/8)((1 + Sign[zerolin[{x, y}, 1, 2]])
 (1+Sign[zerolin[{x, y},2,4]]) (1+Sign[zerolin[{x,y},4,1]]))
```

The shape function for the opposite concave node then is:

```
sfDet[{x_, y_}, a_] :=
((1-zerolin[{x,y},4,a]/twotri[2,4,a])^(twotri[1,2,3]/
                                        twotri[1,3,4])
   *zerolin[{x,y},a,2])/twotri[2,4,a];
sf[4][x_, y__] := left[x, y]*sfDet[{x, y}, 1]
               + right[x, y]*sfDet[{x, y}, 3]
```

Shape functions for the remaining nodes can be found in closed form using the patch test, see §B.3.

Test on a parallelogram. The shape functions are smooth throughout the domain and equal to the functions derived using the general convex element formulation.

```
Clear[xn, yn]
pts = Evaluate[Thread[{Array[xn, 4], Array[yn, 4]}]] =
      {{0, 0},{2, 0}, {2, 1},{0, 1}}
```

The resulting shape functions for nodes-$1, 2, 3, 4$ are:

$$\{(x-2)\ (y-1)\ /2, x\ (1-y)\ /2, x\,y/2, (1-x)\,y/2\} \tag{A.5}$$

On a non-trapazoidal convex element the shape function for node-4 with nodal points: `{{0, 0}, {1, 0}, {2, 2}, {0, 1}}`:

$$\begin{gathered}(x-1)y(\mathrm{sgn}(1-x-y)-1)/2+\\((x-1-2y)(2(x-1)-y)(1+\mathrm{sgn}(2+x-2y))*\\(1+\mathrm{sgn}(2(1-x)+y))(1+\mathrm{sgn}(x-1+y))/72)\end{gathered}$$

On a concave element the shape function for node-4 with nodal points `{{0, 0}, {1/2, 3/4}, {1,1}, {0, 1}}`:

$$1/12\,(1-4y/3)^{\frac{1}{4}}\,(3(1-x)-2y))(1+\mathrm{sgn}(3(1-x)-2y))(1+\mathrm{sgn}(3x-2y))$$

$$1/8(1-2x)^{1/4}(x-2+2y)(1+\mathrm{sgn}(2-x-2y)-(1+\mathrm{sgn}(-3x+2y)).$$

Notice the sign (`Sign[]` or $\mathrm{sgn}(\cdot)$) function is not a smooth function within the given domains.

Appendix B

Methods

B.1 One-dimensional formulation and solution

A governing functional for a one dimensional problem:

$$I(v) = \int_0^\pi \mathcal{K}[v(x)]\mathrm{d}x, \tag{B.1}$$

Let the associated direct formulation be:

$$\mathcal{L}[u(x)] = f(x) \tag{B.2}$$

with corresponding Dirichlet, Neumann or mixed boundary conditions. An approximate solution can be constructed according to the values at distinct nodes along the continuous number line $x \in (0, \pi)$. The test functions need only satisfy the geometric (Dirichlet) boundary conditions, the natural (Neuman) conditions are captured by the divergence expressions in the domain integrals [13, pp.4–5]. Three methods for solution construction according to the finite element construction are the h, p and modal methods. h refers to the distance between nodal points and p to the order of polynomial which is distributing values over the domain [67]. In either case the approximate solution $u(x)$ is described in terms of nodal data u_i and interpolation function $\phi_i(x)$:

$$u(x) = \sum_{i=1}^{n} u_i \phi_i(x) \tag{B.3}$$

The simplest h-version interpolation function is the hat function. The p-version interpolation is a polynomial of order p.

B.1.1 h-method

The minimum can be found according to a hat shaped test function and formulated in finite element form [57, pp. 24–32].

$$[\mathbf{K}]\{\mathbf{u}\} = \{\mathbf{f}\} \tag{B.4}$$

The behavior of any given node u_i is directly coupled only to the its neighboring nodes u_{i-1} and u_{i+1}. Consequently $[\mathbf{K}]$ is a banded symmetric matrix of the form:

$$[\mathbf{K}] = \begin{pmatrix} k_{11} & k_{12} & 0 & 0 & 0 & \cdots \\ k_{12} & k_{22} & k_{23} & 0 & 0 & \cdots \\ 0 & k_{23} & k_{33} & k_{34} & 0 & \cdots \\ \vdots & \vdots & \vdots & \vdots & \vdots & \ddots \end{pmatrix} \tag{B.5}$$

The discontinuities in the derivative of $u(x)$ between elements corresponds with the application of the force or other change in property which occurs at a nodal point.

The error in the approximation $e^h = u - u^h$ is [57, pp. 39–51]:

$$a(e^h, e^h) \leq C_1 h^2 ||u''||_0^2 \leq C_2 h^2 ||f||_0^2 \tag{B.6}$$

where

$$a(\Delta, \Delta) = \int_0^\pi p(\Delta')^2 + q(\Delta)^2 \tag{B.7}$$

$$||u''||_0^2 = \int_0^\pi (u'')^2 \tag{B.8}$$

$$||f||_0^2 = \int_0^\pi (f)^2 \tag{B.9}$$

also, C_1 and C_2 are constants and h is the element division.

B.1.2 p-method

Alternatively, if the continuity at the nodes were assured, the shape function could be constructed according to a Lagrange polynomial, see appendix A.1. The error in such an approximation to a function $f(\cdot)$ is:

$$\epsilon(x) = (x - x_0)(x - x_1)\cdots(x - x_n)\frac{f^{(n+1)}(\xi)}{(n+1)!} \tag{B.10}$$

The order of the polynomial for a model with n number of nodes is $p = n$ and the corresponding order of convergence to a smooth function is order $\mathbf{O}(h^n)$ within the radius of convergence [23, pp. 220–238]. If for the Rayleigh-Ritz approximation the trial function is a polynomial of order p then the stiffness matrix $[\mathbf{K}]$ associated with the Sturm-Liouville problem, equation B.1, is the notoriously ill-conditioned Hilbert matrix [57, pp. 25–26].

While the rate of convergence of p-method seems to much higher than that for the h-method it is not suitable for the construction of a solution where discontinuity occurs at the nodes or if the nodal data is in a bounded set. The h-method construction, on the other hand, can represent discontinuity, does not violate boundedness and — as the number of nodes increases — approaches the equilibrium solution uniformly.

B.1.3 One dimensional modal solution

If instead of increasing the order of the polynomial or decreasing the order of solution a modal method is used instead:

$$\mathcal{L}[\phi_i(x)] = \lambda_i\phi_i(x) \tag{B.11}$$

Where the functions $\phi_i(x)$ are orthogonal and satisfy the boundary conditions:

$$\int_0^\pi \phi_i(x)\phi_j(x)\mathrm{d}A = 0 \quad \text{if} \quad i \neq j. \tag{B.12}$$

The stiffness matrix from such a formulation is diagonal:

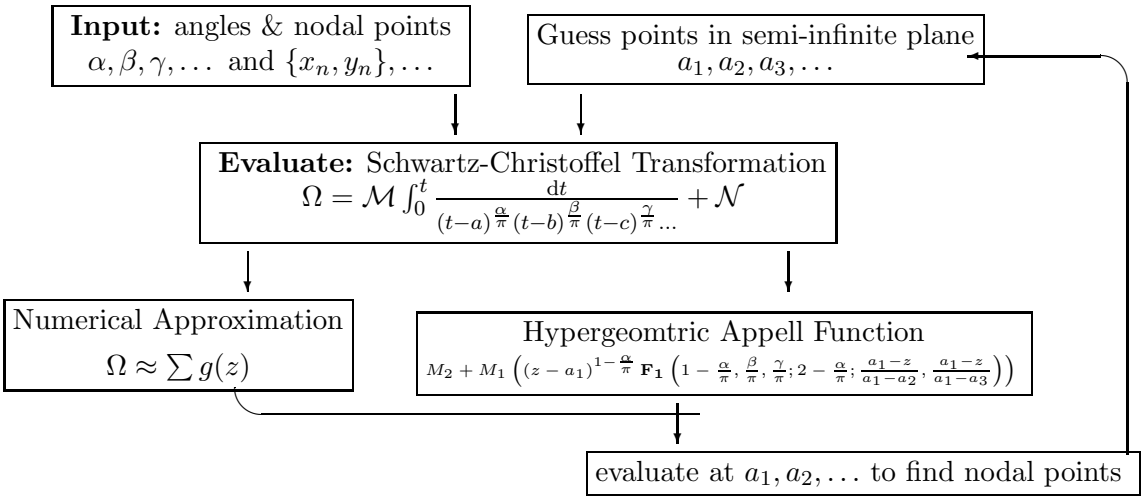
$$K_{ij} = \int_0^\pi \phi_i \mathcal{L}\left[\phi_j\right] \mathrm{d}x = -\lambda_j \int_0^\pi \phi_i \phi_j \mathrm{d}A \tag{B.13}$$

An infinite number of nodes λ_j describe a continuous system exactly. In the limit a modal approximation can represent a piecewise continuous function. Any n nodes describe n distinct modes and approximate the system better than $m < n$ modes would [26, pp.261].

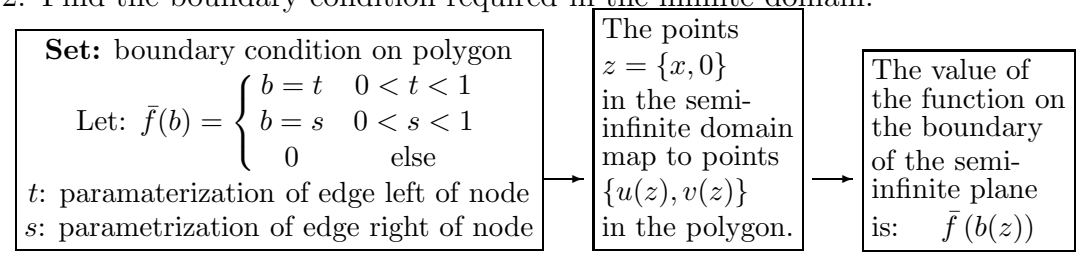
B.2 Conformal Mapping

Process of finding the solution to Laplace's equation on any polygonal domain for a given linear Dirichlet boundary condition

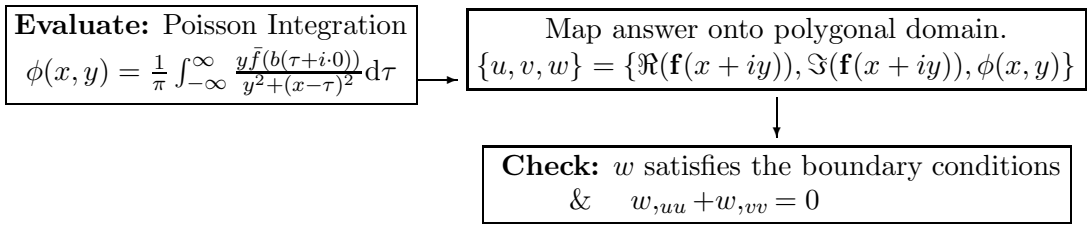
1. Find the mapping that correlates a semi-infinite domain and any given polygon.



2. Find the boundary condition required in the infinite domain.



3. Combine to find solution.



B.3 Shape function generation and boundedness

All four shape functions for a quadrilateral need not be derived separately. Since the set of shape functions must in linear combination satisfy the constancy and linearity requirements, the functions are dependent on one another. Given a shape function $\mathbf{N_1}(x, y)$ which is bounded and smooth within a continuous two-dimensional domain and zero, one, or linear along the boundary the shape functions for the remaining nodes can be found similarly. Within a quadrilateral domain:

$$\mathbf{N_1}(x_j, y_j) = \delta_{1j} \quad \text{and} \quad \begin{array}{c} \mathbf{N_1}(x_1\,(1-t) + x_4\,t, y_1\,(1-t) + y_4\,t) = t \\ \mathbf{N_1}(x_1\,(1-s) + x_2\,s, y_1\,(1-s) + y_2\,s) = s. \end{array} \tag{B.14}$$

On all other boundaries the shape function is zero valued. The remaining shape functions found from the patch test are similarly smooth and linear along the boundary.

Given the patch test requirement for a quadrilateral, see equation 1.7. Along the boundary where $\mathbf{N_1}(x_b, y_b) = 0$, solve the three equations for the three shape functions:

$$N_2(x_b, y_b) = \frac{\triangle(b,3,4)}{\triangle(2,3,4)},\ N_3(x_b, y_b) = \frac{\triangle(b,4,2)}{\triangle(3,4,2)} \text{ and } N_4(x_b, y_b) = \frac{\triangle(b,2,3)}{\triangle(4,2,3)}. \tag{B.15}$$

The resulting equations then are linear valued along the boundary, single valued at their respective nodes and zero valued at the others, solving similarly for the sides adjacent to node-1, $\mathbf{N_1}(x_t, y_t) = t$ find:

$$N_i(x_j, y_j) = \delta_{ij} \quad \text{and} \quad N_i(x_i(1-t) + x_{i-1}t, y_i(1-t) + y_{i-1}t) = t. \tag{B.16}$$

The patch test equations are linear in terms of the shape function. Thus, if the initial shape function is smooth the derived functions will also be smooth. To check the boundedness evaluate the patch test at a point p ($\{x_p, y_p\}$) inside the domain where the first shape function is bounded ($0 < N_1(x_p, y_p) < 1$), let $\alpha_p = N_1(x_p, y_p)$. Solving for the shape functions:

$$N_2(x_p, y_p) = \frac{\triangle(p,3,4) - \alpha_p \triangle(1,3,4)}{\triangle(2,3,4)}, \quad N_3(x_p, y_p) = \frac{\triangle(p,4,2) - \alpha_p \triangle(1,4,2)}{\triangle(3,4,2)}$$

and

$$N_4(x_p, y_p) = \frac{\triangle(p,2,3) - \alpha_p \triangle(1,2,3)}{\triangle(4,2,3)}.$$

For the shape functions to be bounded within a quadrilateral domain the first shape function $\mathbf{N_1}(x, y)$ must satisfy the following additional bounds, define the positive direction with respect to $\triangle(2,3,4) > 0$:

$$\begin{aligned}
&\triangle(\vec{x},3,4) > \mathbf{N_1}(x,y)\triangle(1,3,4) > \triangle(2,3,4) - \triangle(\vec{x},3,4) \\
&\triangle(\vec{x},4,2) > \mathbf{N_1}(x,y)\triangle(1,4,2) > \triangle(2,3,4) - \triangle(\vec{x},4,2) \\
&\triangle(\vec{x},2,3) > \mathbf{N_1}(x,y)\triangle(1,2,3) > \triangle(2,3,4) - \triangle(\vec{x},2,3).
\end{aligned} \tag{B.17}$$

Given a smooth and bounded shape function $\mathbf{N_1}(x, y)$ which does not exhibit any minima and maxima within the domain the remaining bounded shape functions can be derived in closed form.

B.4 Rational polynomial basis functions

The rational polynomial form is flexible enough to represent first order interpolations within all two dimensional and some three dimensional convex shapes. The shape function formulation for any convex polygon can be derived generally as an algebraic collection of functions which are appropriately zero valued and linear around the boundary lines. Define a function $s_i(x, y)$ such that the function is zero along all boundary lines except those adjacent to node i.

$$s_{i\neq j \& i\neq j-1}(x_j + t(x_{j+1} - x_j), y_j + t(y_{j+1} - y_j)) = 0 \quad \forall t \in (0, 1) \quad \text{(B.18)}$$

A function which satisfies this criteria is the product of planes which are set to be zero on each of the non-adjacent boundary lines.

$$l_i(x, y) = Ax + By + C \quad \text{and} \quad l_i(x_i, y_i) = l_{i+1}(x_{i+1}, y_{i+1}) = 0 \quad \text{(B.19)}$$

solving for A and B, C is a scaling factor, find,

$$l_i(x, y) = 2\triangle(\vec{x}, i, i + 1). \quad \text{(B.20)}$$

Define:

$$r(x, y) = \prod_{j=1}^{n} l_j(x, y) \quad \text{then} \quad s_i(x, y) = \frac{r(x, y)}{l_i(x, y) l_{i-1}(x, y)}. \quad \text{(B.21)}$$

n is the number of nodes and the numbering is cyclic, that is point $i = 0$ and point $i = n$ are the same point. The shape function then is

$$N_i(x, y) = \frac{k_i s_i(x, y)}{\sum_{j=1}^{n} k_j s_j(x, y)}. \tag{B.22}$$

The sum of all shape functions is one, this satisfies the first patch test requirement. Along the edges adjacent to node-i the function should be linear along the boundary.

$$N_i(x_i + t(x_{i+1} - x_i), y_i + t(y_{i+1} - y_i)) = Dt + E \tag{B.23}$$

The relationship between k_i and k_{i+1} can be derived from this condition.

$$k_{i+1} \triangle (i, i + 1, i + 2) = k_i \triangle (i - 1, i, i + 1). \tag{B.24}$$

Consequently,

$$k_i \triangle (i - 1, i, i + 1) = k_j \triangle (j - 1, j, j + 1). \tag{B.25}$$

Since $\triangle(a, b, c)$ is the area of the triangle whose nodes are in cyclic order a, b and c, the shape functions then are necessarily positive. This method applies to any convex element with any number of nodes. It does not apply to concave elements since the elongations of the boundary lines would prescribe zero values inside the domain.

Alternatively this shape function representation can derived from projec-

tive geometry, as introduced by Wachspress in 1975, using external intersection points. The solutions are valid within for any convex quadrilateral domain [61]. A shape function for node-i of a general two dimensional finite element can be constructed according to the following formula, see also §3.3 [17]. The node numbering is cyclic. For cyclic node numbering when node-1 is adjacent to node-n and node-m, node-0 = node-n and node-2 = node-m. The order of the numbering is performed according to the right hand rule. A convex element with any number of nodes:

$$N_j^n(x,y) = \frac{\triangle(j-1,j,j+1)\left(\prod_{\forall k \neq j \text{ or } j-1} \triangle(\vec{x},k,k+1)\right)}{\sum_{i=1}^{n} \triangle(i-1,i,i+1)\left(\prod_{\forall k \neq j \text{ or } j-1} \triangle(\vec{x},k,k+1)\right)} \tag{B.26}$$

For computer code and examples see appendix A.2. The shape function for a triangle is derivable from this formula. The general shape function for node a of a convex quadrilateral (a,b,c,d) is:

$$N_a^4(x,y) = \frac{\triangle(d,a,b)\triangle(\vec{x},b,c)\triangle(\vec{x},c,d)}{\left(\begin{array}{l}\triangle(d,a,b)\triangle(\vec{x},b,c)\triangle(\vec{x},c,d) + \triangle(a,b,c)\triangle(\vec{x},c,d)\triangle(\vec{x},d,a) \\ \quad +\triangle(b,c,d)\triangle(\vec{x},d,a)\triangle(\vec{x},a,b) + \triangle(c,d,a)\triangle(\vec{x},a,b)\triangle(\vec{x},b,c)\end{array}\right)}. \tag{B.27}$$

This formulation produces the same shape function for a trapezoid as the standard isoparametric transformation.